

Predicting fatigue crack initiation and propagation in Glare reinforced frames

S.W.F. Spronk

Master of Science Thesis

Predicting fatigue crack initiation and propagation in Glare reinforced frames

MASTER OF SCIENCE THESIS

For the degree of Master of Science in Aerospace Structures at the
Delft University of Technology

S.W.F. Spronk

June 14, 2013

DELFT UNIVERSITY OF TECHNOLOGY
DEPARTMENT OF
AEROSPACE STRUCTURES & DESIGN METHODOLOGIES (ASDM)

The undersigned hereby certify that they have read and recommend to the Faculty of
Aerospace Engineering for acceptance a thesis entitled

PREDICTING FATIGUE CRACK INITIATION AND PROPAGATION IN GLARE
REINFORCED FRAMES

by

S.W.F. SPRONK

in partial fulfillment of the requirements for the degree of
MASTER OF SCIENCE AEROSPACE STRUCTURES

Dated: June 14, 2013

Supervisor(s):

Dr. ir. R.C. Alderliesten

Committee member(s):

Ir. J.M.A.M. Hol

Dr. Dipl.-Ing. T. Beumler, Airbus Deutschland GmbH

Dr. G.S. Wilson, M.Sc., GE Aviation

Preface

It was Professor Marissen with his lectures about fracture of advanced materials who nurtured my interest in fibre metal laminates. I found an opportunity to do a thesis in connection with Airbus which would allow me to explore every aspect of fatigue of this material and which has as an underlying goal the task to make academic knowledge available to the industry. This combination was more than enough reason for me to agree that this would be the perfect way to finish my time at the Delft University of Technology.

Codes are never perfect and future users will always have creative new ways to want to use code in a way that could not be accounted for. Still, I find that the result of my efforts is something to be proud of, and I sincerely hope that my programme will become what it is intended to be and form the basis of a new fibre metal laminate analysis tool from which both the Structural Integrity chair at the faculty of Aerospace Engineering and Airbus can benefit.

I wish here to express my sincere appreciation to my supervisors Dr. ir. René Alderliesten and ir. Jan Hol, who, despite their full agendas, were able to provide me with just the right kind and amount of input to bring the best in me forward during the final 8 months of my study. René especially has proven to be a very good sparring partner to discuss ideas with if I was unsure whether my approach was correct or not.

I would like to thank Dr. Dipl.-Ing. Thomas Beumler for the industry-input into this thesis and the fact that he and Mathias Renner took the time to discuss whether my work suits their needs. I am also grateful to Dr. Greg Wilson for his patience with me and answering my numerous questions. I also thank John-Alan Pascoe, M.Sc. and Dr. Sharif Khan for their help with my code.

Of course I thank my friends, family and Maria for their love, support and at times much needed distraction, especially Sjors, Erik, Rik, Mattia, Birol, Yasser, Lorenz, Mark and Noud have greatly helped me by being so kind to discuss my ideas with me. Without all the help I have received throughout my thesis I would not have come to this great result.

Delft, June 14, 2013

S.W.F. Spronk

Summary

The most highly loaded frames of the newly developed Airbus A400M transport aircraft have glass reinforced aluminium laminate (Glare) straps attached to them to increase their resistance to fatigue damage. These straps were designed using static strength requirements for the frame. Basic justification was done in two steps. Firstly, the frame load was divided between frame and flange on the basis of in-plane stiffness of these parts. Secondly, a fatigue analysis was performed on the strap using an empirical model for fatigue of Glare laminates under tension.

This report contains a thorough explanation of the development of a code which can be used to analyse the fatigue crack initiation and propagation characteristics of the combination of frame flange and Glare strap at once under variable amplitude loading. The choice was made for a modular implementation of a combination of analytical models. This allows the programme to analyse a large variety of cases and allows it to be adapted easily in the case it is decided to continue its development.

The fatigue crack initiation model works in three stages. First, it computes the highest stress cycle occurring in the metal sheets of the laminate, second, it corrects this cycle to match the available SN-data, and third, it finds the corresponding cycles to initiation using the nearest matching SN-curve. Fatigue crack growth calculations are based on an analytical model which applies displacement compatibility at the delamination boundary, to solve for the crack tip stress intensity and subsequently calculate crack- and delamination growth characteristics. These displacements originate from four phenomena. One, the crack opens due to far-field stress in the metal layers. Two, there is also a crack opening effect because of the release of residual stress due to crack- and delamination growth. Three, crack closing occurs due to the bridging effect of the fibre layers. Four, the fibre layers elongate and deform due to the bridging load they sustain. The influence of variable amplitude loading on the laminate is taken into account by implementing the Wheeler yield zone model.

Correct working of the code was verified by assessing whether the modules produced results equal to the codes they were based upon. The parts of the code that were made from scratch were verified by checking whether these parts reacted to input parameter changes in a way that matched expectations. Validation with a variety of test results proved that all the modules and combinations thereof produce results which corresponded to the experiments.

The code that was developed for the research described in this report was used to evaluate Airbus' method of justification of their design of the Glare reinforced frame. It was shown

that the method of justification is unconservative, which is likely due to the assumption that the load through the flange is redistributed to the strap.

A study on ways to improve the design of the Glare reinforced frame flange showed, that the performance of the Glare-reinforced frame flange could be improved by increasing the amount of fibre layer in the cross section relative to the amount of metal.

Table of Contents

Summary	iii
Glossary	ix
List of Acronyms	ix
List of Symbols	ix
1 Introduction	1
2 Definitions	3
2-1 Stress	3
2-2 Dimensions	4
2-3 Coordinate system	4
2-4 Layer terminology	5
2-5 Decimal mark	5
3 Current frame reinforcement design	7
3-1 A400M	7
3-2 Current reinforcement analysis method	9
3-3 Need for a better analysis method	10
3-4 Summary	11
4 Fatigue in fibre metal laminates	13
4-1 Fatigue in general	13
4-1-1 Initiation	15
4-1-2 Crack propagation	15
4-1-3 Variable amplitude	16
4-2 Fibre metal laminates	17
4-3 Fatigue in fibre metal laminates	18
4-3-1 Initiation in fibre metal laminates	18
4-3-2 Crack propagation and delamination growth in fibre metal laminates	20
4-4 Summary	21

5	Program requirements and current solution methods	23
5-1	Introduction	23
5-2	Requirements for the tool	24
5-2-1	Requirements connected to the research question	24
5-2-2	Implementation-related requirements	24
5-2-3	Requirements by Airbus	25
5-3	Current solution methods for fatigue in fibre metal laminates	25
5-4	Required additions to the existing solution methods	26
5-5	Summary	26
6	Solution method for a complete tool	27
6-1	Introduction	28
6-1-1	General assumptions	28
6-2	Static strength	31
6-2-1	Goal	31
6-2-2	Requirements	31
6-2-3	Additional assumptions	31
6-2-4	Method	31
6-3	Fatigue crack initiation	33
6-3-1	Goal	33
6-3-2	Requirements	33
6-3-3	Additional assumptions	33
6-3-4	Method	34
6-4	Constant amplitude fatigue crack propagation	39
6-4-1	Goal	39
6-4-2	Requirements	39
6-4-3	Additional assumptions	39
6-4-4	Method for standard Glare	41
6-4-5	Method for general FMLs	45
6-5	Variable amplitude fatigue crack propagation	49
6-5-1	Goals	49
6-5-2	Requirements	49
6-5-3	Additional assumptions	49
6-5-4	Method for both the Alderliesten and the Wilson model	50
6-6	Summary	53

7	Verification and validation	55
7-1	Introduction	55
7-2	Verification of tool components	56
7-2-1	Static strength	56
7-2-2	Initiation	57
7-2-3	Crack propagation in standard Glare	58
7-2-4	Crack propagation in general FMLs	61
7-2-5	Crack propagation under variable amplitude	63
7-3	Validation of individual modules	66
7-3-1	Static strength estimation	66
7-3-2	Initiation	67
7-3-3	Crack propagation in standard Glare	69
7-3-4	Crack propagation in general FMLs	71
7-3-5	Crack propagation under variable amplitude	74
7-4	Validation of combinations of modules	74
7-4-1	Constant amplitude FCI and FCP	75
7-4-2	Variable amplitude FCI and FCP	77
7-5	The influence of run parameters	78
7-6	Limits of validity	79
7-7	Summary	81
8	Using the model for renewed reinforcement design	83
8-1	Introduction	83
8-2	Evaluation of current design	83
8-3	Reinforced frame design improvement	88
8-3-1	Constraints	89
8-3-2	Variables	89
8-3-3	Room for improvement	89
8-4	Summary	92
9	Evaluation	97
9-1	Complying to the requirements	97
9-2	Recommendations	98
10	Conclusion	101
A	Classical laminate theory	107
A-1	Assumptions	107
A-2	Solution method	108
A-3	Thermal stress	111

Glossary

List of Acronyms

ARALL	Aramid reinforced aluminium laminate
CA	Constant amplitude
CCT	Centre crack tension
CFRP	Carbon fibre reinforced plastic
CLT	Classical laminate theory
COD	Crack opening displacement
CTE	Coefficient of thermal expansion
FCG	Fatigue crack growth (= FCP)
FCI	Fatigue crack initiation
FCP	Fatigue crack propagation (= FCG)
FEA	Finite element analysis
FEM	Finite element method
FML	Fibre metal laminate
GFRP	Glass fibre reinforced polymer
Glare	Glass reinforced aluminium laminate
LEFM	Linear elastic fracture mechanics
L-T	Loading in longitudinal, cracking in long transverse direction
L-S	Loading in longitudinal, cracking in short transverse direction
MSD	Multiple site damage
OL	Overload
RS	Residual strength
SERR	Strain energy release rate
SIF	Stress intensity factor
T-S	Loading in long transverse, cracking in short transverse direction
UD	Uni-directional
VA	Variable amplitude

List of Symbols

Greek Symbols

α	Coefficient of thermal expansion [$^{\circ}\text{C}$]
β	Dimensionless geometry factor
ΔK	Stress intensity ratio [$\text{MPa}\sqrt{\text{mm}}$]
ΔK_{eff}	Effective stress intensity ratio [$\text{MPa}\sqrt{\text{mm}}$]
ε	Normal strain [-]
γ	Shear strain [-]
κ	Curvature [$1/\text{mm}$]
ν	Poisson's ratio [-]
σ	Local stress in material [MPa]
τ	Shear stress [MPa]
θ	Ply rotation [degrees]

Latin Symbols

a	Crack length [mm]
b	Delamination length [mm]
\mathbf{C}	Ply plane stress compliance matrix
C_1	Weibull parameter [MPa]
C_2	Weibull parameter [MPa]
C_3	Weibull parameter [-]
C_4	Weibull parameter [-]
C_{cg}	Paris crack growth coefficient, related to $\frac{da}{dN}$ in [mm/cycle] and to ΔK in [$\text{MPa}\sqrt{\text{mm}}$]
C_{M_x}	Line moment factor: $M_x = C_{M_x} F_S$ [N]
C_{N_x}	Line load factor: $N_x = C_{N_x} F_S$ [N/mm]
C_p	Wheeler retardation parameter [-]
D	Hole diameter [mm]
f	SCF mismatch correction factor [-]
F_S	Applied load factor [-]
F_{Su}	Static strength load factor [-]
K	Stress intensity factor [$\text{MPa}\sqrt{\text{m}}$]
K_t	Stress concentration factor [-]
K_t	Stress concentration factor [-]
m	Wheeler model exponent [-]
M_x	Line moment in x -direction [N]
n_{cg}	Paris crack growth exponent, related to $\frac{da}{dN}$ in [mm/cycle] and to ΔK in [$\text{MPa}\sqrt{\text{mm}}$]

N_f	Number of cycles to failure (Fatigue life) [cycles]
N_i	Number of cycles to initiation (Fatigue initiation life) [cycles]
N_x	Line load in x -direction [N/mm]
\mathbf{Q}	Ply plane stress stiffness matrix
$\overline{\mathbf{Q}}$	Rotated plane stress stiffness matrix ($= \mathbf{T}_1^{-1} \mathbf{Q} \mathbf{T}_2$)
R	Stress (intensity) ratio [-]
r_p	Plastic zone radius [mm]
s	Starter notch length [mm]
S	Nominally applied stress [MPa]
S_a	Stress amplitude [MPa]
S_f	Fatigue limit [MPa]
S_m	Mean stress [MPa]
S_N	Fatigue strength at fatigue life N [MPa]
$S_{u,ci}$	Ultimate compressive strength in direction i [MPa]
$S_{u,s}$	Ultimate in-plane shear strength [MPa]
$S_{u,ti}$	Ultimate tensile strength in direction i [MPa]
S_y	Yield stress [MPa]
t	Thickness [mm]
\mathbf{T}_1	Stress rotation matrix
\mathbf{T}_2	Strain rotation matrix
W	Specimen width [mm]
w	Element width [mm]
y	Global or laminate y -coordinate [mm]
z	Global or laminate z -coordinate [mm]

Subscripts

12	In the 12-plane
1	The ply 1-direction (parallel with the fibres)
2	The ply 2-direction (in-plane and orthogonal to fibres)
0	Initial value
active	The value belongs to a laminate composed of only the layers specified by the user
Al	The value belongs to monolithic aluminium
br	The quantity is related to the bridging phenomenon
complete	The value belongs to the complete laminate
eff	The effective value, corrected to account for crack closure
FML	The value belongs to an FML
FW	The effect of finite width is taken into account
i	The value belongs to crack element i
k	The value belongs to layer k

model	The quantity is a model output
nom	Nominal value, i.e. in the absence of concentrating effect
OL	The value belongs to an overload cycle
peak	Peak value due to concentration
pp	The quantity is related to a prepreg layer, or fibre layer
$S_{m=0}$	Value at zero mean stress
test	The quantity is obtained from test results
tip	The quantity refers to the situation at the crack tip
xy	In the laminate or global xy -plane
x	The laminate or global x -direction
y	The laminate or global y -direction

Superscripts

\circ	Midplane value
max	The value at maximum applied load
mech	Mechanical value, i.e. solely due to applied load
min	The value at minimum applied load
res	Residual stress value
t	The quantity is due to thermal expansion or contraction

Chapter 1

Introduction

Aircraft are designed to be as light as possible to maximise performance. Parts are designed to last only slightly longer than their anticipated service life and are thus as thin as possible to reduce the amount of non-essential weight that is carried on the aircraft to a minimum. This has as a result that the stress levels in the parts are high compared to thicker parts, which causes fatigue cracks of significant length to appear throughout an airframe.

A current solution to tackle excessive fatigue crack growth in some frames of the Airbus A400M military transport aircraft, displayed on the cover of this report, is to apply a hybrid structure solution to the six frames that carry the wing loads and thus endure repetitive loading of a large stress amplitude. The solution consists of adhering a strip of glass reinforced aluminium laminate, or Glare, to the flange of these frames. The fibre layers in Glare have the tendency to bridge cracks resulting from fatigue loading in the metal layers because the fibres are not damaged due to this type of loading.

All aviation authorities require that a design is proven to work well before an aircraft is certified and allowed to take off. Airbus has decided to design and certify the A400M to both civil and military standards, and both standards require Airbus to justify the design of the reinforcement. The available design methods used for the Glare reinforced frame design did not allow any optimization at the time. The design definition was mainly related to residual strength requirements, and the local interaction between the aluminium in a fatigued condition and the Glare could not be predicted. The aircraft justification, however, was performed by a sequence of tests, from coupon to full scale, proving the design is airworthy.

The goal of the research reported in this thesis is to assess the accuracy of the method used for the design for the A400M Glare strap frame reinforcement and determine whether there is room for improving the current design. This is done by developing a tool that can analyse fatigue crack initiation and propagation due to variable amplitude loading of general fibre metal laminates. An analytical tool is developed, because of its potential to be widely applicable, and a wide applicability is preferred, because the underlying goal of the work presented in this thesis is to create a framework which can become the basis of a complete fatigue and damage tolerance toolbox for fibre metal laminates. A framework like this allows

the past and future results of related researches to be bundled into a single solution, which is much more efficient than having a separate dedicated analysis tool for each type of problem.

The problem is tackled as follows. Quantities used throughout the research are defined in chapter 2, so it is fully clear to the reader what they exactly mean. Chapter 3 contains an explanation of the current design method and a definition of what is exactly needed by Airbus. The occurring phenomena are outlined in chapter 4: what is fatigue, what is a fibre metal laminate and what happens when both are combined? Subsequently, in chapter 5, all the requirements that exist for the to-be-developed tool are outlined and the existing models are discussed, after which a choice for model type is made. It is explained in detail how all aspects of fatigue in fibre metal laminates are incorporated into the tool in chapter 6. Chapter 7 contains the description and results of how the tool is verified and validated to ensure it works well. The next step is to actually use the model to find out whether the current design method is accurate and whether there is room for improvement, this is explained in chapter 8. The tool is evaluated on the basis of the requirements in chapter 9. Finally, in chapter 10, the conclusion is drawn whether the goal as set above was met.

Chapter 2

Definitions

Definitions of the several forms of stress and of notch- and crack length are given in this chapter, to make the use and meaning of these quantities clear to the reader. The coordinate system, some basic dimensions, and laminate terminology that are used in this report are also defined.

2-1 Stress

The symbol S is used to denote the nominally applied stress and the symbol σ to denote the local stress throughout this report, following the definitions of Schijve (2009). Subscripts can be used to specify S further, but they will always refer to a quantity that is averaged over the cross-sectional surface the stress acts on. The difference between the two types of stress is illustrated in figure 2-1a.

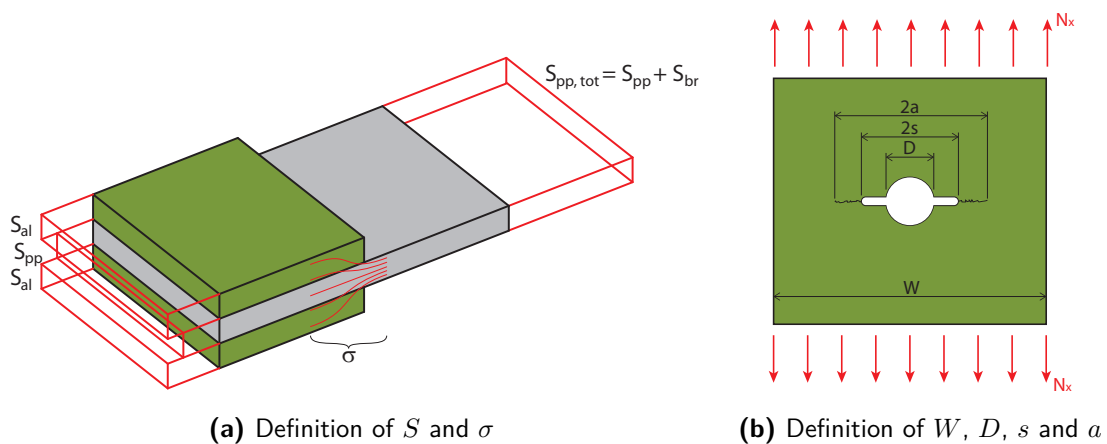


Figure 2-1

2-2 Dimensions

The width of the test specimen W is defined perpendicular to the loading direction, as are the crack length a and the notch length s , see figure 2-1b, where the hole diameter D is also indicated.

2-3 Coordinate system

The coordinate systems used throughout the report are as follows, see also figure 2-2: in general, the x -direction is parallel to the longitudinal direction of the laminate, which in this report also corresponds to the loading direction. The y -direction is the long transverse direction, perpendicular to the x -direction, pointing to the right when looking at the top of the laminate. The z -axis then points downwards to complete the right-handed coordinate system. A positive line moment M_x rotates in the positive y -direction, again according to the right-hand rule, on the face where the normal vector is pointing in the direction of positive x . The positive directions of N_x and M_x are also indicated in the figure. There is a local crack and delamination coordinate system for each ply, which is two-dimensional as any variation in the thickness direction within a ply is assumed to be absent. This coordinate system has axes a and b for crack- and delamination length, respectively. The a -axis of each layer is parallel to the y -axis of the laminate and the b -axis is parallel to the x -axis. The original Alderliesten and Wilson models use a coordinate system in which the x -axis is along the crack and the y -axis in loading direction (Alderliesten, 2005; Wilson, 2013). This system is not used here, because it would imply that 0° plies are perpendicular to the main loading direction, as the ply rotation angle is defined between the 1-axis of a ply and the x -axis of a laminate (Kassapoglou, 2010). In this report, the x -axis, main loading direction and 0° orientation are all aligned.

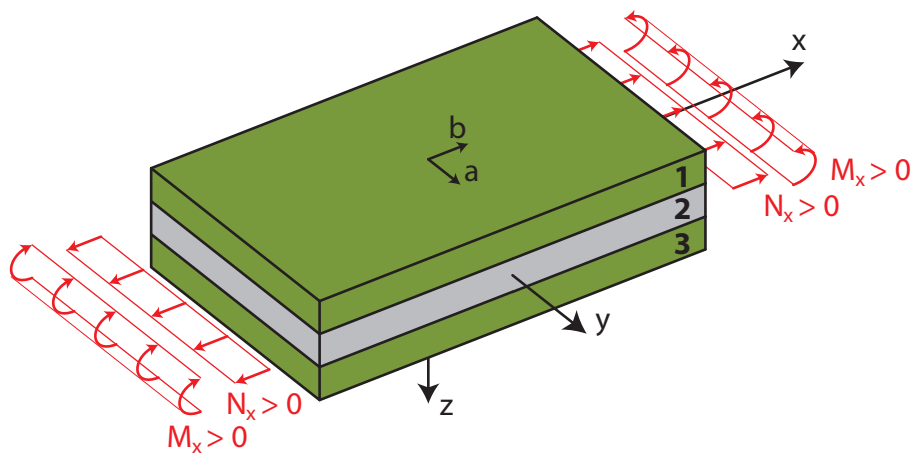


Figure 2-2. Coordinate systems definition

2-4 Layer terminology

Whenever the term 'ply' is used in this report, the author refers to a single sheet of unidirectional prepreg material or a single sheet of metal. Whenever the term 'layer' is written, the author refers to a collection of adjacent plies formed of the same material. A Glare 3 fibre layer thus consists of two fibre plies stacked with a 90 degree orientation difference, see also table 4-1. Even though the term 'prepreg' does not indicate the presence of cured resin and the term 'fibre' does not indicate the presence of any resin at all, both terms are used here to refer to a cured fibre-reinforced plastic material.

2-5 Decimal mark

A full stop is used as decimal mark in this report.

Current frame reinforcement design

- 3-1 A400M
- 3-2 Current reinforcement analysis method
- 3-3 Need for a better analysis method
- 3-4 Summary

3-1 A400M

With numerous transport aircraft in the various fleets of the European NATO nations nearing the end of their service lives, there is a need for a replacement. The Airbus A400M multirole turboprop should be the ideal candidate to replace these aircraft. It outperforms the C-130 Hercules and C-160 Transall aircraft, which will reach the end of their service lives soon, in practically all areas (Airbus Military, 2012).

The A400M has to last at least 10000 flight cycles, or about 30000 flight hours. In doing this, the inner flange of the frame below the rear wing attachment, see figure 3-2, has to endure a combination of both high fatigue loads and severe static tensile loads. To cope with the latter, the frame is manufactured from a high strength alloy, the high fatigue loads are dealt with by reinforcing the high-strength frame using a Glare strap attached to the inner flange, see figure 3-3. The type of Glare used is Glare 2A, because practically the only loads that will be dealt with in this situation are in longitudinal direction. This is a relatively light and cost-effective solution, which significantly increases the fatigue life of the aircraft and thus reduces the required of inspection frequency, compared to when a monolithic variant of the frame is used (Plokker et al., 2009a).

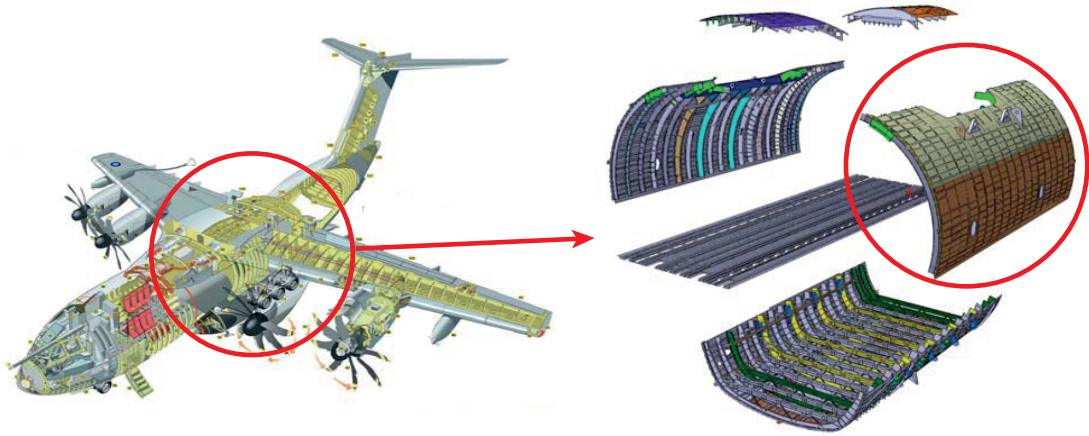


Figure 3-1. The Airbus A400M and its centre fuselage panels (Courtesy Airbus Military)

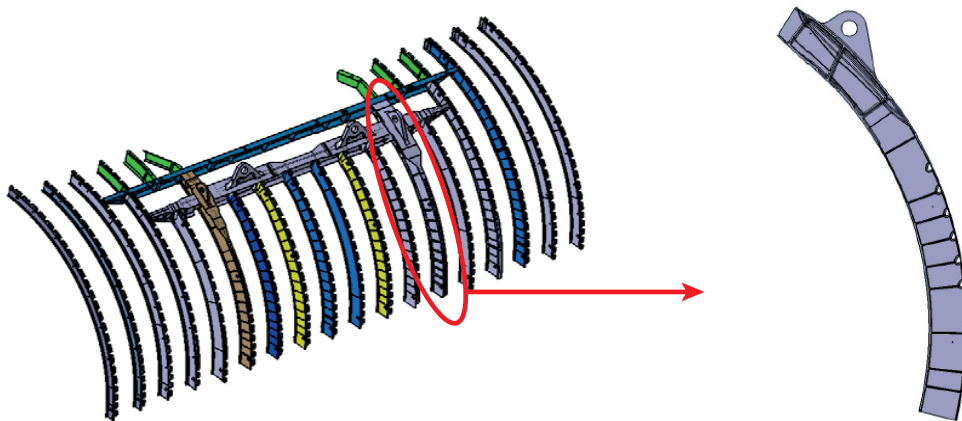


Figure 3-2. The frames of the A400M centre upper fuselage panel, see figure 3-1, and the rear wing attachment frame (Courtesy Airbus Military)

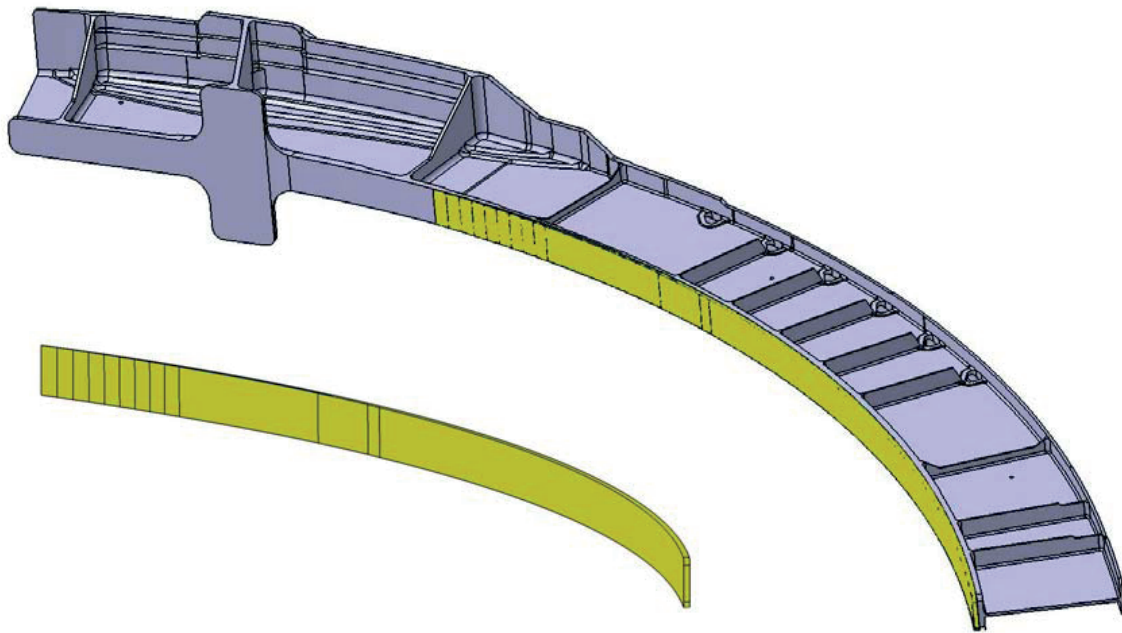


Figure 3-3. The A400M rear wing attachment frame, see figure 3-2, and the Glare strap (Courtesy Airbus Military)

3-2 Current reinforcement analysis method

The design of the Glare straps used to reinforce the rear wing attachment frame is based largely on the residual strength requirements for the frame. This is done by assuming the aluminium flange is fully cracked and the thickness of the intact Glare strap is then taken such that it can cope with the maximum static load, i.e. limit load, that the flange will endure during its lifetime. A thickness ratio of two-thirds Glare and one-third flange thickness was taken and proven sufficient with this method (Plokker et al., 2009b).

A fatigue and damage tolerance analysis was performed to predict the inspection threshold and the inspection interval for the defined design. To this end, representative load spectra were produced equivalent to 10000 flights of the aircraft. The stress levels that the spectrum produces in the reinforced frame were split on the basis of the in-plane stiffness in x -direction of the flange and the strap (Th. Beumler, personal communication, April 4th, 2013). The Glare strap is then analysed to find the crack growth characteristics due to this adapted load spectrum by running an empirical model from the FML F&DT Toolbox (Airbus S.A.S., 2007). The model was run with a Glare 3-12/11-0.4 laminate to simulate solely loading on the reinforcement, because the FML F&DT Toolbox is neither capable of analysing Glare 2 nor asymmetric laminates (Th. Beumler, personal communication, April 4th, 2013).

Residual strength capability was calculated using the Müller method, or metal volume fraction method, which predicts the residual strength on the basis of pristine blunt notch strength minus the blunt notch strength that the damaged material would otherwise have provided (Airbus S.A.S., 2007). It was established that a through crack of 11 [mm] is the maximum

crack length allowed in the reinforcement, if the reinforcement were still able to carry limit load (Th. Beumler, personal communication, April 4th, 2013).

Applying a spectrum that consists of all the cycles the part is assumed to endure during one service life, resulted in the empirical model from the FML F&DT Toolbox calculating a crack length of 1.28 [mm], starting from an initiated crack length of 1 [mm]. The model also predicted that the entire spectrum could be applied almost two more times until the critical crack length was surpassed (Th. Beumler, personal communication, April 4th, 2013).

Constant amplitude tests have also been done on a Glare 2A laminate adhered and bolted to a monolithic plate, where general values for cycles to initiation, crack growth properties and the static strength value have been found that are not specific to the frame under consideration in this research (Klein, 2011). The possibility of failure as a result of the strap delaminating from the frame has been ruled out using a finite element analysis which showed that even an extreme delamination size does not result in large delamination growth (Witasse et al., 2007).

3-3 Need for a better analysis method

There are uncertainties connected to the analysis described in the previous section. The analysis could be overly conservative because of three reasons. One, the crack growth analysis was done on a Glare 3 strap rather than the longitudinally stronger Glare 2A. Two, rather than analysing how many cycles would be needed to reach a crack length of 1 millimetre, a crack of this size was assumed to be present in the structure before the application of the first load cycle. Three, any possible growth retardation effect that severe load cycles might have on light ones is neglected. Non-conservative choices were also made in the research, which include the assumptions that neither a possibly very large crack in the monolithic flange nor a possible internal moment affect the crack growth rate in the strap.

Airbus, like any other aircraft manufacturer, needs to make sure that every part will function as intended during its whole service life, and that not too much structural mass is added to an aircraft, which would result in an inadequate overall aircraft performance. Currently (2013), there is a lack of proper tools at Airbus that can be used to analyse Glare reinforced frames and to ensure the design is durable but not overly conservative.

Although proof of the cycles to failure should ultimately always be given by tests, the amount of tests, and thus total cost of these in a design situation, can be significantly reduced by using properly validated design tools. Even though the validation of such a tool would require tests of its own, it can give a designer the ability to skip sub-component and component level testing phases in some cases, without compromising the adequacy of their design, thus saving a significant amount of time, effort and money that would otherwise be required to carry out these tests. The same advantages exist in the fact that a design tool allows the designer to explore the influence of design changes on the performance of the design, again without the need for a testing programme as large as would be required without the tool.

A design tool is thus needed that can provide a more accurate insight into whether the fatigue life of the reinforced frame under the severest circumstances is long enough to meet the required service life than the current analysis method. As a whole, the Glare strap attached to a monolithic plate can be regarded as a fibre metal laminate in itself, with one thick metal layer on the outside. The aforementioned goal thus requires the tool to be

capable of calculating the fatigue crack initiation and fatigue crack propagation properties of a general fibre metal laminate under variable amplitude tension/bending loading, where the word general indicates that its layers can be of different thickness. A tool that can perform as described above can be used to answer the question of whether the method used to calculate the cycles to failure for the Glare reinforced frame is accurate or not, and to determine if there is room to improve the current design to produce an even lighter and/or longer lasting solution for the Glare reinforced frame.

3-4 Summary

It has been established that the current way of design for the Glare reinforcement for the A400M rear wing attachment frame does not give a certain result, which leads to the goal of the research discussed in this thesis: to assess the accuracy of the method used for the design for the A400M Glare strap frame reinforcement and determine whether there is room to improve the current design, by developing a tool that can be used to analyse fatigue crack initiation and propagation resulting from variable amplitude loading of general fibre metal laminates.

Fatigue in fibre metal laminates

4-1 Fatigue in general

4-1-1 Initiation

4-1-2 Crack propagation

4-1-3 Variable amplitude

4-2 Fibre metal laminates

4-3 Fatigue in fibre metal laminates

4-3-1 Initiation in fibre metal laminates

4-3-2 Crack propagation and delamination growth in fibre metal laminates

4-4 Summary

4-1 Fatigue in general

Ever since the first scientific descriptions of fatigue in the nineteenth century, fatigue has been a failure mode that has widely intrigued engineers in various disciplines (Schütz, 1996). It was August Wöhler in 1870 who first described how a repetition of a load far below the static strength of a structure could induce complete failure of that structure (Schijve, 2009), and his knowledge has been applied in train engineering and other fields all around the world. As soon as aircraft started to fly high enough to create a need for pressurised aluminium fuselages, fatigue problems started to cause problems in aviation, an early and notorious example being the catastrophic explosions of two De Havilland Comet fuselages in 1954.

A stress cycle has several characteristic properties, see figure 4-1. These properties are the mean stress S_m , the stress amplitude S_a , the maximum stress S^{\max} , the minimum stress S^{\min} and the stress ratio:

$$R = \frac{S^{\min}}{S^{\max}} \quad (4-1)$$

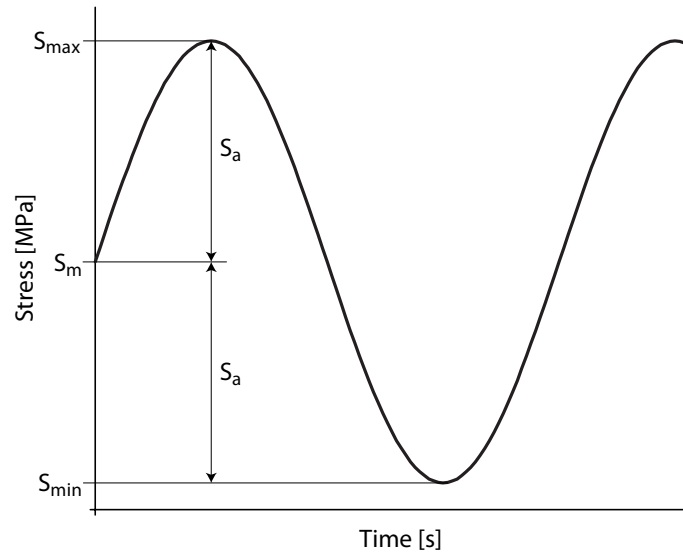


Figure 4-1. Characteristics of a load cycle

however, only two of these quantities are needed to fully define a stress cycle.

When the stress amplitude is high enough, although (much) lower than the static strength, a material can only sustain a finite number of cycles N until it fails. Below a certain stress level S_f , termed the fatigue limit, no damage is done and thus theoretically, an infinite amount of cycles can be applied to the material. Practically, phenomena like corrosion and abrasion constrain the amount of stress cycles to a finite number.

Both S_a and S_m reduce the fatigue life of a specimen when increased. Although the effect of the stress amplitude is much more pronounced than that of the mean stress, the influence of the latter should not be neglected. The decrease in fatigue strength S_N at fatigue life N due to S_m is usually described by the Gerber parabola:

$$\frac{S_N}{(S_N)_{S_m=0}} = 1 - \left(\frac{S_m}{S_{u,t1}} \right)^2 \quad (4-2)$$

or the modified Goodman relation:

$$\frac{S_N}{(S_N)_{S_m=0}} = 1 - \frac{S_m}{S_{u,t1}} \quad (4-3)$$

where $S_{u,t1}$ stands for the ultimate tensile stress in material 1-direction, and it is thus assumed that the fatigue load is also in the material 1-direction. It should be noted that these formulae only account for a tensile mean stress.

The modified Goodman relation of equation 4-3 is used in this research because it is generally a conservative approximation of the mean stress effect (Schijve, 2009).

The fatigue life of an object can be split into two distinctive phases: the initiation phase and the crack propagation phase. Some details of both phases are given below, based on the elaborate description of all aspects of fatigue that can be found in Schijve (2009).

4-1-1 Initiation

The initiation phase is the first part of the fatigue life, in which fatigue cracks emerge from a, seemingly, crack-free stressed object until these cracks have acquired a predefined crack length. Fatigue crack initiation (FCI) results from cyclic slipping of atoms in the crystal structure of the fatigued part, which occurs in practically any repetitively loaded situation. Fatigue crack initiation occurs at a very small scale, so even the tiniest of surface defects can cause a large reduction in the number of cycles required to reach a certain (microscopic) crack length, compared to the case where the surface is polished to perfection. Accurate fatigue initiation predictions are therefore very difficult to make.

The stress field causing the atoms at the surface of a part to slip is rarely homogeneous because parts rarely have straight shapes. Inhomogeneities in a stress field are usually described using the stress concentration factor (SCF) K_t . The SCF is the quotient of the peak stress with the nominal stress, of which the latter is the stress in cases where there is no concentration. Every geometry has a different amount of stress concentration, and the K_t -value therefore is usually obtained using handbooks like Peterson's Stress Concentration Factors (Pilkey and Pilkey, 2008). A larger SCF results in a smaller amount of cycles to crack initiation, due to the higher stress values experienced locally in the material.

4-1-2 Crack propagation

The crack propagation phase, or crack growth phase, starts when the micro crack growth no longer depends on the material surface conditions but rather on the material as a bulk property. This transition is impossible to pinpoint exactly, but is usually defined as a specific crack length in the order of a single millimetre or just below. (Alderliesten, 2009)

The stress intensity factor K has to be used during crack growth, because K_t is infinitely large for a geometry with a radius as small as a crack tip. The stress intensity factor is defined as:

$$K = \beta S \sqrt{\pi a} \quad (4-4)$$

where β is a dimensionless factor depending on the geometry of the structure, S is the remote loading stress and a is the crack length, or the half length from one crack tip to the other in case of a centre crack. The stress intensity is proportional to the stress, so the stress ratio R can also be written as K^{\min}/K^{\max} .

The stress fields for various configurations have been published in books like The Stress Analysis of Cracks Handbook (Tada et al., 2000). In contrast to K_t , which just depends on the geometry, the stress intensity factor K depends on both the geometry and the applied stress and usually carries the unit of $\text{MPa}\sqrt{\text{m}}$. The stress intensity factor is determined by solving analytically the stress field around a crack using linear-elastic stress analysis. Superposition of stress fields is thus allowed, because of the linear-elastic nature of the analysis. The stress intensity functions obtained are only asymptotically correct towards the crack tip, which comprises an area with much smaller dimensions than the crack length a . The plasticity region should again be much smaller, because then this plastic zone is confined within a larger elastic stress field and does not interfere significantly with the validity of the linear-elastic analysis, and, because the boundary of the plastic zone is fully encompassed in an elastic stress field and the influence on the latter is limited to a small region, the same plastic

field will occur in another specimen with a similar elastic field. This allows for a similarity concept to be applied to compare different cases to each other.

Fatigue crack propagation (FCP) in materials tends to behave according to a power law, called the Paris relation, when the stress intensity ratio ΔK is not too small or too large:

$$\frac{da}{dN} = C_{cg}(\Delta K)^{n_{cg}} \quad (4-5)$$

where C_{cg} and n_{cg} are material constants. Most cases of crack growth are said to experience some form of crack closure, changing the stress intensity ratio experienced by the crack tip. An effective stress intensity ratio ΔK_{eff} can then be used rather than ΔK , which takes this effect into account, this will be treated later.

4-1-3 Variable amplitude

The loads an aircraft experiences during its life are far from constant. The crack growth for cases with a non-constant amplitude cannot be computed by simply using equation 4-5. Fatigue life predictions for specimens under variable amplitude loads can be made using the very basic Miner rule. The Miner rule is based on the linear cumulative damage hypothesis, and states that when n_k cycles of a stress amplitude $S_{a,k}$ and corresponding cycles to failure N_k are applied, n_k/N_k of the fatigue life is consumed. So failure occurs when:

$$\sum_k \frac{n_k}{N_k} = 1 \quad (4-6)$$

The Miner rule has many shortcomings, for instance, it assumes that loads below the fatigue limit do not lead to growing damage, while in reality these loads are only incapable of initiating cracks but they could make existing cracks grow. The amount of damage at failure, moreover, is far from constant, because much larger cracks can be existing in a structure with relatively low loads compared to a structure that endures high loads.

The Miner rule also neglects a sequence effect. Tensile loads of a (much) higher amplitude relative to other cycles, termed overloads (OLs), cause more plastic deformation to occur in metal, which results in an excess of material around the crack in the specimen. Two effects are observed: one, the excess of material in the yield zone in front of the crack causes compressive stress, which results in a delay effect on the crack growth. Two, the increase in material volume in the wake of the crack, when the crack has grown beyond the yield zone of a previous OL, causes the crack to be closed while the specimen is still under tension, which reduces the portion of the stress cycle that is making the crack grow. The latter effect is termed plasticity induced crack closure (Alderliesten, 2011).

A simple model that includes some sequence effect is the Wheeler yield zone model (YZM). The Wheeler YZM takes the retarding effect of OLs into account by adding a retardation parameter to the Paris relation, which then becomes (Wheeler, 1970):

$$\frac{da}{dN} = C_p C_{cg} (\Delta K)^{n_{cg}} \quad (4-7)$$

where C_p depends on the plastic zone radius r_p and the crack length of the current cycle and of a high previous load, termed overload (OL): (Khan et al., 2010)

$$C_p = \left[\frac{r_{p,i}}{(a_{OL} + r_{p,OL}) - a_i} \right]^m \quad (4-8)$$

where the subscript OL denotes that the quantity belongs to an overload. The exponent m is to be obtained from fitting the model to test data, the plastic zone radius can be calculated using equation 4-9:

$$r_p = \frac{1}{\pi} \left(\frac{K}{S_y} \right)^2 \quad (4-9)$$

where S_y stands for the yield stress of the material, which is assumed to be equal in all directions.

4-2 Fibre metal laminates

Fokker started to bond sheets of aluminium together after the second world war in 1945, due to the absence of expensive milling machines in his factory. Using this technique, he had the solution in his hands to make fuselages lighter yet more fatigue resistant than their monolithic counterparts. Aluminium has a relatively long fatigue crack initiation phase and a short crack growth period, so, due to the fact that crack initiation has to take place for every single sheet in a laminated aluminium plate, the fatigue life of aluminium is greatly extended by bonding several sheets together instead of milling a part out of a monolithic block. Other beneficial effects are due to the smaller thickness of the sheets, which results in lower stress cycles and more plasticity induced crack growth delay (Schijve et al., 1979).

In the eighties it was found that introducing fibres into the bond between the aluminium sheets could increase the fatigue life even more (Marissen, 1980), a discovery that led to a patent for aramid reinforced aluminium laminate (Schijve et al., 1985), or ARALL, and later to a patent for glass reinforced aluminium laminate (Roebroeks and Vogelesang, 1987), or Glare, see figure 4-2. Fatigue crack growth does not occur in the glass fibre layers present in Glare, so even after a large amount of cycles the material still has load carrying capability. Aircraft with primary structures made out of Glare were flying within a decade of the invention (Vlot, 2001), and 2005 was the year of the maiden flight of the Airbus A380, the first aircraft with large portions of its fuselage made from Glare (Airbus S.A.S., 2012).

The power of fibre metal laminates (FMLs) is that the fibres in the laminate bridge fatigue cracks, see figure 4-3. This bridging means that load is still being transferred through the fibre layers, even if all the aluminium has cracked due to fatigue. The bridging of cracks results in slower crack growth rates than observed in monolithic counterparts, making the crack growth phase the most important phase of the fatigue life of parts produced from Glare. Another benefit of using Glare over aluminium, is that the observed growth rates of fatigue cracks in Glare are approximately constant for the majority of its fatigue life (Alderliesten and Vlot, 2001), making the remaining life much more straightforward to predict.

Glare typically consists of layers made of aluminium 2024-T3, and layers of S2-glass fibres in the FM94 adhesive system (Vlot and Gunnink, 2001). A Glare sheet is defined by a special

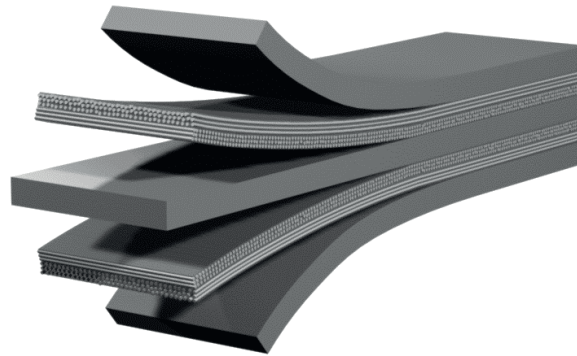


Figure 4-2. Typical layup for a cross-ply Glare laminate (Courtesy R.C. Alderliesten)

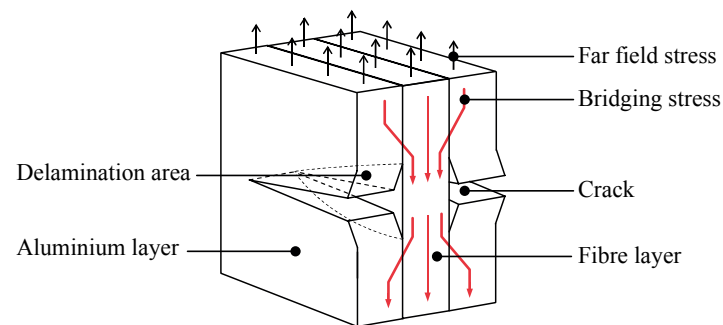


Figure 4-3. Stresses in an FML are bridged by the fibre layers (Courtesy R.C. Alderliesten)

coding system to distinguish between the several different lay-ups that are available. In this system, the layup shown in figure 4-2 is designated Glare 3-3/2-0.3. The first number in this code stands for the Glare grade, see table 4-1. The #/# stands for the number of aluminium and fibre layers, in this case there are three aluminium and two fibre layers in the plate. The last number, 0.3, stands for the thickness of the aluminium layers. The thickness of the glass layers is defined when selecting a certain glare grade. The properties of the aluminium and cured fibre layers can be found in tables 4-2 and 4-3.

4-3 Fatigue in fibre metal laminates

The layered structure of FMLs makes fatigue consideration more difficult than explained in section 4-1. The fibre layers are insensitive to fatigue and thus crack initiation and propagation are limited to the metallic layers. An added effect is the delamination of the prepreg layers from the aluminium layers, which results from the crack bridging phenomenon. The fibre layers can also act as barriers against cracks trying to grow through the thickness the material.

4-3-1 Initiation in fibre metal laminates

Homan (2006) described a relatively straightforward method for calculating FCI in FMLs: he states that a similar stress state in the aluminium layers of an FML compared to a monolithic

Table 4-1. Standard Glare grades (Vlot and Gunnink, 2001)

Glare grade	Subgrade	Metal sheet thickness [mm] & alloy	Prepreg orientation* in each fibre layer**	Main beneficial characteristics
Glare 1	-	0.3-0.4 7475-T761	0/0	fatigue, strength, yield stress
Glare 2	Glare 2A	0.2-0.5 2024-T3	0/0	fatigue, strength
	Glare 2B	0.2-0.5 2024-T3	90/90	fatigue, strength
Glare 3	-	0.2-0.5 2024-T3	0/90	fatigue, impact
	Glare 4A	0.2-0.5 2024-T3	0/90/0	fatigue, strength in 0° direction
Glare 4	Glare 4B	0.2-0.5 2024-T3	90/0/90	fatigue, strength in 90° direction
	-	0.2-0.5 2024-T3	0/90/90/0	impact
Glare 5	Glare 6A	0.2-0.5 2024-T3	+45/-45	shear, off-axis properties
	Glare 6B	0.2-0.5 2024-T3	-45/+45	shear, off-axis properties

* All aluminium rolling directions in standard laminates are in the same orientation; the rolling direction is defined as 0°, the transverse direction is defined as 90°

** The number of orientations in this column is equal to the number of prepreg layers (each nominally 0.133 mm thick) in each fibre layer

Table 4-2. Aluminium 2024-T3 Properties (Alderliesten, 2005)

Description	Value	
	L	LT
Young's modulus [MPa]	72400	
Strength at 4,7% strain [MPa]	420	420
Tensile yield strength [MPa]	347	299
Shear modulus [MPa]	27600	
Poisson's ratio [-]	0.33	
Coefficient of thermal expansion [1/°C]	$2.20 \cdot 10^{-5}$	

Table 4-3. Prepreg properties: S2-glass, FM-73 adhesive, BR-127 primer (Alderliesten, 2005)

Description	Value	
	L	LT
Ply thickness [mm]	0.133	
Young's modulus [MPa]	48900	5500
Shear modulus [MPa]	5550	
Poisson's ratio [-]	0.33	
Poisson's ratio [-]	0.0371	
Coefficient of thermal expansion [1/°C]	$6.1 \cdot 10^{-6}$	$26.2 \cdot 10^{-6}$
Curing temperature [°C]	120	

plate, leads to a similar initiation life. As soon as the occurring stress cycle in the metal layers has been computed using e.g. classical laminate theory (CLT), the fatigue initiation life of the FML can be estimated using standard SN-data of the metal alloy. The crack bridging effect of the fibres can still be neglected at this point, because the fibres are usually not yet effective in crack bridging for cracks with a length below a single millimetre (Alderliesten, 1999). Care should be taken not to neglect the effect of curing stress, because it can have a significant effect on the stress level in a layer.

Usually only the complete fatigue life is known for metals, rather than the crack initiation life. The complete fatigue life of the metal layers can, however, be assumed to be equal to the crack initiation life of those layers, since the fatigue life of monolithic aluminium consists largely of only the crack initiation phase due to very fast crack propagation (Homan, 2006). This assumption is relatively accurate if the initiation phase is assumed to end at a crack length of 1 millimetre (Alderliesten, 2009), and leads to the following conclusion:

$$(N_i)_{\text{FML}} = (N_i)_{\text{Al}} \approx (N_f)_{\text{Al}} \quad (4-10)$$

where N_i stands for the number of cycles to initiation and N_f for the number of cycles to failure, i.e. the fatigue life.

4-3-2 Crack propagation and delamination growth in fibre metal laminates

The crack propagation phase in FMLs is dominated by two phenomena: crack growth in the metal layers and delamination growth at the metal-prepreg interfaces. The former is an opening or mode I type of failure mode, while the latter is an in-plane shearing or mode II type of failure mode.

Standard equations for stress intensity of a mode I crack in metal as described by e.g. Tada et al. (2000) fail to describe the stress intensity at the crack tip for cracks in FMLs larger than 1 millimetre, because the prepreg layer now transfers load across the crack and thus cause a reduction of this stress intensity. A larger stress in the fibres will result in a lower crack growth rate because more load is transferred through the fibre layers rather than around the crack tip. The crack opening has thus also become a function of the prepreg layer deformation, fibre stretching and possibly metal layer shear deformation.

The shear stress between the bridging prepreg layers and the cracked metal layer causes a delamination to occur. The fact that the prepreg layers are delaminated from the surface of the metal layer, allows the fibres to stretch. A shorter delamination length leads to a larger load in the prepreg layers at a certain crack length, and thus to a higher delamination rate because the shear stress on the interface is also larger.

The above two paragraphs imply that crack propagation and delamination growth are balancing phenomena, which is confirmed by the relatively constant crack growth rates seen in FMLs (Marissen, 1988; Alderliesten, 2005). Large values of bridging stress will tend to drop, because they will lead to large delamination growth rates and small crack growth rates. Conversely, small bridging stress values will tend to rise because they result in small delamination growth rates but large crack growth rates.

4-4 Summary

The main conclusions to be drawn from the current chapter are that the required number cycles to initiate a crack is hard to predict accurately, that the cycles to initiation in FMLs can be computed by comparing the stress cycle in the metal layers with standard SN-data of the same metal, and that crack propagation in FMLs is governed by the balancing effect between crack- and delamination growth rate.

Program requirements and current solution methods

5-1 Introduction

5-2 Requirements for the tool

5-2-1 Requirements connected to the research question

5-2-2 Implementation-related requirements

5-2-3 Requirements by Airbus

5-3 Current solution methods for fatigue in fibre metal laminates

5-4 Required additions to the existing solution methods

5-5 Summary

5-1 Introduction

It is important to establish the boundaries of a problem before a solution is sought and implemented. The requirements possible future users of a tool that can calculate the cycles to failure due to fatigue of a fibre metal laminate (FML) are given in this chapter. An overview is provided of the methods which currently exist and which are possibly best suited to meeting parts of these requirements. This chapter is concluded with a discussion of what is still missing with respect to having a tool that fully suits the needs of the users, on the basis of those requirements that are not met when using the existing solutions.

5-2 Requirements for the tool

5-2-1 Requirements connected to the research question

The primary goal of the research reported here is to develop an effective tool that can be used by Airbus to help establish whether its Glare reinforced frame design for its A400M is sound. The clearly connected requirements are thus: the tool should be able to be used to calculate fatigue crack initiation (FCI) and propagation (FCP) due to variable amplitude (VA) loads in a Glare laminate attached to a monolithic plate. This ability will need to be validated in a test situation to ensure that the produced results match reality. These abilities need also to be connected, i.e. it should be possible to continue the propagation calculations once the initiation calculations have been finished, to get to a single answer in terms of cycles to a certain crack length.

It is pointless for an aircraft manufacturer to know the cycles to failure of a certain layer of a fibre metal laminate that is part of a structure, if it remains completely unknown whether the laminate could survive limit load without relying on the layer that has failed. A basic static strength estimation tool that can be used to, at least roughly, estimate the residual strength for parts of the laminate is therefore a minimum requirement. Incorporating a full residual strength model in the tool is not possible given the time available for the research reported here.

5-2-2 Implementation-related requirements

Requirements that are related to the implementation of the models into a programme are stated below.

- The tool needs to be as generally applicable as possible to maximise its usefulness for the aircraft manufacturing industry. All the capabilities of the calculation modules that are used should be exploited.
- It would be inefficient to have a separate program for each different but related type of analysis, considering the many closely related possible applications of the design tool, therefore effort is to be made to make the program as wide and easily expandable as reasonably possible.
- It should be clearly documented what the code calculates exactly if it is to be used for certification purposes.
- The tool should be as fast as possible, yet retain accuracy to allow for a fast design process, which means that simpler models should be included in the tool because they are generally faster to run than more advanced models. This will allow the tool to choose the simplest, optimum model for the specific case to hand.
- The idea is that the tool will eventually form the basis of a new Glare analysis platform for the Structural Integrity chair of the faculty of Aerospace Engineering of the TU Delft, so the code has to be written modularly, clearly, and with a sufficient amount of commenting, to allow future developers to understand the logic of the existing tool, verify the correct working of the code, and create expansions to it, if desired.

- The tool might also be used in an optimising scheme in the future, this will require the load input type to be independent of variables changed by the optimiser.

5-2-3 Requirements by Airbus

Airbus has made several very specific demands. The possibility to halt the crack growth code upon reaching a certain crack size should be built into the tool, so the load case can be updated. The source of these updated loads could be, for example, a finite element analysis. There should also be the possibility to add adhesive layers to the laminate and to use different types of materials for at least the metal layers within one laminate.

5-3 Current solution methods for fatigue in fibre metal laminates

A clear picture exists for FCI. The method by Homan, described in section 4-3-1, has proven to be accurate to predict the cycles until cracks are initiated in FMLs (Homan, 2006), and any method that tries to calculate crack initiation on the basis of the nominal laminate stress or an equivalent quantity, which is normally used to find the cycles to initiation for monolithic materials, would be inferior to the Homan method because the influence of the anisotropy and stiffness variation would not be accounted for. Thus, the Homan method is the only logical choice to calculate fatigue initiation in FMLs.

The situation is not so straightforward for fatigue crack propagation (FCP). Many different methods exist that can be used to describe it, because it is a much more difficult problem compared to the problem of describing crack initiation. Alderliesten (2007b) provided a detailed overview of all the relevant approaches available up to 2007 to describe constant amplitude (CA) FCP in standard Glare. In his paper he divided the various methods into finite element approaches, phenomenological methods and analytical models. The phenomenological methods were found to be incapable of describing FCP in FMLs, because they are too simple to describe the complex mechanisms that occur in the laminate during fatigue cracking. Alderliesten concluded that some of the available analytical and finite element approaches provide a reasonable answer and have great potential, but they were not yet sufficiently mature to provide an accurate answer in a variety of cases. Finite element methods have the added disadvantage over analytical models in that they are often only applicable to a very limited set of situations before the element layout has to be changed. Alderliesten (2007a) chose to develop an analytical approach.

The analytical model for crack growth in standard Glare due to CA load (Alderliesten, 2007a) is based on the models of Marissen (1988) and Guo and Wu (1998). It relies on the principle of superposition of two stress fields at the crack tip: one due to far field loads that cause the crack tip to open, and one due to the bridging of stress through the prepreg layers, which remain intact when fatigue loads are applied. It is subsequently ensured, on a discrete interval along the crack, that the displacement of the crack opening due to these two stress fields is compatible with the elongation of the fibre layers, to find the value of the bridging stress. The bridging stress is in turn used to calculate the stress intensity at the crack tip and the strain energy release rate of delamination, which can be related to the crack propagation rate and the delamination growth rate, respectively. This allows the use of an iterative solution

method to find the crack propagation over time as the growth rates can be used to calculate new crack and delamination lengths that form the basis of a new bridging stress computation.

Alderliesten's original model has been expanded in two ways that are of relevance to the requirements of the research described in this report. One, Khan (2013) has incorporated the model in a calculation that takes into account the effect severe load cycles have on following milder cycles using the Wheeler model, see also section 4-1-3, allowing VA load cases to be modeled with increased accuracy. Two, Wilson (2013) has taken the model to a general level by changing the formulation of bridging stress in the model by Alderliesten to a bridging line load at the delamination boundary and subsequently letting his model solve compatibility on each delamination boundary existing in the laminate under consideration. This expansion adds a large amount of generality to the model, which now allows a simulation of FMLs with varying layer thickness values, different materials per layer, adhesive layers and loading due to a moment.

5-4 Required additions to the existing solution methods

There is a difference between the capabilities of the available methods and what capabilities are required to analyse the Glare reinforced frame, see table 5-1. There are two notable additions that are required. One, the crack propagation model needs to be connected to the initiation model, and two, the VA model and the general FML model need to be combined.

Table 5-1. the available models with their capabilities and the required model

Existing models:				
Name	Type	Loading	Spectrum	Laminate
Homan	FCI	Tension/compression/moment	CA/VA	General FML
Alderliesten	FCP	Pure tension	CA	Standard Glare
Khan	FCP	Pure tension	CA/VA	Standard Glare
Wilson	FCP	Tension/moment	CA	General FML
Required model:				
	Type	Loading	Spectrum	Laminate
	FCI + FCP	Tension/moment	CA/VA	General FML

5-5 Summary

Homan's commonly used fatigue crack initiation model needs to be connected to a model formed from a combination of the VA FCP model by Khan and the model for FCP in general FMLs by Wilson to be able analyse the fatigue properties of a Glare reinforced frame flange.

Solution method for a complete tool

6-1 Introduction

6-1-1 General assumptions

6-2 Static strength

6-2-1 Goal

6-2-2 Requirements

6-2-3 Additional assumptions

6-2-4 Method

6-3 Fatigue crack initiation

6-3-1 Goal

6-3-2 Requirements

6-3-3 Additional assumptions

6-3-4 Method

6-4 Constant amplitude fatigue crack propagation

6-4-1 Goal

6-4-2 Requirements

6-4-3 Additional assumptions

6-4-4 Method for standard Glare

6-4-5 Method for general FMLs

6-5 Variable amplitude fatigue crack propagation

6-5-1 Goals

6-5-2 Requirements

6-5-3 Additional assumptions

6-5-4 Method for both the Alderliesten and the Wilson model

6-6 Summary

6-1 Introduction

The solution method per part of the problem is described in this chapter, i.e.: the goals, requirements, assumptions and method are explained for the static strength, fatigue crack initiation (FCI) and propagation modules, where for the latter two, standard and non-standard Glare, and constant amplitude (CA) and variable amplitude (VA) loading are considered.

6-1-1 General assumptions

Constructing a usable model that will exactly match reality is simply not possible. Simplifying assumptions have to be made in various parts of the analyses to enable the creation of a model that is both implementable and still sufficiently accurate. All the assumptions made during the creation of the tool are listed in this chapter to give the reader and user an idea of the limitations of the tool and its subroutines. This section contains assumptions that apply to the tool as a whole, which are listed below. An overview of the top-layer of the tool is given in figure 6-2. Each calculation module needs some additional assumptions, which can be found in the corresponding sections in which these modules are explained.

- Classical laminate theory (CLT) is assumed to be valid outside of delaminated regions, which implies the assumptions listed below, see also appendix A. (Kassapoglou, 2010; Gürdal and Kassapoglou, 2011)
 - All plies are considered thin relative to their width and length, which usually implies $t < 0.1W$. This assumption is made so the plies can be assumed to be in a state of plane stress, which means $\sigma_z = \tau_{yz} = \tau_{xz} = 0$ and thus free straining in the z -direction.
 - Every ply is assumed to be orthotropic, which means it contains two planes of symmetry.
 - The z -axes of all plies are aligned.
 - All plies are perfectly bonded to each other, which enforces strain compatibility throughout the laminate.
 - The Kirchhoff hypothesis is assumed to be valid, which means that all deformations of the laminate are a function of the mid-plane in-plane deformation, a rotation and a translation in z -direction. This implies that the z -coordinate does not change under deformation and that deformations thus need to remain small, and that a cross-section that was flat before deformation is still flat after deformation.
 - Out-of-plane loads on the laminate are considered negligible, even though the flange is attached to the web of a frame. If it is assumed that an I-beam only carries normal loads in the flanges and only shear load in the web, then, with the help of figure 6-1, it can be seen that for a small section of the frame, the only load that is introduced into the reinforced flange could be a shear force on its surface. This is an in-plane load, and thus the assumption that out-of-plane loads on the laminate are negligible seems plausible.

- Only a load and a moment in x -direction are applied, i.e. N_x and M_x , see also chapter 2. These loads are assumed to be in sync because, for the Glare reinforced frame, they have the same source, namely the wing of the A400M which is attached to the frame. These loads are thus assumed always to be a scalar multiple of each other, the value of which can be given as an input to the tool.
- The influence of transverse stresses in width or thickness direction of the laminate on the stress state in longitudinal direction are assumed to be negligible. There are, namely, no loads applied in transverse or thickness direction.
- Cut-outs are assumed to have a smooth surface and thus require FCI before propagation. They are also assumed to be of constant dimension through the thickness.
- If a hole is present in the laminate, it is considered to be an open hole. This means that interference stresses and bearing stresses are absent and that there is no load carrying capability across the hole.
- Any load introduction effects are ignored, so the applied load can be regarded as a uniform applied stress.
- The amount of out-of-plane bending is assumed to be negligible considering the thickness of the flange analysed, so secondary bending influences are assumed to be of insignificant influence, see also the end of section 8-2.
- All the curing cycles the laminate may have undergone are assumed to have the same elevated temperature, thus each layer can be regarded as experiencing the same temperature difference between curing and testing. This is confirmed for the case of the Glare reinforced frame (Th. Beumler, personal communication, May 7th, 2013).
- Any possible local stress raising effect of a cracked layer on the adjacent layers other than a global redistribution of stress is assumed to be negligible. This assumption implies that there is no equivalent of stress concentration or intensity factor in the thickness direction of the laminate. It stems from the assumption that the dimensions of a crack are assumed to be small compared to the in-plane dimensions of a cracked layer.
- Delamination is assumed only to occur as a result of metal layer cracking. The strap is assumed not to delaminate on its own e.g. as a result of the curvature of the frame being reduced by the load it carries. This assumption is supported by the results of an analysis by Witasse et al. (2007), which show that even a very large delamination does not result in excessive delamination growth.
- Buckling on any scale, i.e. global structural buckling, crippling of the flange or fibre buckling, as a result of compressive parts of a load cycle are not taken into account because the research focuses on the combination of crack- and delamination growth as a failure mode. This means highly compressive cycles might not be modelled correctly.

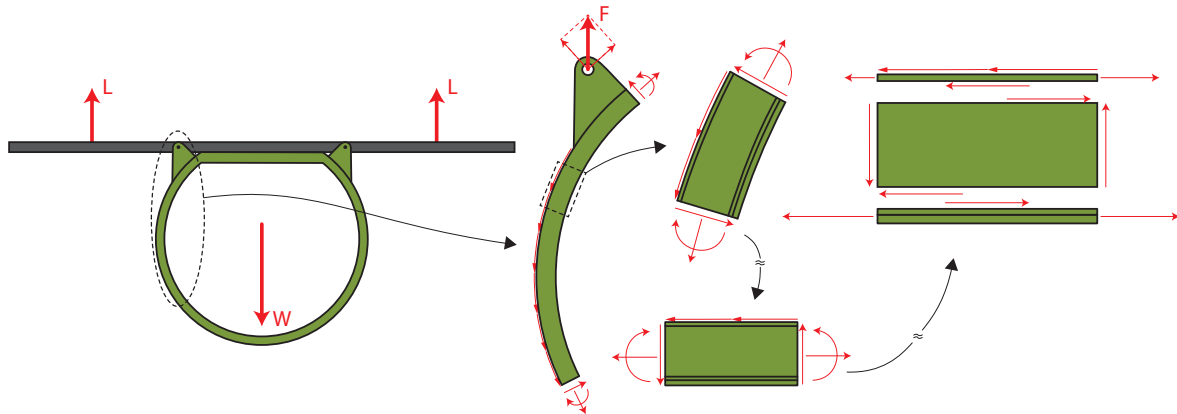


Figure 6-1. Simplifying a part of the frame onto which a wing is attached. The left figure is a schematic front view of the cross-section of the A400M. The figure to its right is a part of the frame that carries the wing loads, the figure to its right again a part. The figure below it is a rectangular simplification, the rightmost figure a blown-up version with simplified loads as well.

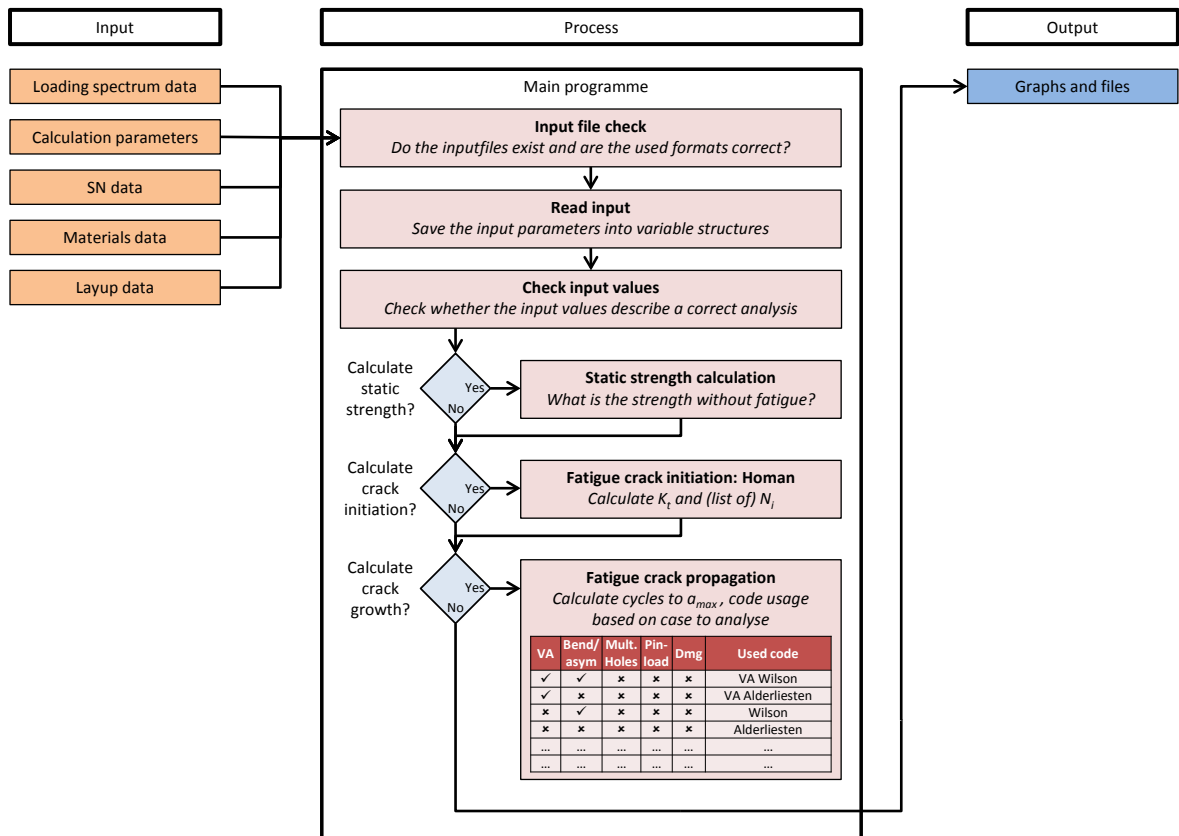


Figure 6-2. Overview of the top-layer of the code.

6-2 Static strength

6-2-1 Goal

The goal of the static strength module is to estimate the static strength of the fibre metal laminate and to provide a through-the-thickness stress distribution.

6-2-2 Requirements

The user needs to have the possibility to exclude plies in the static strength analysis, to estimate strengths as if these plies were fully cracked, and the stress distribution at failure needs to be shown.

6-2-3 Additional assumptions

The following assumptions have to be made, additional to the ones mentioned in section 6-1-1.

- All materials are assumed to behave elastically up to failure. No yielding effect is taken into account.
- The laminate is assumed to behave as a beam, and any effect of stress in y and z -direction is thus ignored. This assumption implies that a stiffness-weighted linear calculation can be used to compute the redistribution of stress as a result of a layer's inability to carry loads.
- 'Inactive' layers due to cracking are assumed to be only outer layers or collections thereof, which means the laminate keeps behaving as a whole.
- The release of residual stress due to a layer being fully cracked is assumed to have no significant effect on the stress state of the rest of the laminate.
- The laminate is assumed to be pristine: free of any cut-outs, notches and/or cracks.

6-2-4 Method

The static strength of the FML is estimated in the steps explained below, see also figure 6-3.

The z -coordinate of the neutral axis is first calculated on the basis of the in-plane stiffness in x -direction, since that is the main loading direction:

$$\bar{z} = \frac{\sum_{k=1}^N z_k^{\circ} A_{11,k} t_k}{\sum_{k=1}^N A_{11,k} t_k} \quad (6-1)$$

where z_k° stands for the mid-plane z -coordinate of ply k , defined from the top of the laminate, see also figure 2-2. The definition of the in-plane stiffness term A_{11} can be found in appendix A.

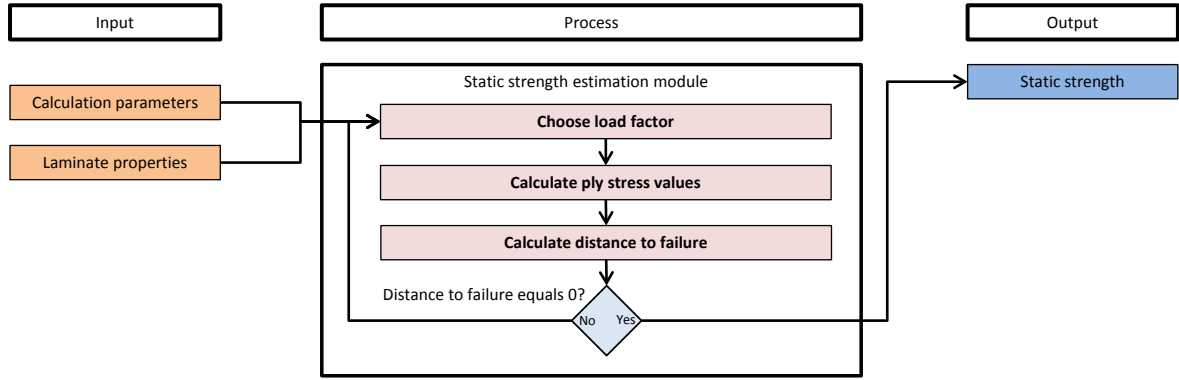


Figure 6-3. Overview of the static strength estimation module.

The vertical shift of the neutral axis is found by performing the calculation again, excluding the inactive layers this time:

$$d\bar{z} = \bar{z}_{\text{complete}} - \bar{z}_{\text{active}} \quad (6-2)$$

When only inner layers of the laminate are set to be inactive, the bending stiffness is overestimated by the program. In reality the laminate is split into two thinner laminates, but the program still calculates the properties as if it were one. The influence of any residual stress that would be released if a layer is completely cracked is also neglected.

The following load vector is assumed to act on the laminate:

$$\begin{Bmatrix} \bar{N} \\ \bar{M} \end{Bmatrix} = \begin{Bmatrix} N_x \\ N_y \\ N_{xy} \\ M_x \\ M_y \\ M_{xy} \end{Bmatrix} = F_S \begin{Bmatrix} C_{N_x} \\ 0 \\ 0 \\ C_{M_x} + d\bar{z}C_{N_x} \\ 0 \\ 0 \end{Bmatrix} \quad (6-3)$$

where F_S is the load that is taken to find out whether the laminate fails or not. The ratio between the factors C_{N_x} and C_{M_x} is thus maintained. The moment resulting from the shift in neutral axis is added with the factor $d\bar{z}C_{N_x}$ to M_x .

The ply stress values are computed using CLT, see appendix A, which includes the residual stress resulting from the curing process. These stress values are calculated on both the top and bottom of each ply, where the severest value is used to estimate the onset of failure.

The Tsai-Wu failure criterion, although not entirely based on physical phenomena, is a useful and widely used method to define failure of composites according to Kassapoglou (2010) and is used here to find out whether failure occurs within the laminate. The criterion is described with the equation below:

$$\frac{\sigma_1^2}{S_{u,t1}S_{u,c1}} + \frac{\sigma_2^2}{S_{u,t2}S_{u,c2}} - \sqrt{\frac{1}{S_{u,t1}S_{u,c1}} \frac{1}{S_{u,t2}S_{u,c2}}} \sigma_1 \sigma_2 + \dots + \left(\frac{1}{S_{u,t1}} - \frac{1}{S_{u,c1}} \right) \sigma_1 + \left(\frac{1}{S_{u,t2}} - \frac{1}{S_{u,c2}} \right) \sigma_2 + \frac{\tau_{12}^2}{S_{u,s}^2} \geq 1 \quad (6-4)$$

where $S_{u,ti}$ is the ultimate tensile strength in direction i , $S_{u,ci}$ the ultimate compressive strength in direction i , and $S_{u,s}$ the ultimate in-plane shear strength. The values σ_1 and σ_2 are the local stresses in the 1- and 2-direction of a ply, see appendix A for the definition. As soon as equation 6-4 surpasses a value of 1 for one or more layers, the laminate is said to have failed. The static strength F_{Su} of the laminate is estimated by choosing such a value, that highest value of the Tsai-Wu criterion is exactly equal to 1.

6-3 Fatigue crack initiation

6-3-1 Goal

The goal of the fatigue crack initiation (FCI) module is to provide a list of the cycles to initiation for the metallic plies of the laminate.

6-3-2 Requirements

The Homan method is to be implemented. This method has to be implemented such that the most appropriate SN-curve is selected by the program according to the load case occurring in the layer and the material it is made of. The programme should be capable of handling both uniform and moment loads as an input and it should contain an optional native stress concentration factor (SCF) calculation.

6-3-3 Additional assumptions

- Cracking is considered to be a local effect considering the crack size during initiation compared to in-plane dimensions, and the connected load redistribution is assumed to be dealt with within the layer itself and surrounding prepreg layers. The possibly present added stress raising effect a cracked metal layer has on neighbouring metal layers is thus assumed not to influence significantly the cycles to initiation of the latter.
In other words: the SCF is assumed to be dominant in each metal layer and hardly affected by cracks in neighbouring metal layers, and it thus still dictates the FCI.
- Layers with a saw-cut are assumed to have a negligible initiation phase, because the surface quality of the inside of such a cut is assumed to be very rough and can thus be considered as already cracked.
- Even though a moment might be applied to the laminate, each ply is assumed to be in a state of uniform stress at the mid-plane value.
- The stress field during the curing cycle is assumed not change as a result of creating a cut-out other than that it disappears where material has been removed. This assumption is based on the assumption that all cut-outs have a constant dimension through the thickness of the laminate and that straight and vertical cross-sections remain straight and vertical after removal of the cut-out material. This means that when material is removed, the residual stress field which existed in the volume of the cut-out is taken with it, in contrast to stress fields due to externally applied loads which have to flow around

cut-outs. This difference is because the direction of flow of curing stress is essentially in thickness direction because plies with different coefficients of thermal expansion are stacked, even though the field itself is a uniform tension field in all in-plane directions. This vertical direction of flow results in an absence of load transfer in the in-plane direction, and thus the piece of material removed retains its residual stress field, leaving the residual stress in the material left behind completely unchanged.

- The effect of the angularity and directionality of the laminate on the stress concentration is assumed to be equal for each metal layer, regardless of the position this layer has within the laminate or its thickness. This means the method as described in Homan (2006) is used for all layers in the laminate, including the flange.

The validity of this assumption is questionable, because the outer surface of a thick metal layer like the flange is likely not experiencing the influence of the Glare strap as much as the inner surface. An alternative would be to use the SCF for monolithic materials instead, thus assuming the anisotropy of the Glare strap does not influence FCI in the flange, but there are two arguments against this choice. One, because a thin layer does experience the effect of anisotropy on its SCF, the monolithic SCF is to be taken only for metal layers above a certain thickness, but no literature exists to date (2013) to substantiate any choice of this thickness. Two, the angularity and directionality of a laminate can both increase or decrease the SCF with equation 6-6, so it is unknown for a general laminate whether treating a thick layer differently from the other layers is a conservative choice or not. The Glare 2A strap was found to have a strong decreasing effect on the SCF of the flange in this specific case, so neglecting this effect in the flange would be conservative in this case, but the extent of this conservatism remains unknown.

The choice was thus made to use the Homan method in spite of its questionable accuracy. More research is necessary to find out whether the Homan model suffices for general laminates or a new method needs to be developed.

- A metal layer is assumed to have a crack of 1 millimetre length after initiation.
- The cycles to failure for a monolithic aluminium layer are assumed to be representative for the cycles to initiation of a metal ply, because for the latter a length of 1 millimetre is taken (Alderliesten, 2009).
- The highest stress value is assumed to occur at the sides of the notch in the metal layers, with respect to the loading direction (Homan, 2006).
- The SCF is assumed to be the same for both tensile and compressive stress, because only tensile stresses are assumed to be the cause of crack initiation.

6-3-4 Method

The FCI module calculates the flights to initiation for each layer in the laminate. An overview of the implementation is given in figure 6-4. First, the SCF is calculated, which is used to calculate the peak stress in each layer from the far-field ply stress values obtained using CLT. Using this peak stress, the stress cycle experienced in each layer can be defined for each load level in the spectrum. This stress cycle is then converted to match the conditions of the

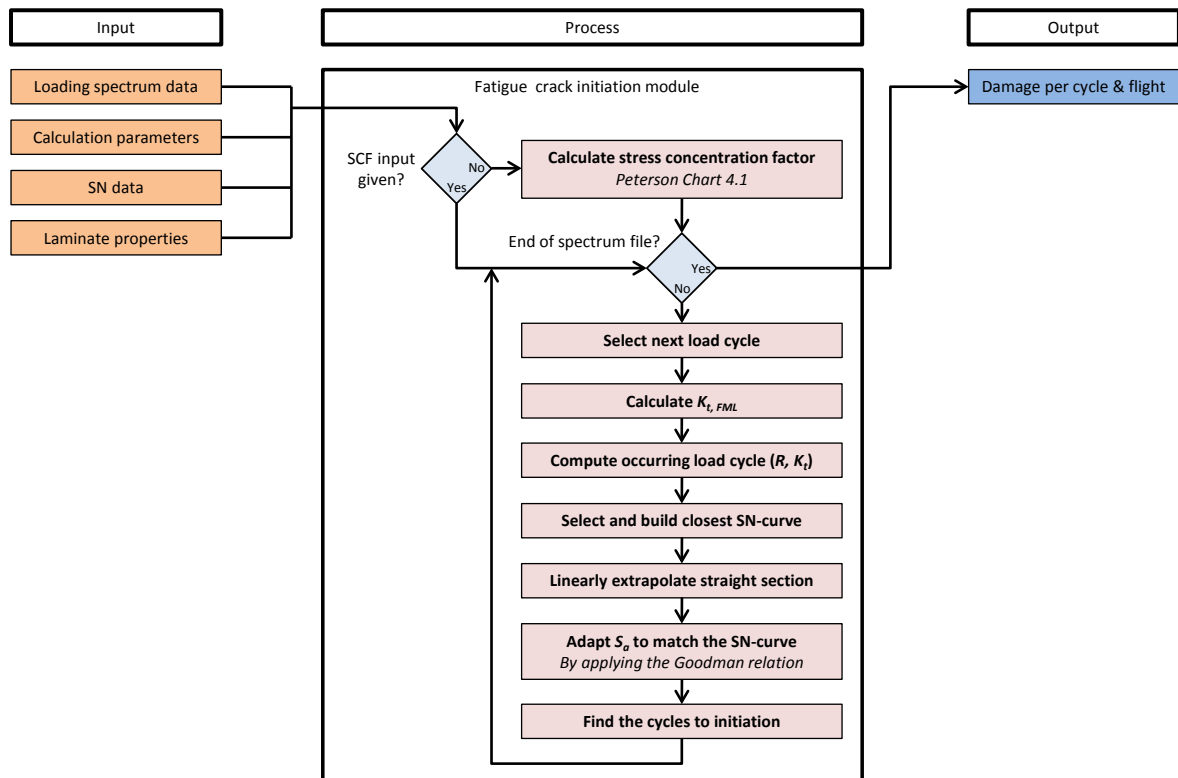


Figure 6-4. Overview of the FCI module.

nearest matching SN-curve, which in turn is used to find the cycles to crack initiation for each load level, for each layer. The inverse values, which stand for damage per cycle, are multiplied with the corresponding number of cycles to get the damage per flight per load level, which in turn is summed to obtain the damage per flight for a single application of the whole spectrum for each layer. This number is again inverted to produce the flights to crack initiation.

Stress concentration factor

The goal of this section is to find a SCF which is representative for an anisotropic plate of finite width, for which no equations are readily available. Homan (2006) stipulates that the ratio of stress concentration in an infinitely wide FML to the concentration of an infinite isotropic plate is equal to that same ratio for plates of finite width, or:

$$\frac{K_{t, FML, FW}}{K_{t, Al, FW}} = \frac{K_{t, FML}}{K_{t, Al}} \quad (6-5)$$

where K_t stands for the SCF and the subscripts Al and FW stand for aluminium and finite width.

The SCF of an infinite anisotropic plate with a circular hole has been solved by Lekhnitskii (1968), and can be used to find the highest SCF for an infinitely large FML plate, occurring

at the sides of the hole:

$$K_{t, \text{FML}} = 1 + \frac{\sqrt{2(r+a)}}{r} \quad (6-6)$$

where a is the angularity of the laminate and r the directionality:

$$a = \frac{c_{12} + \frac{c_{66}}{2}}{c_{11}} \quad (6-7)$$

$$r = \sqrt{\frac{c_{22}}{c_{11}}} \quad (6-8)$$

where c_{11} , c_{12} , c_{22} and c_{66} are elements from the laminate compliance matrix in laminate coordinates, which is the ply-thickness-weighted sum of the inverse of the rotated stiffness matrix for each ply, see also appendix A:

$$\sum_{k=1}^N \bar{Q}_k^{-1} = \begin{bmatrix} c_{11} & c_{12} & 0 \\ c_{21} & c_{22} & 0 \\ 0 & 0 & c_{66} \end{bmatrix} \quad (6-9)$$

The SCF for a circular hole in an infinitely large isotropic plate can also be calculated using equation 6-6, in which case $a = 1$ and $r = 1$ and so $K_{t, \text{Al}} = 3$.

The SCF for a hole in an isotropic plate under tension is described in Peterson (1974):

$$K_{t, \text{Al, FW}} = \frac{\sigma_{\text{peak}}}{S_{\text{nom}}} = 2 + 0.284 \left(1 - \frac{D}{W}\right) - 0.600 \left(1 - \frac{D}{W}\right)^2 + 1.32 \left(1 - \frac{D}{W}\right)^3 \quad (6-10)$$

where D is the hole diameter and W the plate width.

Inserting equations 6-6, 6-10 and $K_{t, \text{Al}} = 3$ into equation 6-5 results in an equation for the stress concentration in an FML of finite width:

$$K_{t, \text{FML, FW}} = \left(\frac{K_{t, \text{FML}}}{K_{t, \text{Al}}}\right) K_{t, \text{Al, FW}} = \frac{1}{3} \left(1 + \frac{\sqrt{2(r+a)}}{r}\right) K_{t, \text{Al, FW}} \quad (6-11)$$

Peak stress

The peak stress $\sigma_{k, \text{peak}}$ in each layer k is calculated by multiplying the nominal mechanical stress $S_{k, \text{nom}}^{\text{mech}}$ occurring in the layer by the SCF and then adding its residual stress S_k^{res} :

$$\sigma_{k, \text{peak}} = K_{t, \text{FML, FW}} \cdot S_{k, \text{nom}}^{\text{mech}} + S_k^{\text{res}} \quad (6-12)$$

where the nominal mechanical stress is calculated by only elevating the mechanical stress as a result of the reduced cross-section:

$$S_{k, \text{nom}}^{\text{mech}} = (S_{k, \text{ff}} - S_k^{\text{res}}) \left(\frac{W}{W - D}\right) \quad (6-13)$$

where $S_{k, \text{ff}}$ is the far-field stress in layer k calculated using CLT. The occurring SCF as defined by the ratio of peak stress to nominal stress is not constant due to the presence of residual stress. Its value is therefore calculated again:

$$K_t = \frac{\sigma_{k, \text{peak}}}{S_{k, \text{nom}}} \quad (6-14)$$

where the total nominal stress in a layer is the sum of the nominal mechanical stress and the residual stress:

$$S_{k, \text{nom}} = S_{k, \text{nom}}^{\text{mech}} + S_k^{\text{res}} \quad (6-15)$$

The occurring stress ratio at the cross-section of the point of interest is also different to the applied stress ratio, and is therefore also recalculated:

$$R_{\text{nom}} = \frac{S_{k, \text{nom}}^{\text{min}}}{S_{k, \text{nom}}^{\text{max}}} \quad (6-16)$$

Correcting for a different load cycle

The stress cycle at the peak stress point has to be converted to match the mean stress level that was used in the tests to produce the data for the SN-curve with which the amplitude of this stress cycle is to be compared. The modified Goodman relation, equation 4-3, is used to this end.

The mean stress and stress amplitude occurring in the ply can be calculated using equations 6-17 and 6-18, see also figure 4-1.

$$S_{m, \text{nom}} = \left(\frac{1 + R_{\text{nom}}}{2} \right) S_{k, \text{nom}}^{\text{max}} \quad (6-17)$$

$$S_{a, \text{nom}} = \left(\frac{1 - R_{\text{nom}}}{2} \right) S_{k, \text{nom}}^{\text{max}} \quad (6-18)$$

The stress amplitude for zero mean stress is calculated using Goodman:

$$S_{a, \text{nom}}|_{S_m=0} = \frac{S_{a, \text{nom}}}{1 + \frac{S_{m, \text{nom}}}{S_{u, t1}}} \quad (6-19)$$

A Goodman function with the same stress amplitude for zero mean stress exists with the stress ratio R_{SN} that was used to generate data for the SN-curve from which the cycles to initiation will be read. This function is described in equation 6-20:

$$S_{a, \text{SN}} = S_{a, \text{nom}}|_{S_m=0} \left(1 - \frac{S_{m, \text{SN}}}{S_{u, t1}} \right) \quad (6-20)$$

in which the mean stress is still an unknown.

The mean stress of a load cycle in the SN-curve can be written as a function of the corresponding stress amplitude with use of the stress ratio. From equation 6-18, it follows for any load cycle that:

$$S_{\text{max}} = \left(\frac{2}{1 - R} \right) S_a \quad (6-21)$$

in which the denominator will never be zero because $R = 1$ means there is no load variation. Hence for the mean stress of a load cycle described with the SN-curve, it follows that:

$$S_{m, \text{SN}} = S_{\text{max}, \text{SN}} - S_{a, \text{SN}} = \left(\frac{2}{1 - R_{\text{SN}}} - 1 \right) S_{a, \text{SN}} \quad (6-22)$$

Equation 6-20 can thus be rewritten using equation 6-22 to obtain a relation for $S_{a,SN}$ that is solely dependent on terms that are known and gives the stress amplitude in the SN-data that is equivalent to the stress amplitude $S_{a,nom}$ occurring in a metal layer:

$$\begin{aligned}
 S_{a,SN} &= S_{a,nom}|_{S_m=0} \left(1 - \frac{\left(\frac{2}{1-R_{SN}} - 1\right) S_{a,SN}}{S_{u,t1}} \right) \\
 &= S_{a,nom}|_{S_m=0} - S_{a,nom}|_{S_m=0} \left(\frac{\frac{2}{1-R_{SN}} - 1}{S_{u,t1}} \right) S_{a,SN} \\
 &= \frac{S_{a,nom}|_{S_m=0}}{1 + S_{a,nom}|_{S_m=0} \left(\frac{\frac{2}{1-R_{SN}} - 1}{S_{u,t1}} \right)} \quad (6-23)
 \end{aligned}$$

The stress amplitude is also corrected for a mismatch between the stress concentration factor in the analysed situation and the factor used in the test data. This is done by multiplying the calculated stress amplitude with a factor f , which is described using equation 6-24:

$$f = \begin{cases} \frac{K_t}{K_{t,SN}}, & K_t > K_{t,SN} \\ 1, & \text{otherwise} \end{cases} \quad (6-24)$$

Flights to initiation

The SN-curve is constructed from four Weibull parameters C_1 to C_4 in a manner described in HSB 63110-02 (IASB, 1994):

$$\log_{10}(N_i) = C_3 \left[\ln \left(\frac{C_2 - C_1}{S_a - C_1} \right) \right]^{\frac{1}{C_4}} \quad (6-25)$$

which produces a typical S-shaped curve, see the solid line in figure 6-5. N_i has been written in equation 6-25 to indicate that the curve is used to calculate cycles to crack initiation rather than failure, even though the data used to generate SN-curves is usually cycles to failure.

Stress amplitudes below the fatigue limit are also damaging when they have been preceded by cycles with a stress amplitude above the fatigue limit. SN-curves from the input data are therefore adapted by continuing the slope of the straight centre section down until $N_i = 10^9$, as is explained in Schijve (2009), which is visualised in figure 6-5 using a dashed line. The equation for the dashed line is constructed from the point of maximum slope on a log-log scale. This slope is calculated using a central finite difference scheme because of the discrete environment of the code. Stress amplitudes that fall below the linear continuation are given 10^9 cycles to initiation, as is shown using the vertical dashed part of the line in the figure.

Stress amplitudes which surpass the highest stress amplitude of the curve produced with the input coefficients are given a single cycle to initiation.

The inverse of the cycles to initiation for each load level is taken and is subsequently multiplied with the amount of cycles for the corresponding level to obtain the damage per flight for each load level. These values are summed up to obtain the damage per flight for the whole spectrum, of which in turn the inverse is taken to obtain the amount of flights the structure can take before crack initiation takes place. The spectrum is thus assumed to represent one flight cycle.

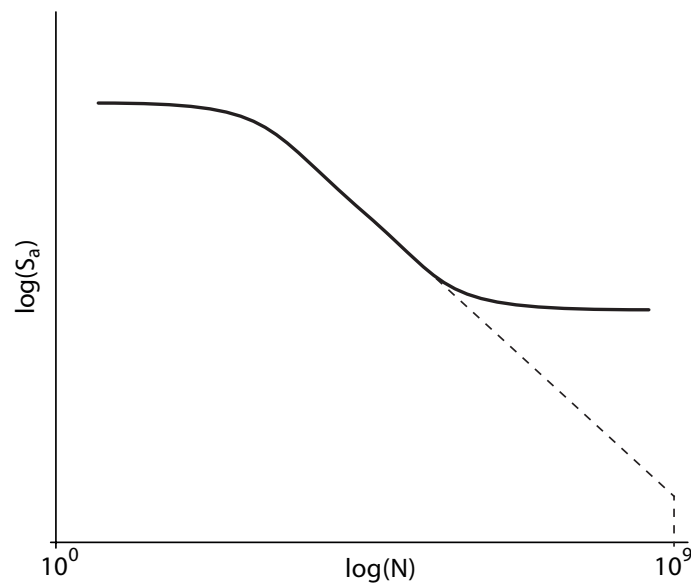


Figure 6-5. A typical Wöhler curve including linear continuation of straight part

6-4 Constant amplitude fatigue crack propagation

6-4-1 Goal

The goal of this module is to describe fatigue crack propagation (FCP) due to CA loads starting from an already cracked laminate. This initial crack can be only in part of the layers in case where Wilson's general FML code is run rather than the Alderliesten model, and initially intact plies can initiate during the growth of others, according to a list of cycles to initiation provided by the crack initiation code.

6-4-2 Requirements

Both the Alderliesten code and the Wilson code should be implemented, so results can be compared, and the programme can select the simpler and thus faster analysis method for the problems that do not require the elaborate model. There should be an option to halt the analysis and update the far-field applied loads. As mentioned in the goal, the Wilson code should be adapted to handle partial and delayed initiation. Parameters controlling the numerical accuracy, and thus run time, should be a user input rather than hard-coded quantities.

6-4-3 Additional assumptions

A different set of additional assumptions is required for the crack propagation module, this set is given and discussed below.

- The initial delamination shape and the shape for the tip of the crack are assumed to be parabolic, because the delamination shapes observed in fatigue-loaded Glare usually

reasonably resemble a parabola (Alderliesten, 2007a).

Assuming an initial delamination shape is necessary because the model needs to work from a delamination shape to get started, although after a series of calculation steps the delamination will evolve to the same shape regardless of several different initial shapes (Alderliesten, 2007a).

The delamination shape at the crack tip has to be assumed rather than calculated because firstly, the delamination growth cannot be calculated if there is not yet a delamination present at that part of the crack that has just been incremented and secondly, because the delamination rate calculation used in the Alderliesten model does not regard neighbouring elements, which results in the absence of natural suppression of extreme delamination growths. A shape thus needs to be enforced for the elements close to the tip to avoid numerical problems. A parabolic shape is used, as was the case in the original model, since it was the most accurate for Glare 3 and 4B (Alderliesten, 2005). In this research, it is assumed to be also accurate for Glare 2A. The parabolic delamination shape is calculated using the following equation:

$$b(a_s) \sqrt{a - \frac{y - a_s}{a - a_s}} \quad (6-26)$$

where a is the current crack length, a_s is the crack length at which the approximation starts, y is the coordinate along the crack and varies from a_s to a in the parabola, and $b(a_s)$ is the delamination length at $y = a_s$, which determines the height of the parabola.

- It is assumed that the shear deformation of the prepreg layers can be written as a result of far-field stress in the aluminium layers. Wilson (2013) points out that the only reason the shear deformation in the fibre layers exists is the fact that the fibres are carrying added bridging stress, and that the far-field stress in the aluminium layers is thus the incorrect quantity to base the fibre layer deformation upon. Still, the far-field stress in the aluminium layers is used in the Alderliesten model to calculate the fibre layer deformation that occurs during bridging, see equations (6.15) and (6.16) in his thesis. This assumption thus has to be made here to support this model.
- The calculation Alderliesten (2005) implements, requires the assumption that the deformation of the prepreg layers remains small.
- All stress gradients in y - and z -direction are ignored, because the equations are all one-dimensional in x -direction. It is assumed that a ‘flow’ of stress in the transverse direction is absent in the prepreg layers, which is deemed a reasonable assumption regarding the relatively low in-plane shear stiffness of the prepreg layers (Alderliesten, 2005). Direct interaction between bar elements is thus assumed not necessary to calculate the crack- and delamination growth properties.
- The delamination length is assumed to be constant in an element and the bridging load evenly distributed along the width, again because the used equations are one-dimensional in x -direction to get a closed-form expression for delamination growth (Alderliesten, 2005).
- It is assumed that the strain energy release rate can be seen as the sole driving factor for delamination growth in order to solve for the bridging stresses (Marissen, 1988;

Alderliesten, 2007a). The energy release rate and delamination growth are related through a Paris-type equation (Alderliesten, 2004).

- The influence of anisotropy of the metal ply on the bridging stress is assumed to be negligible (Marissen, 1988).
- The crack opening due to metal layer deformation as a result of the bridging loads can be assumed to be negligible compared to the prepreg layer deformation and fibre elongation, because of the high relative stiffness of the metal layer (Guo and Wu, 1999).
- The influence of the laminate anisotropy on the crack opening shape is neglected. Marissen (1988) argues that the influence on the accuracy of the solution for the stress intensity factor is acceptable for ARALL. It is assumed that this is also the case for the Glare reinforced frame flange.
- Linear elastic fracture mechanics (LEFM) is applied to the metal plies in the FML. This requires the underlying assumption that there is only small-scale yielding at the crack tip so the stress intensity field remains the dominant loading parameter (Marissen, 2011). This seems a reasonable assumption because enclosing a metal layer in prepreg layers does not seem to be a reason for significantly more yielding to occur.
- It is assumed that the relation found between the crack tip stress intensity and crack growth rate in experiments with thin monolithic aluminium sheets is also representative for the case where these sheets are incorporated in Glare, thus in this step the influence of the anisotropy of the laminate is also neglected.
This assumption, along with the previous two, are the main assumptions of the Alderliesten FCG model.
- The crack opening shape is assumed to be elliptic (Marissen, 1988), which seems to be a reasonable assumption regarding the measured crack opening shapes for Glare 3 (Alderliesten, 2005).
- It is assumed that each metal layer cracks in an equal manner, which means one prepreg/metal/prepreg combination analysis suffices to describe the entire laminate. The surface layers are only bridged on one side, but it is thus assumed that the single-side bridging of these layers has a negligible influence on the crack growth properties of the laminate as a whole.
- The laminate is assumed to be under pure tension for the Alderliesten model.
- It is assumed that crack closure is the cause for a low stress intensity values not to follow the Paris equation, and that the absolute stress intensity ratio needs to be replaced with an effective stress intensity ratio (Plokker, 2005).

6-4-4 Method for standard Glare

Alderliesten (2005) provides a very accurate description of how his model works. Therefore, only a summary of the logic of the method is given while referring to his work and the changes made with respect to this original implementation are mentioned, rather than copying all the equations into this report. An overview of the code is given in figure 6-6.

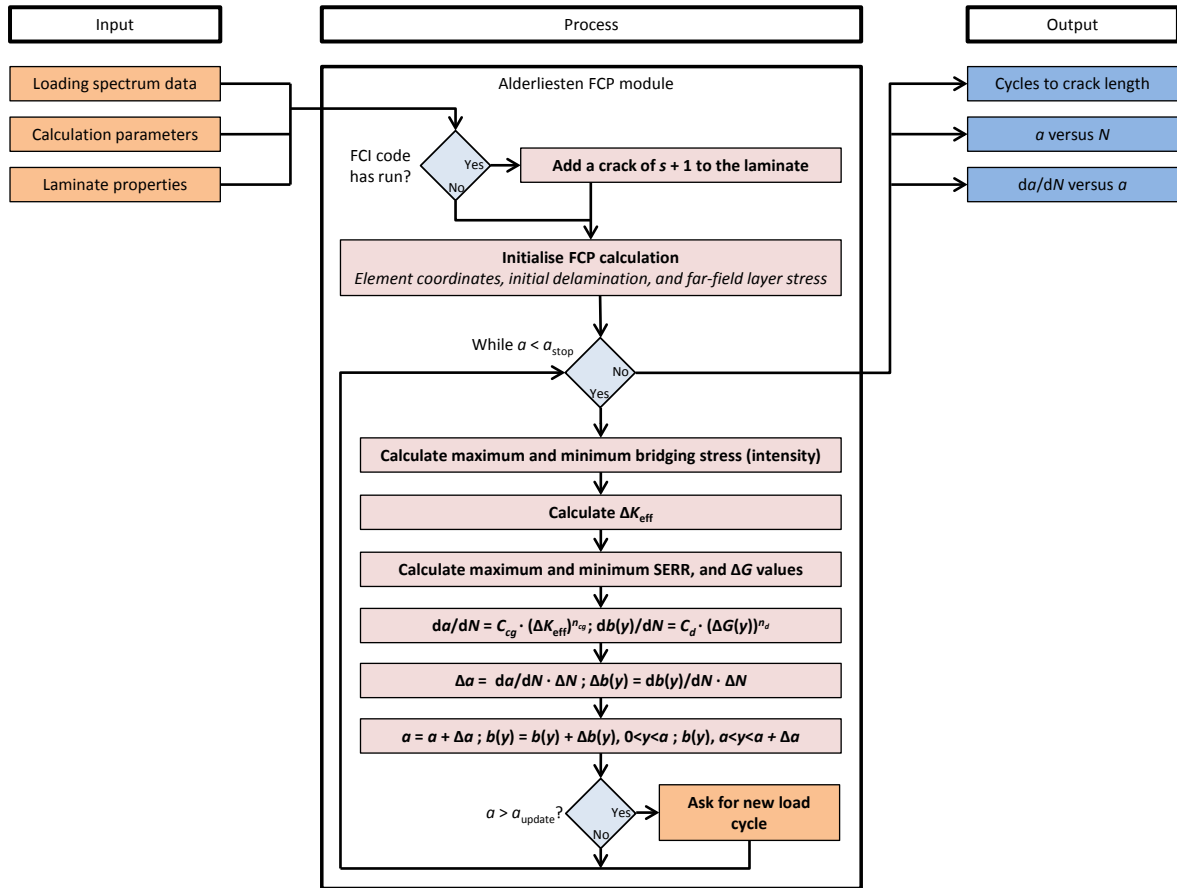


Figure 6-6. Overview of the implementation of the Alderliesten FCP model in the tool connected to the current research.

The Alderliesten crack growth model for Glare iteratively carries out the steps below to find the number of cycles to reach a certain crack length. The numbers between brackets refer to equations in the dissertation connected to the Alderliesten model (Alderliesten, 2005).

1. Calculate the crack opening due to maximum and minimum far-field stress (6.6).
2. Calculate the deformation of the prepreg layer under maximum and minimum far-field stress (6.10-6.12).
3. Calculate the bridging stress intensity (6.27;6.28) by applying displacement compatibility at the crack surface (6.19) at maximum and minimum far-field stress. This displacement is comprised of the results of the two previous steps, the extension of the fibre layer due to a combination of far-field fibre stress and bridging stress (6.9), and due to the reduction of crack opening due to the fibre bridging effect (6.7;6.18;A.18-A.21). This displacement compatibility requires a discrete solution, because an integration of the non-uniform bridging stress cannot be carried out.
4. Calculate the effective stress intensity ratio from the far-field stress intensity and the bridging stress intensity (6.1;6.29), again at maximum and minimum far-field stress.

5. Compute the maximum and minimum delamination energy release rates (6.24;6.25).
6. Calculate the crack- and delamination growth rates from the effective stress intensity ratio (6.30) and the strain energy release rate ratio (6.4), respectively.
7. Apply the calculated crack- and delamination increments to the current coordinates and interpolate to find the updated delamination shape as Alderliesten (2005) describes in appendix C of his dissertation.

The changes between the implementation of the model connected to the research described in this report and the original code are explained below.

- Rather than keeping the width of each element along the crack the same, a element width which decreases towards the tip was chosen. The midpoint coordinates and element widths are now described according to a function by Shebychev to improve convergence of the model (Wilson, 2007):

$$y_i = s + (a - s) \sin \left(\frac{2n_i - 1}{2N} \frac{\pi}{2} \right) \quad (6-27)$$

and

$$w_i = (a - s) \cos \left(\frac{2n_i - 1}{2N} \frac{\pi}{2} \right) \frac{\pi}{2N} \quad (6-28)$$

- A change is made to use CLT instead of a metal volume fraction (MVF) approach, to make this module consistent with the others in the tool. Although both models are equivalently accurate to describe the in-plane extensional displacements, there are still small differences between the results of both implementations, which stem from the two differences given below.

- The proposed tool calculates the second in-plane Poisson's ratio on the basis of in-plane extensional stiffness values rather than assuming $\nu_{21} = \nu_{12}$ (Kassapoglou, 2010):

$$\nu_{21} = \frac{E_2}{E_1} \nu_{12} \quad (6-29)$$

- The rotated thermal expansion coefficients are calculated by use of the strain rotation matrix T_2 in the classical laminate theory (Tsai and Hahn, 1980), see also appendix A. The thermal expansion vector for a ply in laminate coordinates becomes the following:

$$\begin{bmatrix} \alpha_x \\ \alpha_y \\ \alpha_{xy} \end{bmatrix} = T_2 \begin{bmatrix} \alpha_1 \\ \alpha_2 \\ 0 \end{bmatrix} = \begin{bmatrix} \alpha_1 \cos^2(\theta) + \alpha_2 \sin^2(\theta) \\ \alpha_1 \sin^2(\theta) + \alpha_2 \cos^2(\theta) \\ (\alpha_1 - \alpha_2) \cos(\theta) \sin(\theta) \end{bmatrix} \quad (6-30)$$

where α is the coefficient of thermal expansion and the subscripts 1 and 2 indicate that the value is in the local 1- or 2-direction of a ply, respectively, and the subscripts x and y indicate that the value is in the laminate x - or y -direction,

respectively. Equation 6-30 is used instead of the equations used by Alderliesten, which state:

$$\begin{bmatrix} \alpha_x \\ \alpha_y \\ \alpha_{xy} \end{bmatrix} = \begin{bmatrix} \alpha_1(\cos \theta + \sin \theta) \\ \alpha_1(\cos \theta + \sin \theta) \\ 0 \end{bmatrix} \quad (6-31)$$

- The calculation of the deformation of a unidirectional (UD) prepreg layer due to shear stress was adapted to use the formulae for UD prepreg layers (equations (B.47), (B.52) and (6.15) of Alderliesten (2005)) instead of the equation for cross-ply (CP) layers (equations (B.62), (B.70), and (6.16) of Alderliesten (2005)), even though the influence on the final result is minimal. The tool now selects which equations to use on the basis of the type of plies found.
- Crack closure is seen as the cause of decelerated crack growth for low values of the stress intensity, as was written in the additional assumptions in section 6-4-3. Schijve (1981) mentions that good correlation between the crack growth rate and effective stress intensity ratio was found for Aluminium 2024-T3 when the following equation was used:

$$\Delta K_{\text{eff}} = (0.55 + 0.33R + 0.12R^2) (1 - R) K^{\text{max}} \quad (6-32)$$

Plokker (2005) shows that this equation also provides a good correlation between the crack growth rate and effective stress intensity for the aluminium sheets in Glare. Rensma (2007) argues that it is the stress intensity ratio at the crack tip, rather than the far-field ratio, that is leading for the crack growth rate, because a difference between these two exist due to the presence of residual stress, see also section 6-3-4. The equation for the effective stress intensity ratio then becomes:

$$\Delta K_{\text{eff}} = (0.55 + 0.33R_{\text{tip}} + 0.12R_{\text{tip}}^2) (1 - R_{\text{tip}}) K_{\text{tip}}^{\text{max}} \quad (6-33)$$

instead of the one used by Alderliesten:

$$\Delta K_{\text{eff}} = (1 - R^{1.35}) K_{\text{tip}} \quad (6-34)$$

about which doubts were already expressed in the dissertation by Alderliesten (2005). Using a different equation for ΔK_{eff} means that different Paris crack growth relation parameters C_{cg} and n_{cg} are required to provide an accurate fit with the test data rather than the ones provided by Alderliesten (2005) in table 6.2 of his dissertation. Khan et al. (2010) use $C_{cg} = 1.27 \cdot 10^{-11}$ and $n_{cg} = 2.94$, but the source mentioned only provides a ground for the Paris delamination growth parameters. A good correlation with test data by Homan (2002) was obtained using these values, see figure 6-7, and thus they are considered accurate.

- Alderliesten uses the Dixon finite width correction factor (FWCF), but Wilson (2013) shows, with test results, that effect of a finite width on the crack growth in the metal layers of FMLs is practically absent, most probably as a result of the effect of fibre bridging, see also the test data in figure 7-19. The proposed implementation, therefore, does not make use of a FWCF.

- The influence of the residual stress in the metal layers that is released when these layers crack and delaminate from the surrounding prepreg layers is neglected in the original code, but taken into account in the implementation connected to this research. Two effects are actually occurring, as illustrated in figure 6-8, which is a 2D representation of a FML.

From situation 1 to 2, the laminate is brought to room temperature from the curing temperature. It has a length that reaches line A at curing temperature. The cool-down makes the metal layers want to shrink to more than the prepreg layers, e.g. a difference between line C and B, respectively. Situation 3 is what actually happens when the laminate is cooled, because the layers are attached to each other: the laminate obtains a length D which is between C and B. The sum of the tensile stress in the metal layers balances the sum of the compressive stress in the fibre layers at this point. No displacement occurs when only a crack is added in the central metal layer of the system, because the layer is still supported by the fibre layers along its full length. Two displacements arise if the metal layer also delaminates from the adjacent fibre layers. One, the metal layer contracts along the length where it is unrestricted by the prepreg layers, creating a crack opening even though no external load is applied, i.e. the room between lines F and G. Two, the laminate as a whole expands because part of the compressive stress in the fibre layers has been released, as indicated with line E.

In the research described in this report, the former is taken into account but the influence of the latter is assumed to be negligible, because the crack is assumed to be small compared to the in-plane dimensions of the laminate and thus an overall increase in length of the laminate is restrained by the intact parts of the laminate that surround the crack.

6-4-5 Method for general FMLs

The model for FCP in general FMLs of Wilson (2013) adds the capability to calculate crack growth in FMLs containing cracks of different length, layers of different thickness and material, and extra adhesive layers, as well as FMLs undergoing a load case that includes a moment. Figure 6-9 contains a schematic overview of the logic of the model.

The most important changes with the Alderliesten model are that Wilson (2013) calculates the amount of bridging by applying a displacement compatibility on the delamination boundary rather than the crack flanks, and that multiple layers are now responsible for bridging a crack rather than just the adjacent prepreg layer.

A different set of assumptions is used for the Wilson model. Any assumptions from the list given in section 6-4-3 that are not used, or used differently, in this module are given first, followed by additional assumptions that had to be made by Wilson to get to an answer.

- Changes with respect to the assumptions for the Alderliesten model in section 6-4-3 are given below.
 - All metal layers can now crack differently, so analysing one metal layer is no longer sufficient to characterise the entire laminate.

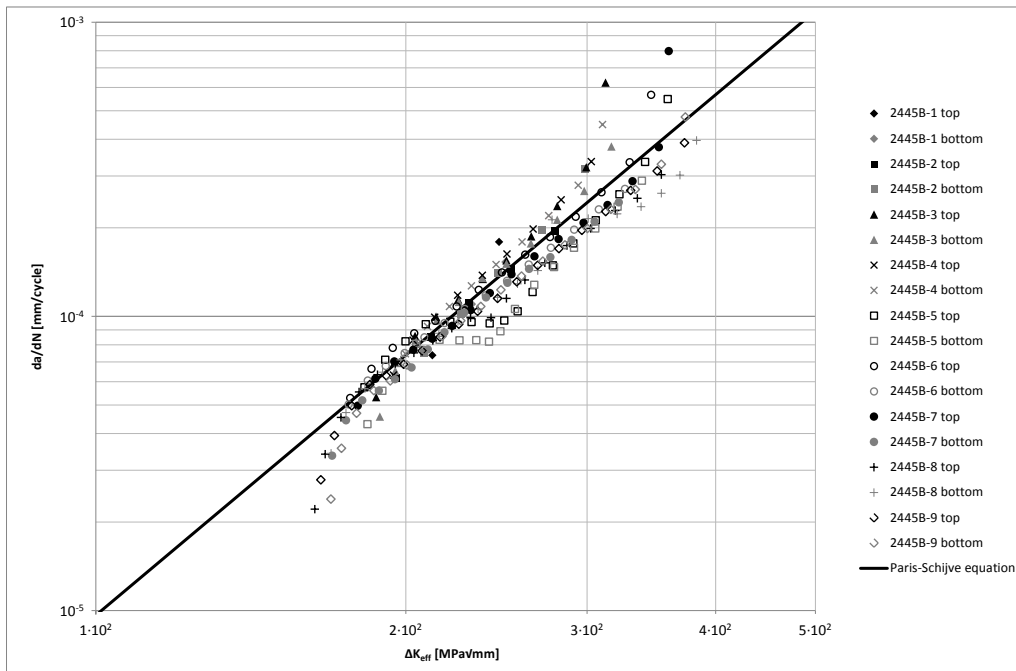


Figure 6-7. Fitting equation 6-32 to test data from Homan (2002)

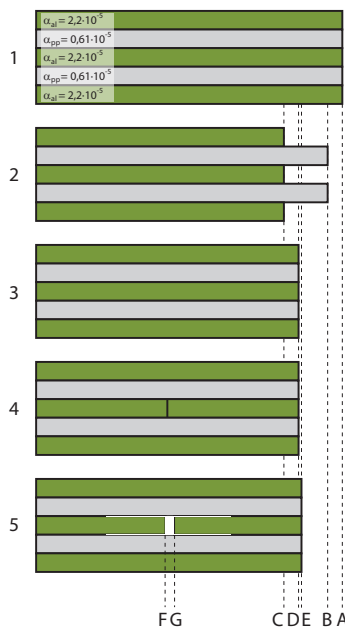


Figure 6-8. The effect of residual stress on crack opening

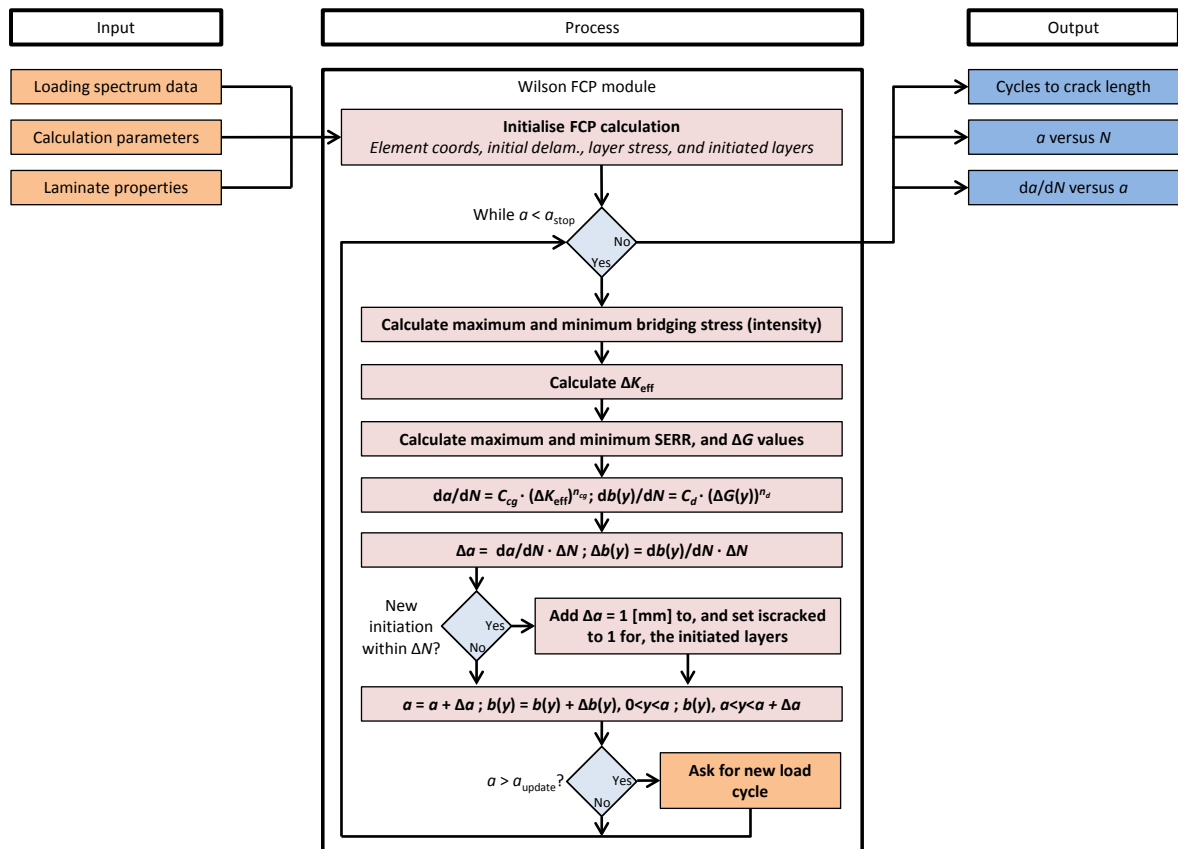


Figure 6-9. Overview of the implementation of the Wilson FCP model in the tool connected to the current research.

- The loading case can include a moment next to the pure tension in the case of the Alderliesten model.
- The altered delamination increment calculation does not show the extreme delamination growths as seen in the Alderliesten code, so the assumed parabolic tip delamination is only applied to the initial delamination and no longer on the delamination tip during analysis.
- The prepreg layer deformation is now written as a result of a line load which affects half of the thickness, rather than a far-field metal layer stress deforming the layer as a whole. This change is made to incorporate the effect of different shear stress values on either side of a prepreg layer and also allows internal moments to be taken into account correctly.
- Any layer that is on at least one side attached to another layer is assumed to contribute to bridging of the crack. This needs the bar elements along the crack to contain vertical segments for each new delamination situation, and in each segment the CLT is assumed to be valid.
- It is assumed for the laminates under consideration that taking the effect of secondary bending into account as described with the neutral line model (NLM) does not add to

the accuracy (Wilson, 2013). The NLM is probably only valid for very thin laminates because these bend relatively easily out of plane.

- The amount of delamination growth per cycle is assumed to be small. The SERR is calculated based on the strain energy of all the bridging material below and above the delamination, which are thus both assumed constant as the delamination extends, which is a good approximation if the extension remains small (Wilson, 2013).

The model works basically in the same way as the Alderliesten model it is based upon, although the method now needs to solve for compatibility at the delamination boundary of each delaminated interface rather than on one crack flank (Wilson et al., 2009). The steps it takes iteratively to get to an answer in the form of a number of cycles to reach a specific crack length is given below. The numbers between brackets refer to equation numbers in the dissertation connected to the Wilson model (Wilson, 2013). The author notes that at the time of writing this report, Wilson's dissertation was still in the draft stage and the equation numbers are thus probably not correct with respect to the final version of his work.

1. Calculate the crack opening due to maximum and minimum far-field stress (4.9;4.10).
2. Calculate the bridging stress by applying displacement compatibility at each delamination boundary (4.52-4.60) at maximum and minimum far-field stress. This displacement is comprised of the results of the previous step, the reduction of crack opening due to the bridging effect (4.11-4.14), the deformation of a prepreg layer under maximum and minimum shear stress (4.25), and due to the elongation of the bridging material resulting from a combination of far-field fibre stress and bridging stress (4.50;4.51). If adhesive layers are added their deformation is calculated with (3.7;3.8) rather than (4.25). This displacement compatibility requires a discrete solution, because an integration of the non-uniform bridging stress cannot be carried out.
3. Calculate the effective stress intensity ratio (3.13;3.19;3.20) from the far-field stress intensity (3.14) and the bridging stress intensity (3.15-3.17), again at maximum and minimum far-field stress.
4. Compute the strain energy release rate for each delamination (5.23) from the strain energy above the delamination boundary (5.10), the strain energy below the delamination boundary (5.14), and the work done due to delamination growth (5.22), using the coefficients that ignore the moment due to the NLM (3.9-3.12).
5. Calculate the crack- and delamination growth rates from the effective stress intensity ratio (3.21) and the strain energy release rate ratio (3.22;3.23), respectively.
6. Apply the calculated crack- and delamination increments to the current coordinates and interpolate to find the updated delamination shape (3.24-3.26).

The numerical implementation of the Wilson method can have a problem termed leapfrogging at times. The delamination growth calculations on either side of a layer can start to influence each other in such a way that they amplify each other, which can be attributed to the fact that

a fast-growing delamination would be directly slowed down in reality, but is allowed to grow at its initially fast pace for an entire increment in the discrete environment of the model. This creates an overshoot which amplifies the growth on the other side, creating the same effect repeatedly. Wilson has implemented an extensive detection and mitigation scheme, which reduces the growth of both delaminations at the average speed of the two as soon as leapfrogging has been detected (Wilson, 2013).

A second side-effect of the numerical implementation is a relatively large amount of noise in the crack growth calculation. Wilson (2013) uses a 10-point smoothing function to produce a smooth plot from the output data. The tool connected to this report does not make use of this smoothing.

Another difference of the implementation of the Wilson module in the tool connected to this report, as compared to the original code, is that it allows for delayed initiation to take place if no cracks are present in the input situation. On the basis of a list of cycles to initiation for each layer, as received from the FCI module, the Wilson code commences with a crack propagation analysis with a 1 millimetre crack and parabolic delamination for the layers with the lowest cycles to initiation. The crack propagation analysis is performed in a standard way until the number of cycles to initiation for another layer has been surpassed, at which point the code creates a 1 millimetre crack and parabolic delamination shape in this layer as well. This continues until either all layers have a crack and the code runs again as normal, or as soon as one of the layers has reached the maximum crack length and the simulation finishes with some uninitiated layers.

6-5 Variable amplitude fatigue crack propagation

6-5-1 Goals

The goal of the variable amplitude (VA) addition is to make both the Alderliesten and Wilson modules capable of handling a load spectrum rather than solely a CA load, including a load history effect, while not removing functionality. Only one elaboration is given for the VA addition, because this addition is practically equal for both the Alderliesten and the Wilson model.

6-5-2 Requirements

Two models are to be implemented: linear damage accumulation (LDA) and the Wheeler yield zone model (YZM). The choice for the Wheeler YZM stems from Khan (2013), who found that this relatively simple model was already sufficient to describe the history effects occurring in Glare. The reason for this is probably that fibre bridging reduces the relative effect plasticity has on the crack growth. Next to adding the VA capability, none of the functionality as mentioned in section 6-4 should be lost as a result of the addition.

6-5-3 Additional assumptions

- The LDA model is based on the assumption that every load cycle has a distinctive amount of damage it does regardless of what preceded the cycle. Tests show that load

history effects do occur (Khan et al., 2010), so this model most likely overestimates the crack growth rate of the laminate under tensile VA loading, because the history effects for this type of loading are mainly causing slower crack growth rates (Schijve, 2009).

- The YZM is based on the assumption that crack growth is slowed down after application of a large tensile load, termed overload (OL), only due to the increased size of the yield zone connected to this OL as compared to the case the loading was CA. This increased yield zone is an excess of material in front of the crack tip, which causes compressive stresses to exist and thus reduce the severity of the crack-opening stress field, thereby slowing crack growth.
- Khan (2013) has found that a value of 2 for the Wheeler model exponent results in accurate predictions. It is assumed that this is also the case for the research described in this report, although the origin of this value is not clearly stated by Khan.

6-5-4 Method for both the Alderliesten and the Wilson model

A VA input spectrum requires the loop of either section 6-4-4 or section 6-4-5 to be applied many more times than for CA, because rather than simply changing the number of cycles so the calculated crack growth rate produces exactly the user-set value of the maximum crack growth increment, the code now has to calculate the growth rates for each different load level in the spectrum and add the contributions to crack growth until the desired increment has been reached before it can start updating the delamination shape. This means that, especially for spectra with a lot of different light load cycles, many calculation loops are needed per growth increment, in contrast to the single loop for CA loading, no matter what severity. Schematic overviews of the logic of the code for the VA Alderliesten and the VA Wilson model can be found in figures 6-10 and 6-10.

A method termed dynamic programming was applied to prevent excessive amounts of calls to the functions within the loop. The input spectrum is analysed and each unique load level is given a load identification number before the crack growth calculation loop is started. The result of each calculation loop is saved in a database and before each new entry of the loop, the database is checked whether a calculation result already exists for the current load level. The result from the database is used if this is the case, the calculation loop is run otherwise. As soon as the desired crack growth increment has been reached, the delamination shape is updated and the database is emptied because the calculated values are no longer valid. The dynamic programming change resulted in a reduction to a tenth of the original calculation time for some spectra, allowing for much more runs to be performed in the same time as compared to the original.

The implementation of the YZM as found in the code of Khan (2013) recalculates the x -coordinate of the end of the yield zone as soon as the current load is larger than the next. This method, however, assumes that the end of the yield zone due to the previous larger load cycle always lies at a lower x -coordinate than the end of the current load cycle, if the current load is larger than the next. This leads to an overestimation of the crack growth rate, especially if a large overload is applied, followed by a small load, which in turn is followed by an even smaller load, because the crack growth during the last load cycle should be significantly slowed down as a result of the yield zone of the first load cycle because the first load cycle

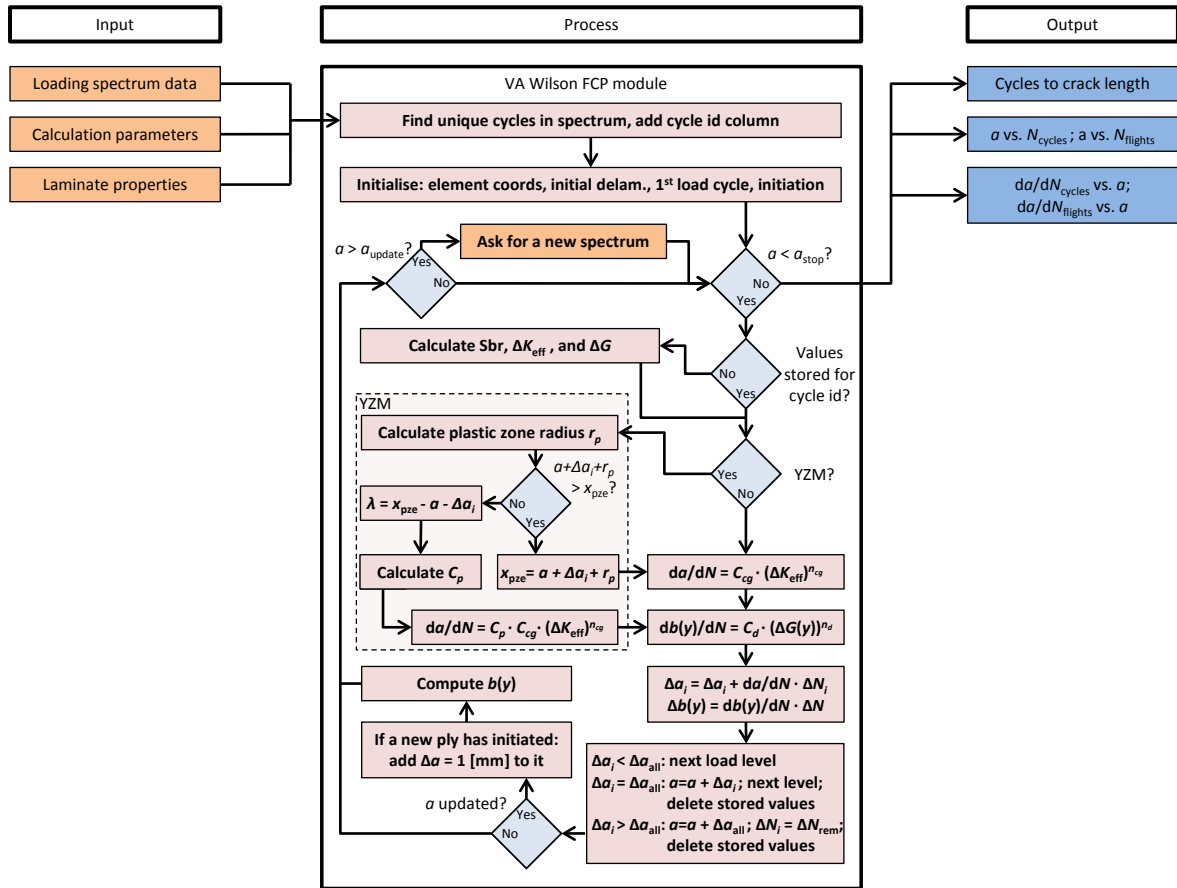


Figure 6-11. Overview of the implementation of the Wilson FCP model for VA loading in the tool connected to the current research.

plasticity-induced retardation so the retardation parameter is calculated using equation 4-8 and the crack growth rate using equation 4-7.

Sadly, the method above is also not perfect. The stress intensity value can be overestimated for certain combinations of initial delamination size factor b_0 and initial crack size, causing retardation to occur even when the loading is CA. An extra check is therefore included, which neglects retardation if the applied load cycles have been equal or only increasing since the first applied load cycle. The method explained in the previous paragraph is activated as soon as a load cycle is detected that is lower than any of the cycles applied since the very first applied load cycle.

Running the Wilson module for general FMLs with VA loading results in wrong behaviour of the leapfrog mitigation scheme. A VA version of this mitigation scheme needs the number of cycles each load level that was applied since the previous delamination shape update, and to scale the delamination rates accordingly as soon as leapfrogging is detected. The implementation of a suitable leapfrog mitigation for VA loading is not straightforward, and is left as a recommendation for future work. The Wilson module with VA loading is therefore run without leapfrog mitigation, and it did not produce any unreasonably large delaminations for the analyses carried out in this research.

6-6 Summary

The implementations of the static strength module, the FCI module and the standard and general FCP modules for both CA and VA load cases have been explained, along with all the assumptions made, and schemes implemented to reduce unwanted numerical side-effects. A working model that can analyse the Glare strap reinforced frame flange was produced, which starts with FCI analysis on the pristine object and then continues with FCP analysis to calculate the number of cycles or flights that can be applied before a certain crack length is reached.

Verification and validation

7-1 Introduction

7-2 Verification of tool components

7-2-1 Static strength

7-2-2 Initiation

7-2-3 Crack propagation in standard Glare

7-2-4 Crack propagation in general FMLs

7-2-5 Crack propagation under variable amplitude

7-3 Validation of individual modules

7-3-1 Static strength estimation

7-3-2 Initiation

7-3-3 Crack propagation in standard Glare

7-3-4 Crack propagation in general FMLs

7-3-5 Crack propagation under variable amplitude

7-4 Validation of combinations of modules

7-4-1 Constant amplitude FCI and FCP

7-4-2 Variable amplitude FCI and FCP

7-5 The influence of run parameters

7-6 Limits of validity

7-7 Summary

7-1 Introduction

The results of two checks related to programming are provided in this chapter. These checks are verification and validation. Firstly, for verification, the results of the code produced in the research described in this report are compared to the results of the original versions of

parts of this code. The parts of the code that are made from scratch are verified by checking whether these parts react to input parameter changes in a way that matches expectations. Secondly, the outcomes of the program are compared with test results available in literature, which allows conclusions to be drawn about the validity of the code.

7-2 Verification of tool components

For the work discussed here, performing a verification basically means finding out whether the code that is created is what the author intended to create. This might sound superfluous, but it is far from that, because the chance is high that for large programmes for example there is an error in the logic, applying the model in a discrete environment has had unwanted side-effects, or simply a coding error has been made.

Verification is performed by checking whether the outcomes of modules react to input variations in a way that matches expectations, and, if applicable, whether the module as implemented in the tool produces the same result as the original version of the code.

7-2-1 Static strength

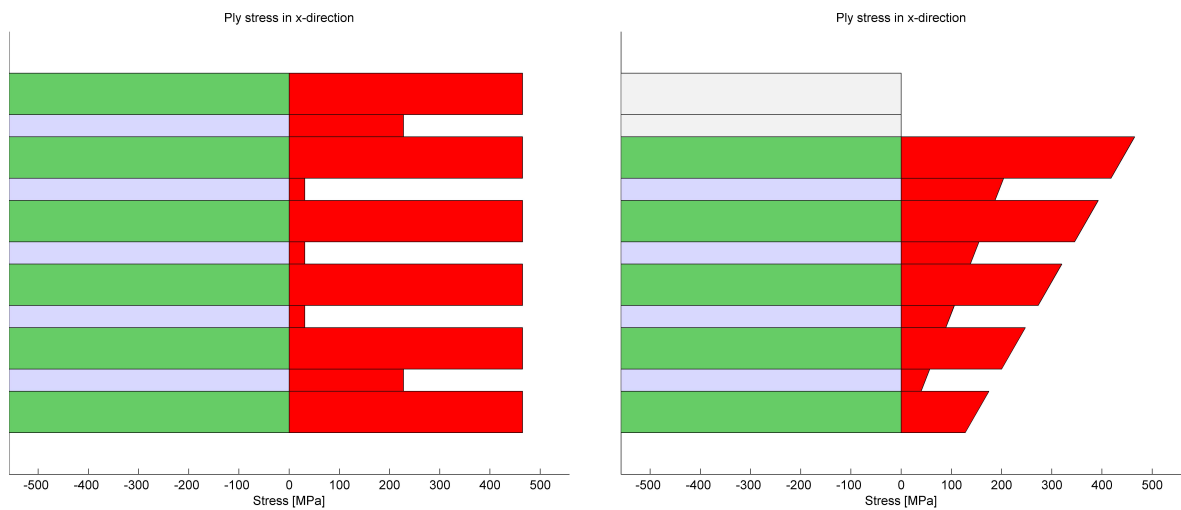
The static strength estimation module was made from scratch, so only a basic verification can be performed: a check on whether the produced outcomes seems to be logical.

The first verification of the static strength estimation module is to determine whether the produced stress distributions make sense. The stress distribution in x -direction at failure is given for two different laminates in figure 7-1. An illustration of the laminate is shown on the left of each figure and the estimated stress distribution at failure on the right.

The module captures correctly the behaviour that layers of higher stiffness attract more load, because the layers with the highest stiffness, i.e. the metal layers, show the largest stress in figure 7-1a, followed by the 0-degree prepreg layers, and the layers with the lowest internal stress are the 90-degree prepreg layers, where the last are also the plies with the least stiffness in x -direction. As the laminate has 90-degree layers, the critical load should drop because the metal layers carry a larger percentage of the applied load. The module reproduces the effect correctly: the critical load has become $1.5 \cdot 10^3$ [N/mm] versus $1.7 \cdot 10^3$ [N/mm] in the case of standard Glare 2A-6/5-0.5, which is not shown here.

The stress redistribution as a result of removing layers also matches expectations, see figure 7-1b. Two layers have been removed from the top of a this time standard Glare 2A laminate, resulting in a downwards shift of the neutral axis with respect to the far-field condition, where these top layers are assumed to be fully functioning. The downwards shift should result in a negative line moment according to the definition in figure 2-2, which is perfectly reproduced by the static strength estimation module. The load that can be carried should also be greatly reduced, because the top active layer reaches the ultimate stress much sooner than in the pristine case. This is reproduced by the code: the critical load has dropped to $0.8 \cdot 10^3$ [N/mm].

The input values of static strength for the material are recovered as soon as a single layer is entered and examined under a uni-axial load, thus the correct behaviour of the static strength estimation module is verified with this and the aforementioned outputs.



(a) Glare 2A-6/5-0.5 with the three middle prepreg layers 90 degrees rotated

(b) Glare 2A-6/5-0.5 with the two upper layers shut down

Figure 7-1. Stress distributions in x -direction at failure for different laminate configurations

7-2-2 Initiation

Verifying on the basis of a comparison with the original code is considered not useful for the fatigue crack initiation (FCI) module, because the module has been changed in so many ways that the number cycles to initiation calculated with the code as implemented in the tool will definitely be different than the answer of the code it is based upon. Verification will thus be based solely on checking whether the produced results are as expected.

A basic check for correct functioning is to enter Weibull parameters in the input file for a material and analyse a monolithic plate of the same material using the FCI module. A constant amplitude (CA) input load cycle should retrieve a number of cycles to crack initiation that follows exactly the Weibull curve generated from the parameters when the values for R and K_t , as used in the simulation, match the ones given along with the SN-data. The example parameters that are used to generate a Weibull curve for this test can be seen from table 7-1. This produces equation 7-1 for the cycles to initiation as a function of stress level, based on

Table 7-1. Example SN-curve parameters

C_1	C_2	C_3	C_4	K_t	R
122	219	4.93	10.31	1.1	0.1

equation 6-25.

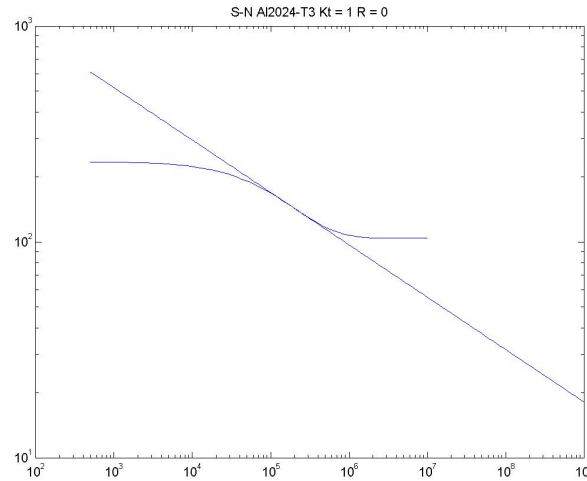
$$N_i = 10 \left(4.93 \left[\ln \left(\frac{219 - 122}{S_a - 122} \right) \right]^{10.31} \right)^{\frac{1}{1.1}} \quad (7-1)$$

The results match well, as can be seen from table 7-2, indicating that the initiation module does its job correctly.

A Wöhler curve as produced by the FCI module is shown in figure 7-2, showing that the linear continuation as described at the end of section 6-3-4 also works well.

Table 7-2. Comparing FCI module results to equation 7-1

S_a	Equation 7-1	FCI module
150	$1.08 \cdot 10^5$	$1.07 \cdot 10^5$
175	$4,95 \cdot 10^4$	$4,90 \cdot 10^4$
200	$1.79 \cdot 10^4$	$1.74 \cdot 10^4$

**Figure 7-2.** A Wöhler curve produced by the initiation module

Initiation analysis of a Glare 2A-6/5-0.4 laminate under tension-bending with positive bending produces the lowest number of cycles to initiation for the metal layer with the highest ply number, which means it is the bottom layer, see the output from the output file for this analysis below. This behaviour can also be regarded as correct, looking at the coordinate system definition in figure 2-2.

#	metal	Damage/flight	Flights to initiation
1	1	1.0000e-009	999999999
3	1	7.0486e-008	14187158
5	1	6.6472e-007	1504390
7	1	3.0430e-006	328618
9	1	9.5124e-006	105126
11	1	2.3484e-005	42582

7-2-3 Crack propagation in standard Glare

The implementation of the Alderliesten fatigue crack propagation (FCP) module is verified by comparing a graphical output of the crack growth rate to the original code, a running version of which is made available to the author. The crack growth rate is chosen, because it is the best for revealing whether the trends in the results of both models match. The finite-width correction in the original version has been removed because it changes the result to such a large extent that comparison becomes rather difficult. The equation for the effective

stress intensity, as used by the original code, had also already been changed to the Schijve equation, see equation 6-33. The codes are used to analyse three different cases to verify whether outputs match:

1. Glare 3-4/3-0.54; $W = 500$ [mm]; $s = 37.5$ [mm]; $a_0 = 38$ [mm]; $S^{\max} = 100$ [MPa]; $R = 0.05$
2. Glare 2A-3/2-0.2; $W = 600$ [mm]; $s = 30$ [mm]; $a_0 = 31$ [mm]; $S^{\max} = 80$ [MPa]; $R = 0.05$
3. Glare 4B-8/7-0.3; $W = 600$ [mm]; $s = 0$ [mm]; $a_0 = 3$ [mm]; $S^{\max} = 120$ [MPa]; $R = 0.05$

All the settings, which were partially hard-coded in the original code, were set equal for both versions of the code. Several of the results from both models are shown in figures 7-3, 7-4, and 7-5 below.

It can be seen from these images that the behaviour of both models is very similar, which shows that the Alderliesten model is correctly implemented. The relatively small difference in crack growth rate can be attributed to the changes in implementation discussed in section 6-4-4 which are not mentioned further here.

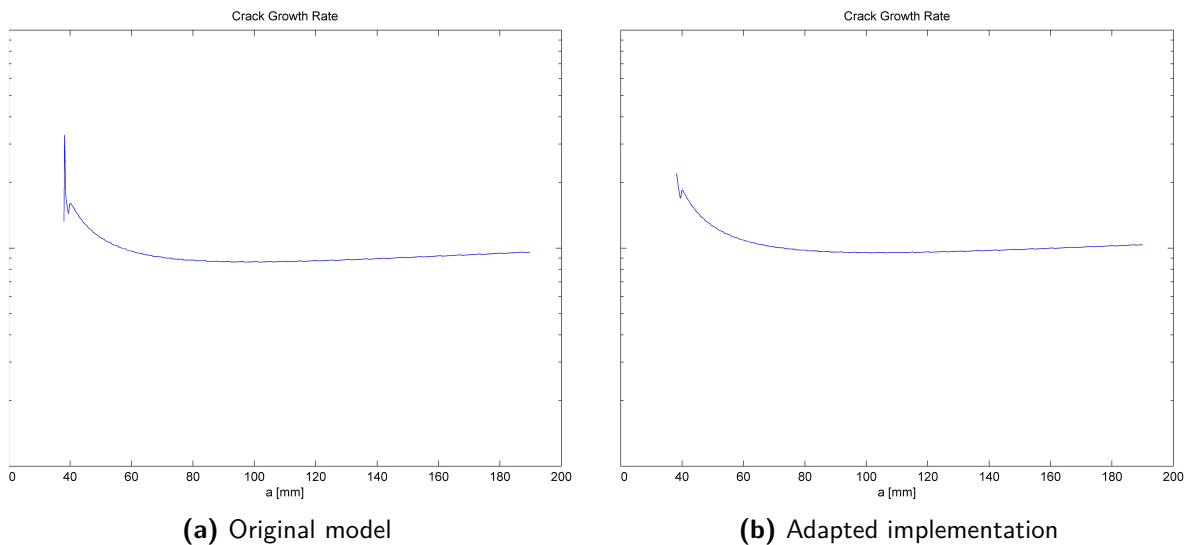


Figure 7-3. Comparing the adapted Alderliesten FCP model output with original for Glare 3-4/3-0.54

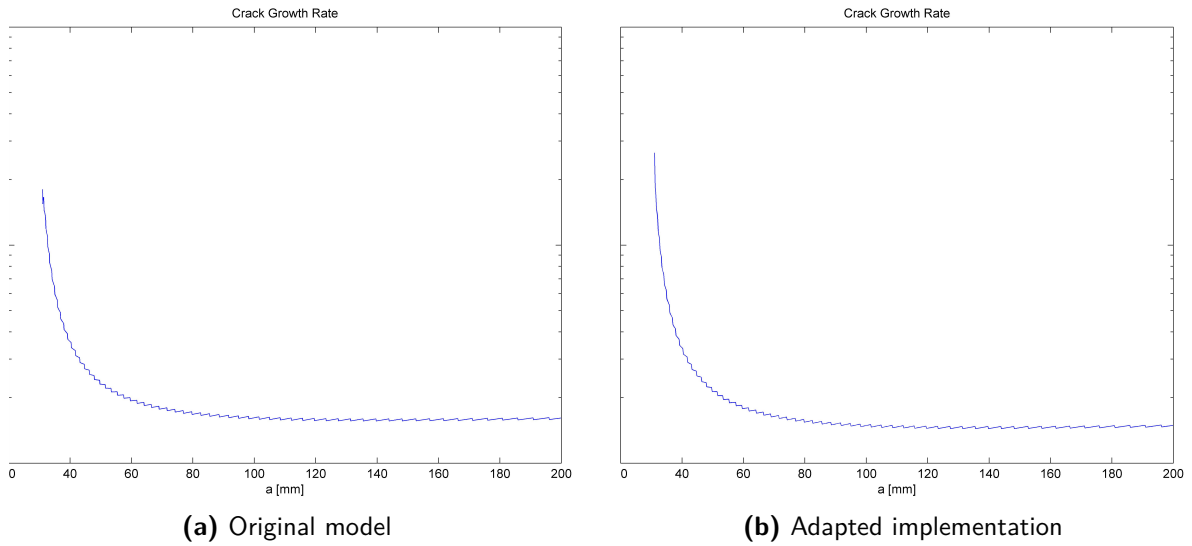


Figure 7-4. Comparing the adapted Alderliesten FCP model output with original for Glare 2A-3/2-0.2

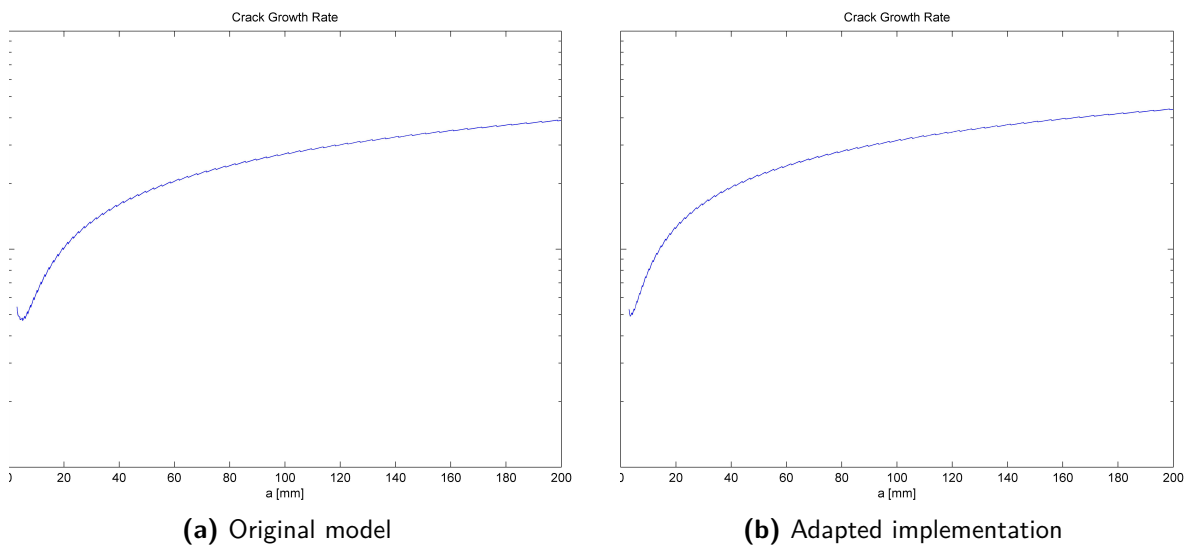


Figure 7-5. Comparing the adapted Alderliesten FCP model output with original for Glare 4B-8/7-0.3

7-2-4 Crack propagation in general FMLs

The Wilson code is verified in the same manner as the Alderliesten code. The 10-point result smoothing, mentioned in section 6-4-5, is not used to produce the results of the original code. The results of the following cases are compared in figures 7-6, 7-7, and 7-8 below. The different colours are used merely to distinguish between the crack growth rates connected to the different cracks existing in the laminate.

As can be seen from the figures, the results match perfectly for the first two test cases and acceptably for the third case. The behaviour of the original and adapted implementation of the Wilson model is still very similar for the third test case. The code is thus deemed to work properly, especially considering the exact match of behaviour in the first two test cases. The cause of the crack growth rate of the adapted implementation being 20 % higher than that computed using the original code is unclear.

1. Glare 2A-7/6-0.5; $W = 200$ [mm]; $s = 5$ [mm]; $a_0 = 6$ [mm]; $S^{\max} = 100$ [MPa]; $R = 0.05$; pure tension
2. Glare 2A-7/6-0.5; $W = 600$ [mm]; $s = 0$ [mm]; $a_0 = 3$ [mm]; $S^{\max} = 120$ [MPa]; $R = 0.05$; Tension/bending
3. [0.60 [mm] Al2024-T3 / 0.24 [mm] FM-94 / 0.60 [mm] Al2024-T3 / 0.24 [mm] FM-94 / 0.266 [mm] 0° S2 & FM-94 / 1.00 [mm] Al2024-T3 / 0.266 [mm] 0° S2 / 0.24 [mm] FM-94 / 2.00 [mm] Al2024-T3]; $W = 600$ [mm]; $s = 30$ [mm]; $a_0 = 31$ [mm]; $S^{\max} = 80$ [MPa]; $R = 0.05$; pure tension

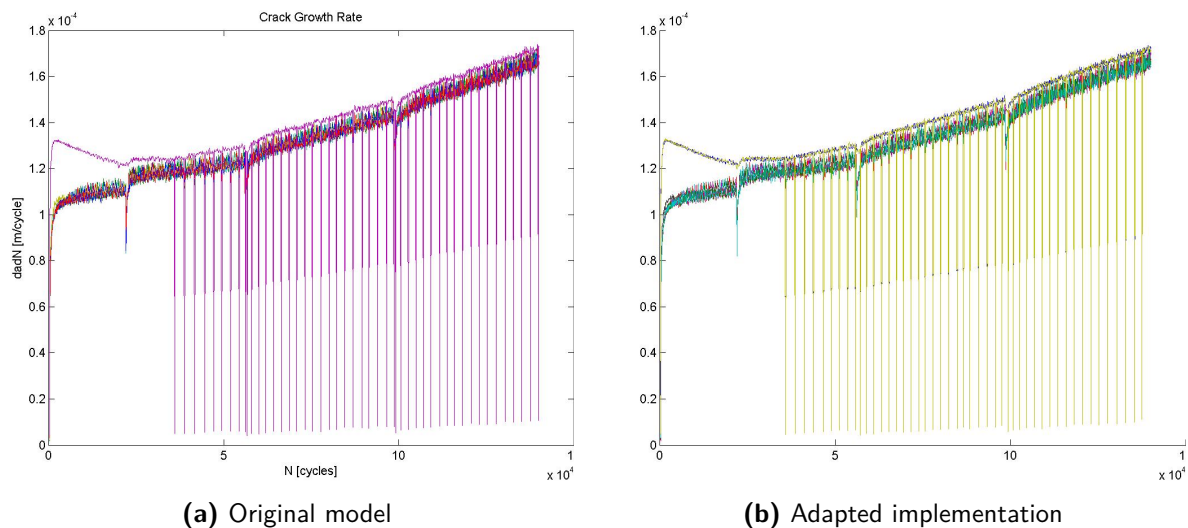


Figure 7-6. Comparing the adapted Wilson FCP model output with original for Glare 2A-7/6-0.5 under pure tension

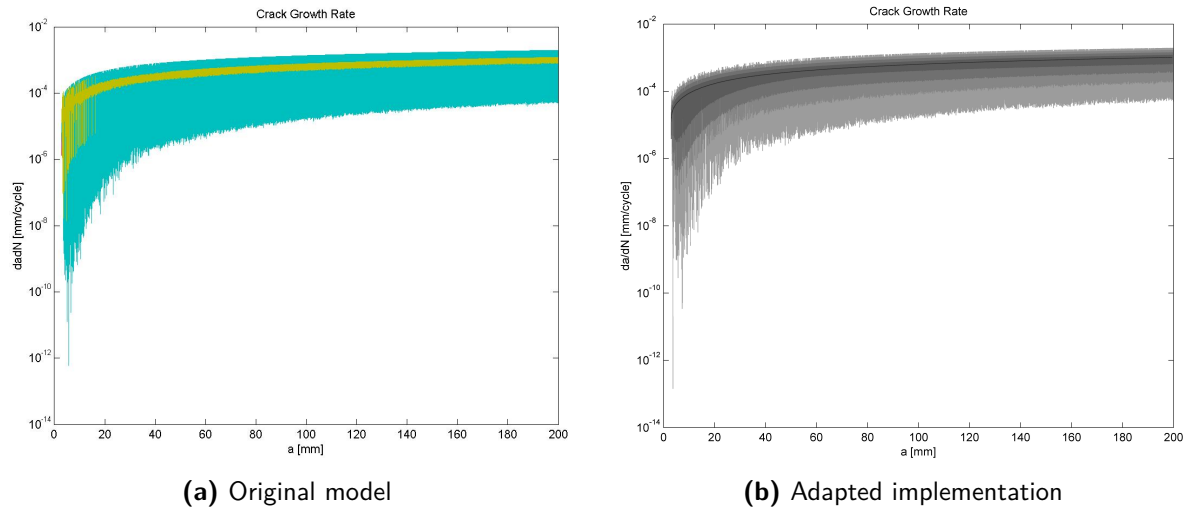


Figure 7-7. Comparing the adapted Wilson FCP model output with original for Glare 2A-7/6-0.5 under combined tension and bending

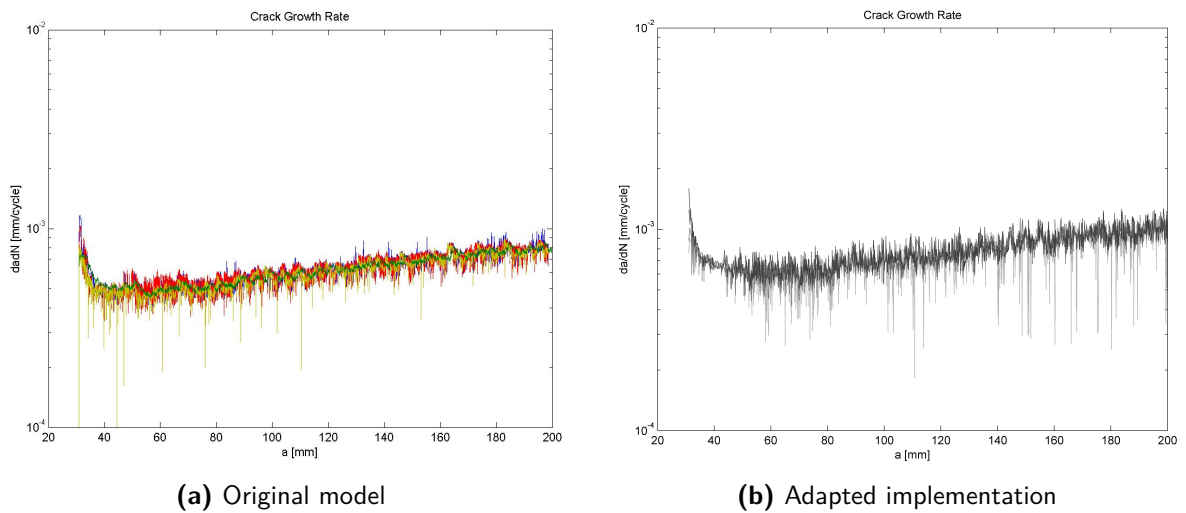


Figure 7-8. Comparing the adapted Wilson FCP model output with original with an asymmetric laminate containing also adhesive layers

7-2-5 Crack propagation under variable amplitude

The correct behaviour of the variable amplitude (VA) Alderliesten model is verified by comparing the results with figures of the output from the Khan model (Khan et al., 2010), because it is unclear how to run the original code properly, and how to retrieve results from it. Only the yield zone model (YZM) is verified, because firstly, that is only model for which original code data is available and secondly, the linear damage accumulation implementation is practically the same as that for the YZM apart from a small amount of lines of code which manage crack growth retardation.

Khan et al. (2010) cite four characteristic load cycle histories: a single overload (OL), multiple OLs, block loading low load - high load and block loading high load - low load. The VA Alderliesten FCP module output is compared with the figures from the paper for all four types of loading, see figures 7-9 until 7-12. As can be seen, all the characteristic behaviour of the 'predictions'-curves in from the paper is closely copied by the VA FCP module and the value of the crack growth rate is also a good match along the curve, although the crack lengths at which the characteristics occur do not match. This difference can be attributed to the fact that the VA FCP code does not trigger the OL application or load block switch on the basis of crack length reached, but on the number of cycles given in the input spectrum. The mismatch of application is thus merely a result of an incorrect number of cycles being applied before a switch in load level is chosen. This is also the cause of the crack growth rate jumping to a higher level again, see figure 7-12b, because simply the end of the spectrum had been reached before the crack length had reached its goal, causing the program to start again from the beginning of the spectrum file, and thus applying cycles of a high load level again.

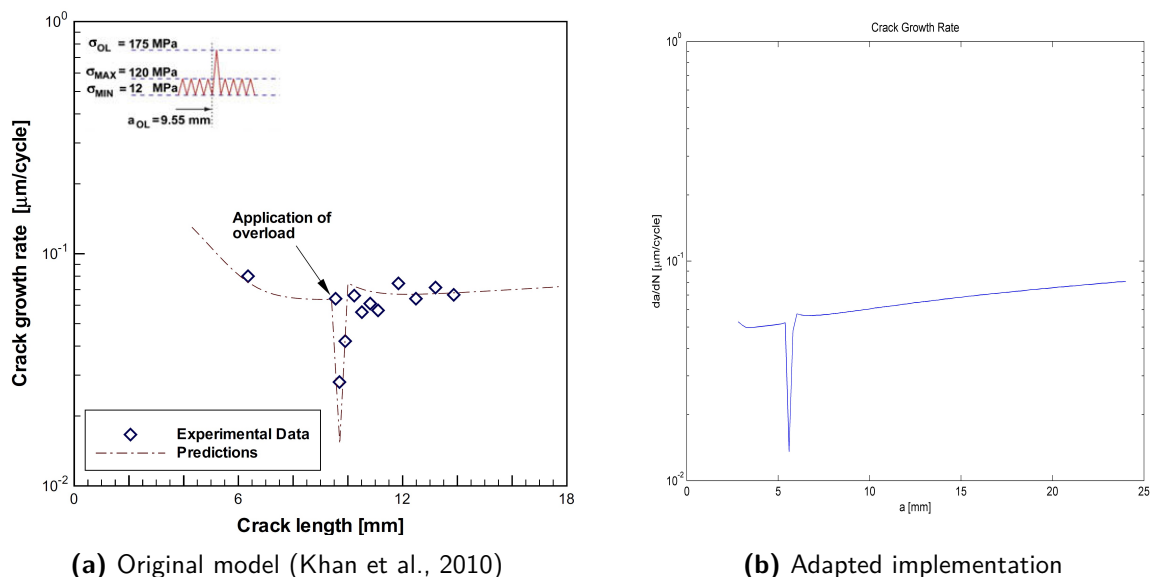
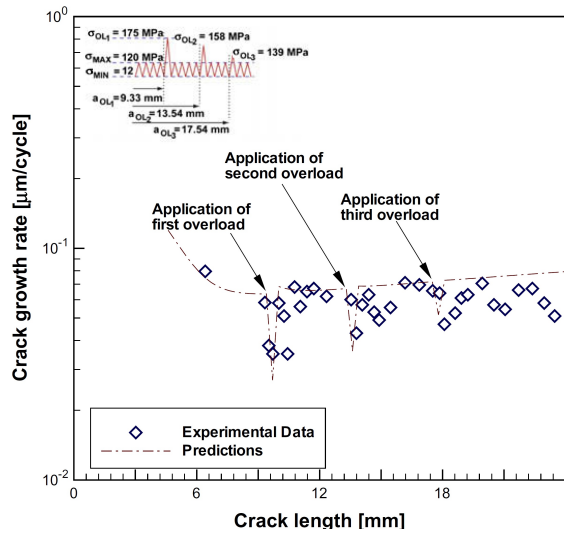
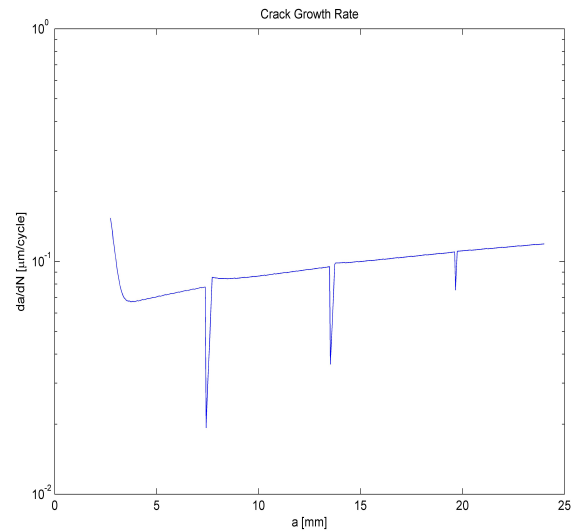


Figure 7-9. Comparing the adapted VA Alderliesten FCP model output with the original for a load history with a single overload

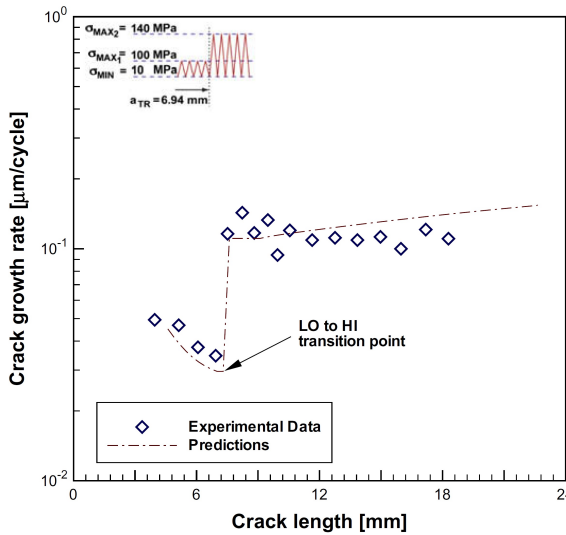


(a) Original model (Khan et al., 2010)

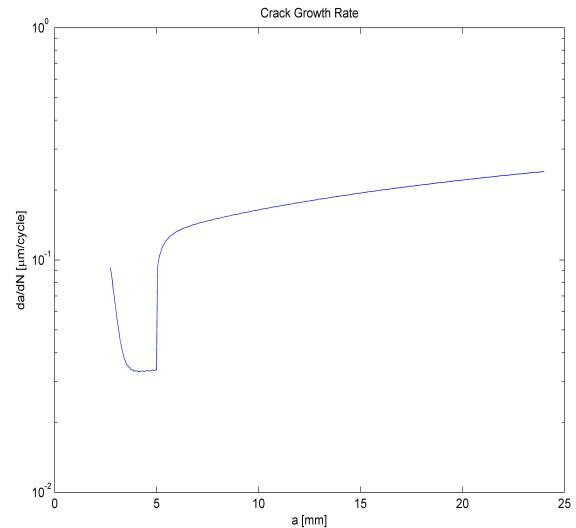


(b) Adapted implementation

Figure 7-10. Comparing the adapted VA Alderliesten FCP model output with the original for a load history with multiple overloads



(a) Original model (Khan et al., 2010)



(b) Adapted implementation

Figure 7-11. Comparing the adapted VA Alderliesten FCP model output with the original for a load history with a low load block followed by a high load block

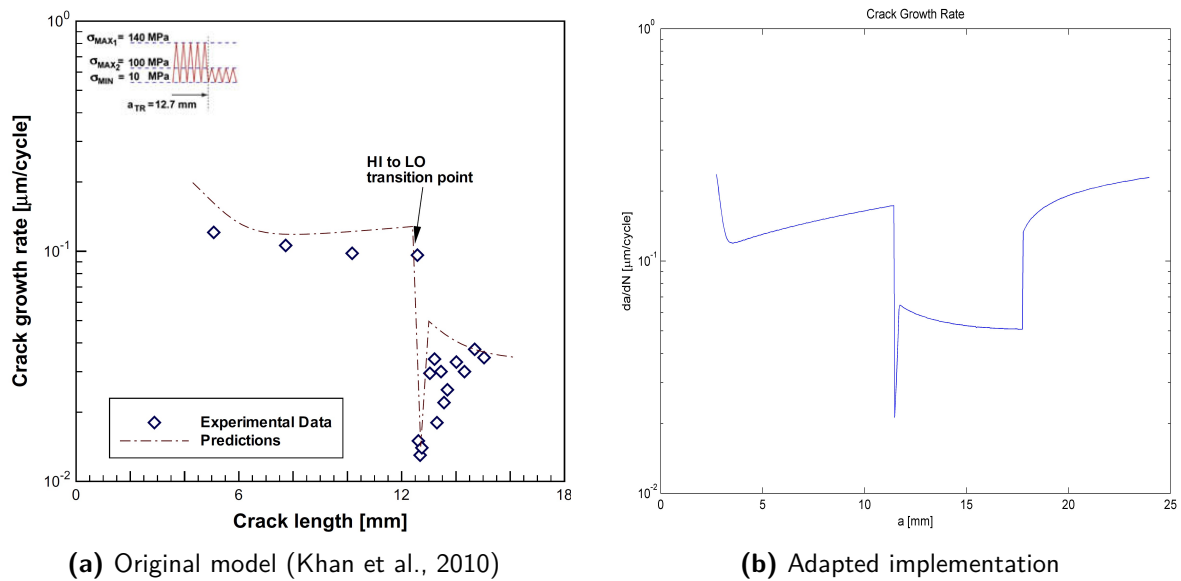


Figure 7-12. Comparing the adapted VA Alderliesten FCP model output with the original for a load history with a high load block followed by a low load block

The VA Wilson FCP code is verified on the basis of the same test case, see figures 7-13 and 7-14. Only the first two cases are run, because of the long runtime required to get to a result. Even though the same spectra are used to create these figures as the ones that have been used to create figures 7-9b and 7-10b, the OLs are occurring at yet another crack length, because the crack growth rate calculated by the Wilson code does not exactly match the crack growth rate obtained by the Alderliesten code. This results in the third OL not being applied for the multiple OL spectrum, because only two low spikes can be seen in figure 7-14.

The VA versions of both the Alderliesten and the Wilson FCP module are also tested with CA cases from sections 7-2-3 and 7-2-4, respectively. The produced graphs are exact matches with the results coming from the CA counterparts and are thus not shown here. This shows that the original capabilities of the module have not been altered by the VA additions, apart from the fact that adding VA capability increases the runtime tenfold for either model.

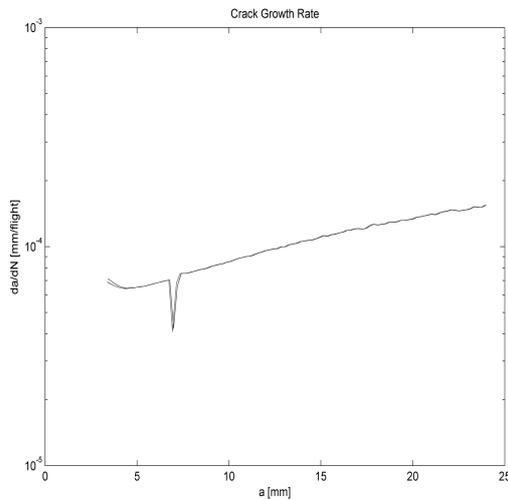


Figure 7-13. Running the spectrum with a single overload with the VA Wilson FCP module

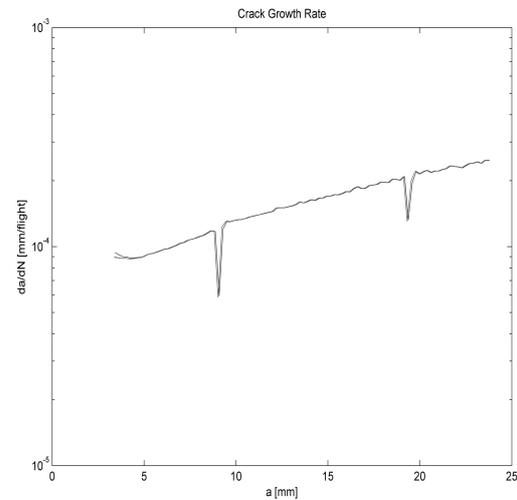


Figure 7-14. Running the spectrum with multiple overloads with the VA Wilson FCP module

7-3 Validation of individual modules

Validation is about answering the question of whether a correct object, in this case the correct code, has been produced, rather than whether the code has been produced correctly, the latter question was answered in the previous section on verification. The findings on whether the code is capable of first, being used to assess the accuracy of the previously used design method for the Glare reinforced frame flange of the A400M and two, being used to find room for improvement of the design that resulted from this method, i.e. the goals of this research, are collected in this section.

Validation is performed by checking whether the outcomes of the modules match reality in the form of test results. This match needs to be confirmed in both the magnitude of the results and the trend they show.

7-3-1 Static strength estimation

A static strength test on a Glare 2A-16/15-0.4 FML attached to a 5.2 millimetre-thick Al7085-T7068 plate with an interface of two zero-degree prepreg layers and an adhesive layer showed yielding at an average stress of about 360 [MPa] and failed at an average stress of about 450 [MPa] Klein (2011).

The material properties for Al7085-T7651 shown in table 7-3 were taken from MMPDS-06 (William J. Hughes Technical Center, United States., 2011), and it was assumed that these values should also match the values for heat treatment T7068 well.

The static strength module estimates failure of the same laminate at a line load of $5.57 \cdot 10^3$ [N/mm], or an average stress of $\frac{5.57 \cdot 10^3}{16} = 348$ [MPa] because the laminate thickness is 16 [mm], using the maximum stress criterion. An average failure stress of 353 [MPa] is estimated using the Tsai-Wu criterion.

Table 7-3. Aluminium 7085 Properties (William J. Hughes Technical Center, United States., 2011)

Description	Value	
	L	LT
Young's modulus [MPa]	69600	
Tensile ultimate strength [MPa]	517	503
Compressive ultimate strength [MPa]	496	503
Shear modulus [MPa]	26900	
Poisson's ratio [-]	0.33	
Coefficient of thermal expansion [$1/^\circ C$]	$2.47 \cdot 10^{-5}$	

This is a very good match, considering the amount of variables in the laminate and how severe the assumptions are that were made to implement of the static strength module.

7-3-2 Initiation

Accurately predicting the cycles to initiation is very difficult. First, the phenomenon is highly dependent on material surface quality and even the smallest defect can have a tremendous effect on the amount of cycles that is needed to reach a 1 millimetre crack length. Second, the exact condition of the surface quality is often not known. Third, the SN-curves to compare the data against are on their turn based on a collection of cycles to initiation containing their own amount of scatter, and an exactly matching SN-curve, i.e. with the same K_t , R and for exactly the same material and environmental conditions, is not always available. Finally, the load cycle that causes the crack initiation to occur might not be precisely known, due to the variability of residual stress levels, inaccuracies in the model that calculates stress levels, or because the dimensions of the test object are not exactly as stated, and a small error in the stress amplitude is amplified by the fact that it is used to find the cycles to initiation on a logarithmic scale, especially for low stress amplitudes. All the above are reasons to consider a prediction that is less than 10 times different from test results to be fairly accurate.

Table 7-4 contains the SN-curve data for the various materials that is available to the author

The test results for crack initiation in standard Glare due to pure tension of Homan (2006) are compared to output from the FCI module at the same applied stress levels in figure 7-15. The results match very closely in terms of value and trend for all three test cases, although the match is not as good as for the other test data for the high and low stress amplitudes of the test at $K_t = 1.06$, but these tests are the most sensitive to surface quality.

Table 7-4. Weibull parameters for a few materials that can be used to construct SN-curves using equation 6-25

Material	C_1	C_2	C_3	C_4	K_t	R	Source
Al2024-T3	30	235	4.08	3.49	2.7	0.17	(Homan and Schra, 2002)
Al2024-T3	122	219	4.93	10.31	1.1	0.1	(Homan and Schra, 2002)
Al2024-T3	104	235	5.19	9.01	1.0	0.0	(IASB, 1986)
Al2024-T3	63	235	4.59	5.26	2.0	0.0	(IASB, 1986)
Al2024-T3	53	235	4.32	3.86	2.5	0.0	(IASB, 1986)
Al2024-T3	35	235	3.92	2.52	3.6	0.0	(IASB, 1986)
Al2024-T81	25	494	2.22	1.14	4.4	0.0	(ASM International, 1995)
Al2024-T81	96	459	3.83	2.14	1.0	0.0	(ASM International, 1995)
Al7475-T761	63	211	5.08	8.05	1.0	0.1	(IASB, 1987)
Al7475-T761	36	211	4.48	4.16	2.5	0.1	(IASB, 1987)
Al7475-T761	35	211	4.04	3.88	3.6	0.1	(IASB, 1987)

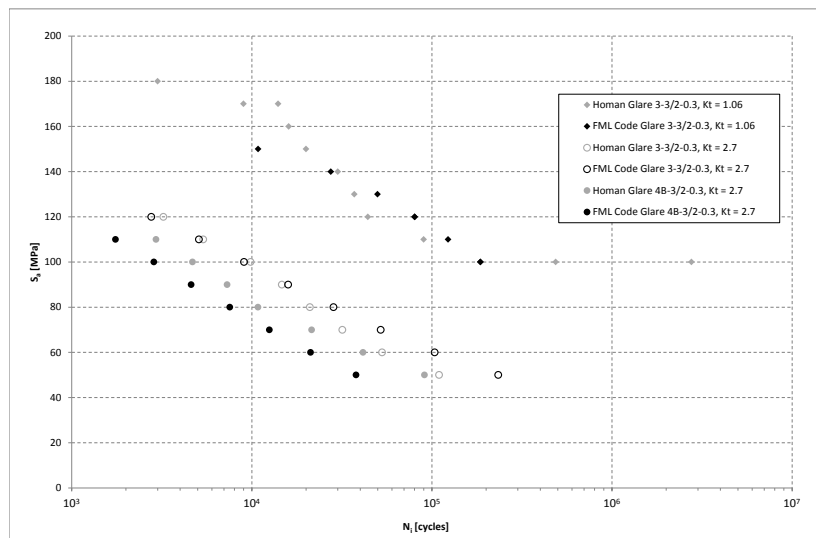


Figure 7-15. Comparing FCI module outputs with Glare test data by Homan (2006)

Randell (2005) has tested standard Glare specimens with an open hole under combined tension and bending. The crack initiation results of these tests are displayed in table 7-5, along with the predictions from the FCI module. Note: because the bending factor used by Randell (2005) was not properly defined, it is not certain whether setting the ratio of mid-plane strain to outer surface strain equal to the factor mentioned in the report produces the correct amount of bending. The column named Factor in table 7-5 is the ratio of FCI code N_i value to the N_i value found by Randell. The maximum normalised factor is the maximum value of either the factor or its inverse for initiation of that layer. This column is added because the author considers a factor of 0.5 equally accurate as a factor of 2.0, and thus the values in the rightmost column allow for an easy comparison. The column termed # refers to the specimen ID given by Randell, where L stands for the left side and R for the right side.

It can be concluded from the Factor column in table 7-5 that the FCI model almost consistently underestimates the cycles to crack initiation for the surface layer and consistently overestimates the cycles to crack initiation for the second subsurface layer. Applying a moment that is too severe compared to the test situation because of the uncertainty mentioned in the previous paragraph could be an explanation for this behaviour. Another explanation for the increasing overestimation of the cycles to crack initiation as the layers are initiated later, could be that the assumption that the presence of a crack in one layer does not affect crack initiation in the others is invalid.

The rightmost column of table 7-5 still shows that the match between test results and FCI model predictions are reasonable in terms of both value, especially for the first subsurface layers, and trend. The deeper the layer, the lower the bending moment, and thus the more cycles to crack initiation that are required, as reflected in the test results and the model output.

So far, only the CA FCI results have been validated. The author recommends validating whether the crack initiation module also produces correct results for VA spectrum loading.

7-3-3 Crack propagation in standard Glare

Validation of the Alderliesten FCP model was done by Alderliesten (2005). This also validates to a certain extent the implementation of this model for the research described in this report, because in section 7-2-3 it was established that results produced from both models were practically the same.

From figure 7-16 it can be seen that the agreement of the adapted implementation agrees with the test data given by Alderliesten (2005). The blue line is the output of the Alderliesten module as included in the tool for Glare 3-4/3-0.54 under a stress of 100 [MPa] with a load ratio of 0.05. The squares and diamonds show test results and the lower solid black line shows the output of Alderliesten's model in its original form. The most striking difference is that the result of the adapted implementation in the tool becomes horizontal towards larger crack lengths instead of increasing, which is solely due to the absence of a finite width-correction. The vertical shift is due to all the other differences mentioned in section 6-4-4. Agreement with the test data is still fair, and more conservative than the original model for lower crack lengths.

Wilson (2007) pointed out the relatively bad convergence of the Alderliesten FCP code, and suggested a varying element width that is biased towards the crack tip. This is also

Table 7-5. Comparing FCI module results with test data by Randell (2005)

Specimen	Layer	Randell #	N_i	FCI code N_i	Factor	Max. norm. factor				
Glare 2A-5/4-0.4 $W = 100$ $S_a = 80$	surface layer:	1L	66000	14153	0.21	4.66				
		1R	66000		0.21					
	1 st subsurface:	1L	108000	92346	0.86	1.62				
		1R	150000		0.62					
	2 nd subsurface:	1L	258000	1692308	6.56	6.56				
		1R	300000		5.64					
Glare 2A-5/4-0.4 $W = 50$ $S_a = 80$	surface layer:	2L	40000	12679	0.32	3.15				
		2R	40000		0.32					
		4L	35000		0.36					
		4R	30000		0.42					
	1 st subsurface:	2L	100000	92346	0.92	1.52				
		2R	70000		1.32					
		4L	110000		0.84					
		4R	140000		0.66					
	2 nd subsurface:	2L	150000	1692308	11.28	11.28				
		2R	150000		11.28					
		Glare 2A-5/4-0.4 $W = 50$ $S_a = 100$	surface layer:		5L		30000	6048	0.20	4.96
					5R		20000		0.30	
6L	25000			0.24						
6R	25000			0.24						
1 st subsurface:	5L		40000	47231	1.18	1.18				
	5R		55000		0.86					
2 nd subsurface:	6L	45000	558671	1.05	6.98					
	6R	55000		0.86						
	5L	100000		5.59						
	5R	80000		6.98						
Glare 2A-6/5-0.4 $W = 50$ $S_a = 100$	surface layer:	7L	40000	39424	0.99	1.27				
		7R	50000		0.79					
	1 st subsurface:	7L	45000	96924	2.15	2.15				
		7R	50000		1.94					
	2 nd subsurface:	7L	80000	283726	3.55	5.67				
		7R	50000		5.67					
	Glare 2A-6/5-0.4 $W = 100$ $S_a = 100$	surface layer:	8L	70000	42581	0.61	1.64			
			8R	50000		0.85				
			9L	40000		1.06				
			9R	40000		1.06				
		1 st subsurface:	8L	70000	105126	1.50	1.75			
			8R	60000		1.75				
9L			60000	1.75						
9R			60000	1.75						
2 nd subsurface:		8L	80000	328618	4.11	5.48				
		8R	60000		5.48					
		9L	70000		4.69					
		9R	70000		4.69					

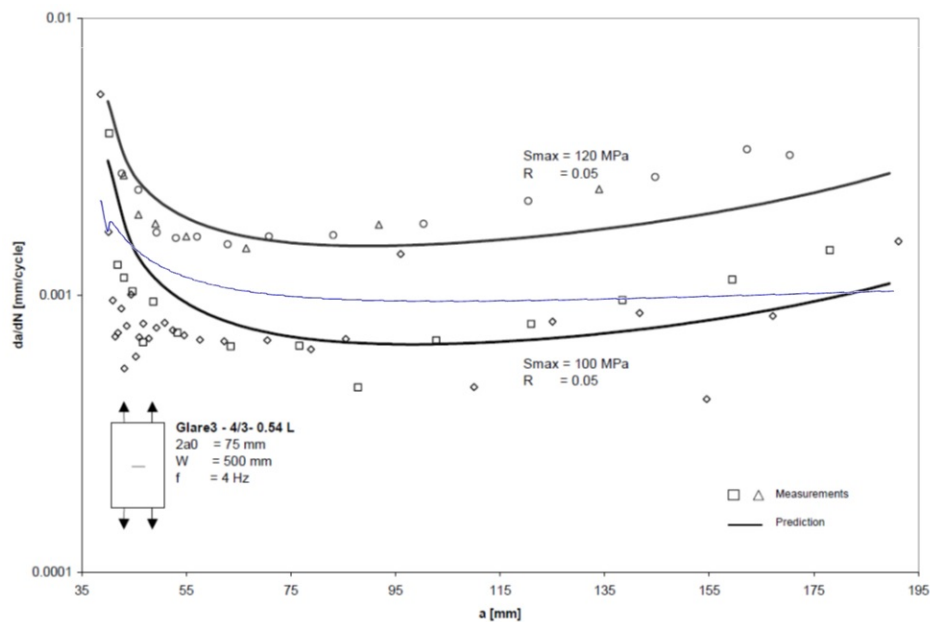


Figure 7-16. Comparing the adapted Alderliesten FCP module output with original output and test data by Alderliesten (2005)

implemented in the adapted implementation of the model, see section 6-4-4. The convergence issue has not been solved with this solution, because the crack tip stress intensity still relies largely on the user-specified maximum tip-element width, see figure 7-17. From figure 7-18 it can be seen that there is still convergence, but this convergence is not towards the correct answer. At a w_{max} of about 0.01 [mm], the Alderliesten model starts predicting a crack growth rate that is too low. A reason for this could be that the model diverges from reality, because in real life the fibres could delaminate in bundles rather than fibre per fibre, so reducing the element width below this bundle size does not create a delamination shape that is more accurate. This explanation suggests that the Wilson FCP model should show the same non-converging behaviour. This is not the case, as can be seen in the next section. Alderliesten advises no specific element width in his dissertation, but a value of around 0.01 [mm] seems to work rather accurately.

Alderliesten (2005) tested a large amount of Glare 3 and Glare 4B specimens to validate his model, but no Glare 2A laminates were tested. The model is expected to behave well for Glare 2A laminates because two different Glare grades have been modelled successfully. Since no Glare 2A data was available to the author, it is recommended that the results of the model are first validated using Glare 2A data before relying on the model for predictions.

7-3-4 Crack propagation in general FMLs

A near exact match between the original Wilson code and the version that is part of the tool that is developed for this research is shown in figures 7-6, 7-7, and 7-8, which means the code in the tool connected to this report works exactly in the same manner as the original. The steps taken by Wilson (2013) to validate the model therefore also validate the version which is included in the tool.

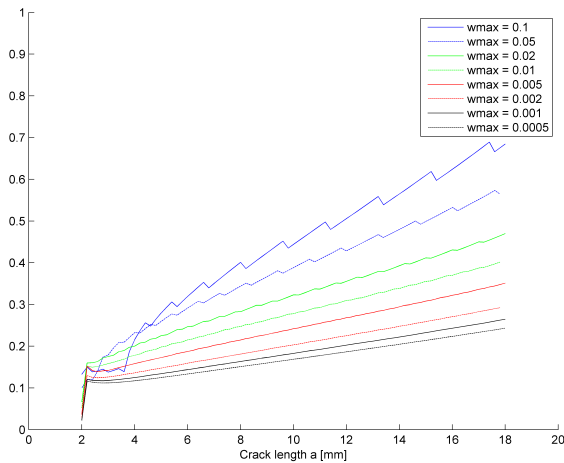


Figure 7-17. Calculation of crack growth rate with several values for w_{\max}

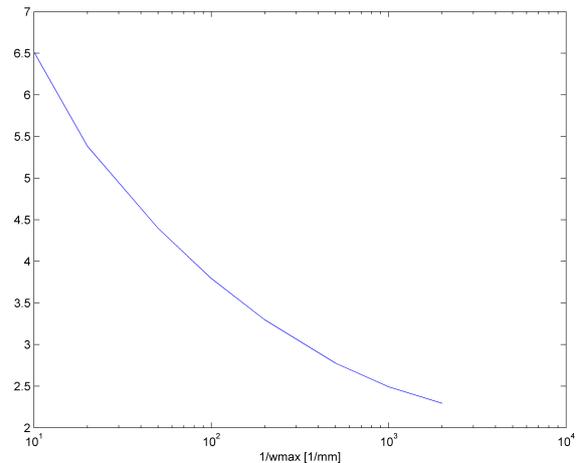


Figure 7-18. Convergence of the crack growth rate at a crack length of 16.6 [mm]

An example of the agreement between model and test results for a laminate including thick Al2024-T3 layers and extra adhesive layers, laminate 0 taken from the dissertation of Wilson (2013), is given in figure 7-19. Multiple model output curves are given in the figure, they all belong to the same run, but describe cracking in a different metal layer. The two curves that start differently from the rest are the bottom and top surface layers. Several test results are given in the figure, all of which are taken from Wilson's dissertation. The specimen that was tested up to a crack length of about 90 [mm] is also modelled using the Wilson FCP code in the tool of this research; it can be seen that the order of magnitude of the crack growth rate matches reasonably, but the trend does not: the model shows a too fast increase of crack growth rate. This is consistent with the results of the runs given in Wilson's dissertation, hence there is a general problem with the code rather than one solely connected to the implementation in the tool. Wilson attributes this to an overprediction by the model of the growth of internal delaminations with respect to the test situation, which is supported by destructive inspections of tested specimens. This overprediction, Wilson says, is likely to be caused by the tendency of delaminations to grow together in his model, which in its turn might be due to the manner in which leapfrogging is detected and mitigated in the code.

An example of the agreement of the Wilson model in the case where bending is applied to a standard Glare laminate is given in figure 7-20. The coloured lines indicate the adapted implementation of the Wilson FCP model, the thick black lines the original. It can be seen that the trends are copied very well, but that the values are off. Since the other comparisons had good matches for both, this shows that the moment applied to the model is probably not the same as in the test results, as already mentioned in section 7-3-2.

The Wilson code has no convergence issue, as can be seen by the excellent agreement between the crack growth rates of figures 7-21a and 7-21b: even though the coarse mesh shows a much larger variation, this variation is exactly around the curve that is produced with the finer mesh. Again a multitude of curves is seen in both figures, although much clearer in figure 7-21a, which shows the results for a large element size. Every curve describes the crack growth rate of a different metal layer during the same analysis. For the larger element size, the difference in behaviour of the surface layers is larger compared to the smaller element size. It

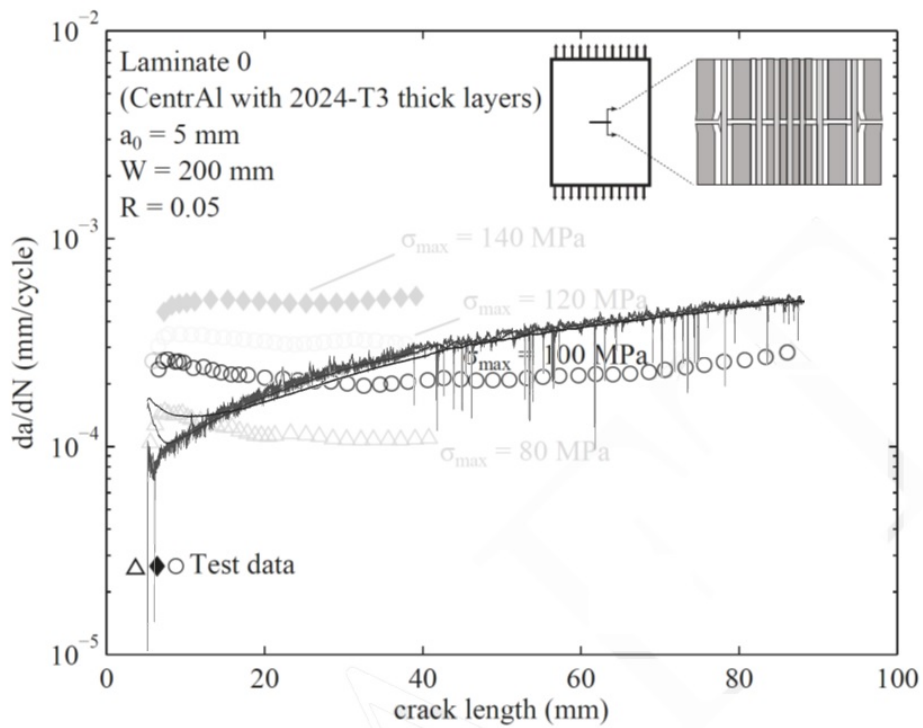


Figure 7-19. Comparing adapted Wilson FCP module output with test data by Wilson (2013)

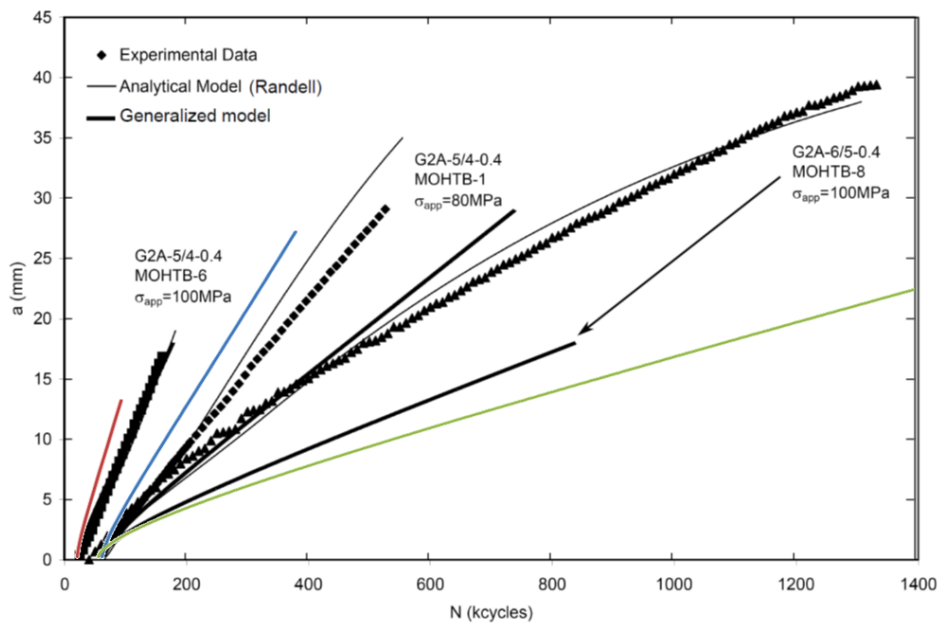


Figure 7-20. Comparing adapted Wilson FCP module output with test data by Randell (2005)

can be seen in figure 7-21a, that the top and bottom metal layer show a higher crack growth rate yet with deeper peaks, compared to the subsurface layers.

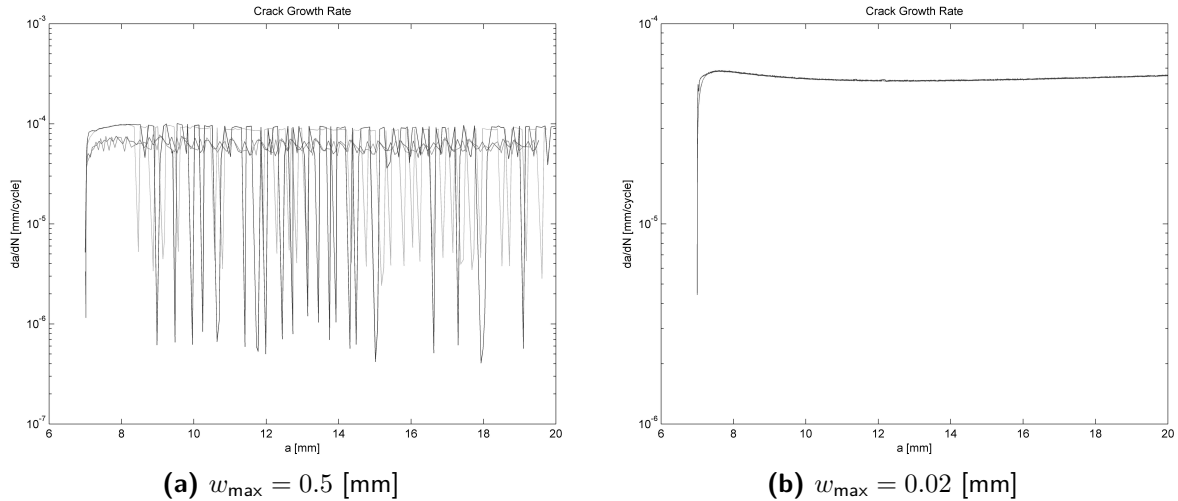


Figure 7-21. Analysing Glare 2A-4/3-0.4 with the Wilson FCP code for different values of w_{\max}

7-3-5 Crack propagation under variable amplitude

Validation of the VA model is performed on the basis of the test results given by Khan (2013), which were included in the figures in section 7-2-5. It can be seen that the adapted models follow all the trends and magnitudes of the test data correctly. The match for the VA Alderliesten model can possibly be improved by using a different maximum element width from the 0.01 [mm] used to produce the curves. The moment of application of the overload or different load block can be adapted by choosing a different number of cycles.

The new formulation of the yield zone model seems to have improved the accuracy of the VA code. This can be concluded by comparing the adapted model output, shown in figure 7-22b, with the test results and original model output, shown in 7-22a. The graph produced by the adapted model is below the one of the original code. This means that the new formulation takes into account more crack growth retardation than the formulation by Khan, and it can be seen from comparing the figures that it results in a better match between the model output and the test data.

7-4 Validation of combinations of modules

The tool that is developed for the research described in this report is intended to be used to predict the fatigue life of specimens from a pristine part to a certain crack length that is larger than a millimetre. This means that a combination of two modules working together also needs to be validated. There is some test data available to compare the output of the combined use of modules to, this comparison is made in this section.

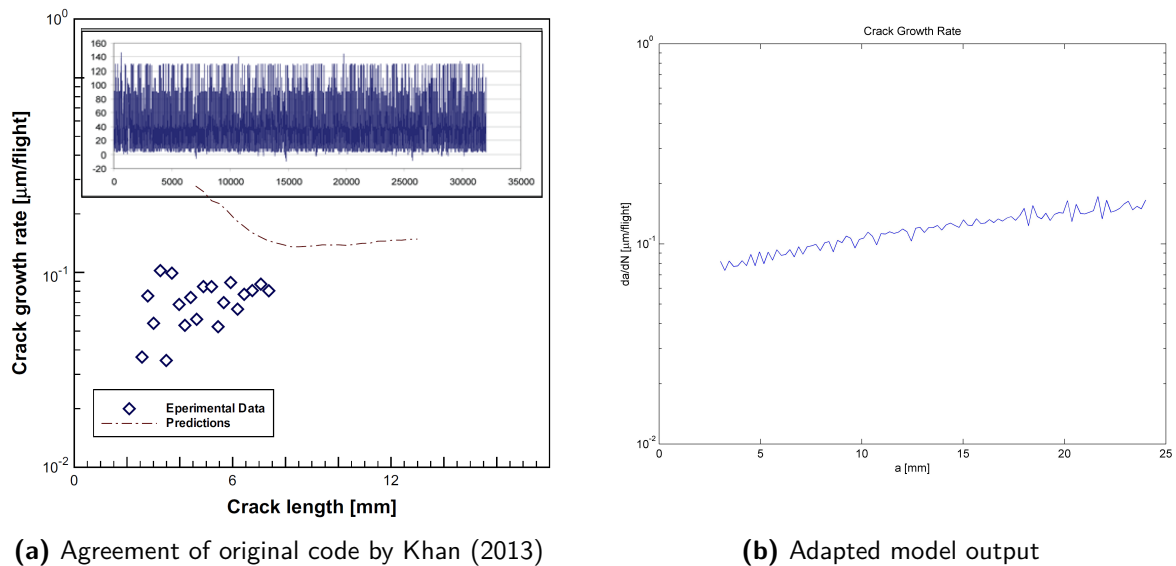


Figure 7-22. Comparing the agreement of the new VA Alderliesten model with the original for 'Spectrum 2' (Khan, 2013)

7-4-1 Constant amplitude FCI and FCP

Randell (2005) tested Glare 2A open hole specimens in combined tension and bending up to failure. Since no starter notch was applied to the specimens, crack initiation also needed to take place. Running the FCI and Wilson FCP module with delayed crack initiation produces the grey lines shown in figure 7-23a. The longer, black lines are results from Randell's own model. The trends match, i.e. the first ply that initiates has the highest slope, but the values do not. It can be seen that the crack growth model assumes a crack of 1 [mm] when a ply initiates. It was already known that a large variation in cycles to initiation was to be expected. Running the Wilson FCP module with delayed initiation using the cycles to crack initiation from Randell (2005) produces the gray lines in figure 7-23b. The points of initiation now line up, but the slopes are still not accurate. The accuracy is approximately equal to the original Wilson FCP model (Wilson, 2013), but where Wilson used three cracked plies from the start, the implementation connected to the research described in this report inserts the cracks when the respective plies have surpassed their cycles to crack initiation.

There is test data available for the cycles to small crack lengths of a Glare 2A-16/15-0.4 FML attached to a 5.2 millimetre-thick Al7085-T7068 plate with an interface of two zero-degree prepreg layers and an adhesive layer subjected to purely tensional CA load cycles (Klein, 2011). This requires a combination of the FCI and generalised FCP modules, because even though the tests had been done to find the cycles to crack initiation for different stress levels, the crack detection was delayed until cracks emanated from underneath the unloaded bolts that were also installed. The smallest observable crack had a length between 7 and 8 [mm], because of the bolt size and detection equipment used.

No FCI properties of Al7085-T7068 were available to the author that could be read by the code, since the only source of data found that contained fatigue properties of this material used a different equation to describe the SN-curve and fitting a different type of curve was

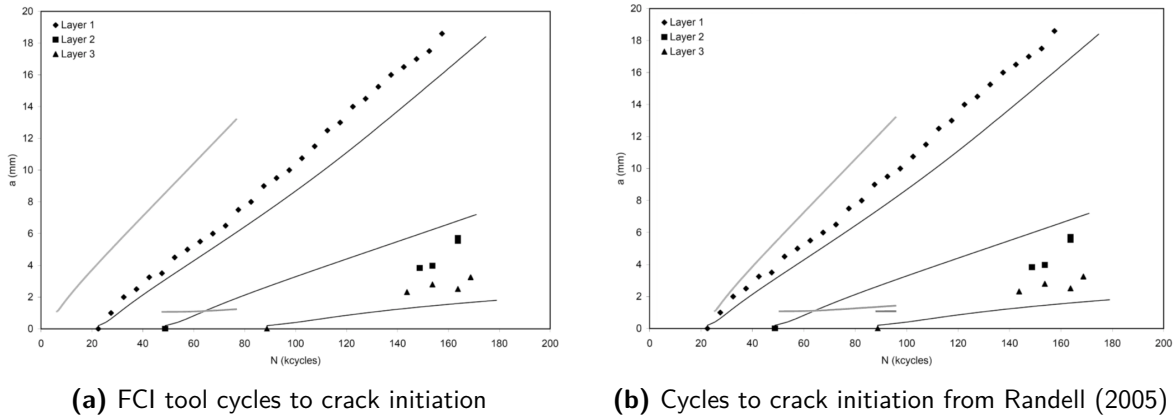


Figure 7-23. Comparing the VA Wilson FCP model output with delayed crack initiation with test data by Randell (2005), the grey lines are produced by the Wilson model

not easily done and therefore not carried out for this validation (William J. Hughes Technical Center, United States., 2011; IASB, 1994). The material is assumed to behave similar to Al7475-T761 in terms of initiation, Weibull parameters for that material were available to the author, see table 7-4. It is recommended that, to increase the accuracy of the FCI prediction, either Weibull parameter data is generated for Al7085-T7068, or the compatibility of the tool is expanded so it can handle more types of descriptions of SN-curves.

Crack propagation properties of Al7085-T7068 were provided by Airbus in the form of Paris parameters and Elber law constants, see table 7-6 (Th. Beumler, personal communication, May 13th, 2013). The Elber law matches the Schijve equation, see equation 6-33, in the tensile stress regime when the quadratic term of the latter is set to zero. The given values for the Elber law are therefore simply entered into the Schijve equation, because the stress ratio for tests was 0.1, indicating there was only tensile stress applied on the specimens. The equation for the effective stress intensity ratio in Al7085-T7068 thus becomes:

$$\Delta K_{\text{eff}} = (0.70 + 0.3R_{\text{tip}}) (1 - R_{\text{tip}}) K_{\text{tip}}^{\text{max}} \quad (7-2)$$

Table 7-6. Al7085-T7068 crack growth properties provided by Airbus (Th. Beumler, personal communication, May 13th, 2013), related to crack growth in [mm/cycle] and stress intensity in [MPa√mm]

C_{cg}	$2.406 \cdot 10^{-7}$
n_{cg}	1.5
Elber A parameter	0.70
Elber B parameter	0.3

The results of the tests and the predictions made with the model can be found in table 7-7. The #-column contains the specimen number from the test, followed by the testing stress amplitude, the crack length measured in the test, the cycles to the given crack length, the cycles to crack initiation by the model and the cycles to the given crack length by the model, respectively. The rightmost two columns show the factor of test result to model prediction and the normalised version of this factor, similar to the one in the rightmost column in table 7-5.

The results show a good match, considering the amount of variation that can be expected in the results of crack initiation experiments. This shows to some extent that it is a reasonable assumption to take the Glare-influenced K_t value rather than the monolithic value, although more testing is required to form a definitive answer on the accuracy of this assumption. It was a crack on the monolithic aluminium side that reached the indicated crack length first in all the model outputs and all the test results.

Table 7-7. Comparing model results with tests from Klein (2011), $R = 0.1$ and using equation 6-10 for K_t

#	S_a [MPa]	a_{detect} [mm]	N_{test}	$N_{i,\text{model}}$	N_{model}	factor	norm. fact.
1	100	7	18219	13517	20072	1,10	1,10
2	75	8	38873	56832	59670	1,53	1,53
4	125	7	10766	1994	7297	0,68	1,48
5	87,5	8	22445	26906	34288	1,53	1,53
6	62,5	8	52505	108773	111727	2,13	2,13
7	50	8	109797	237855	241975	2,20	2,20
8	39	7	3000000	568193	572955	0,19	5,24
10	45,31	8	626900	335867	340621	0,54	1,84

The results of two FCP tests from Klein (2011) and the corresponding model outputs are shown in figure 7-24. Only the leading cracks are shown in the figure, even though fatigue cracks emerged from all eight bolts in both tests.

The point of crack initiation in the flange is given a larger number of cycles to initiation than test results in both cases, which could be an indication that the reduction in stress concentration due to the anisotropy of Glare 2A is not experienced as strong by the flange as it is by the thin metal layers of the Glare strap. The crack growth in the flange is also slightly overestimated by the model in both cases, although the agreement is still reasonable as was also found above. The stress intensity as calculated for the crack tip in the monolithic layer might be less valid for the flange because metal layer deformation could start to play a role in the equation for bridging stress. The data set, however, is far too small to draw a more specific conclusion than that the model shows a reasonable agreement with the test data. More testing is advised to investigate the influence of the flange on the crack propagation in the reinforcing strap.

The author advises that more validation is done to make sure moments and thick monolithic layers are modelled correctly by the program, even though the program already shows a reasonable match for combined tension and bending load cycles.

7-4-2 Variable amplitude FCI and FCP

No test data was available to the author for VA FCI followed by FCP. The author recommends strongly that this data is generated to provide validation of this part of the model before it is used for predictions, although the previous sections suggest that it will work properly. A description of the validation for the VA part is given in subsection 7-3-5 and for the FCI and FCP parts in subsections 7-3-2 and 7-3-4, validating all subcomponents of the complete code. The CA variant of combined FCI and FCP also works well, see subsection 7-4-1.

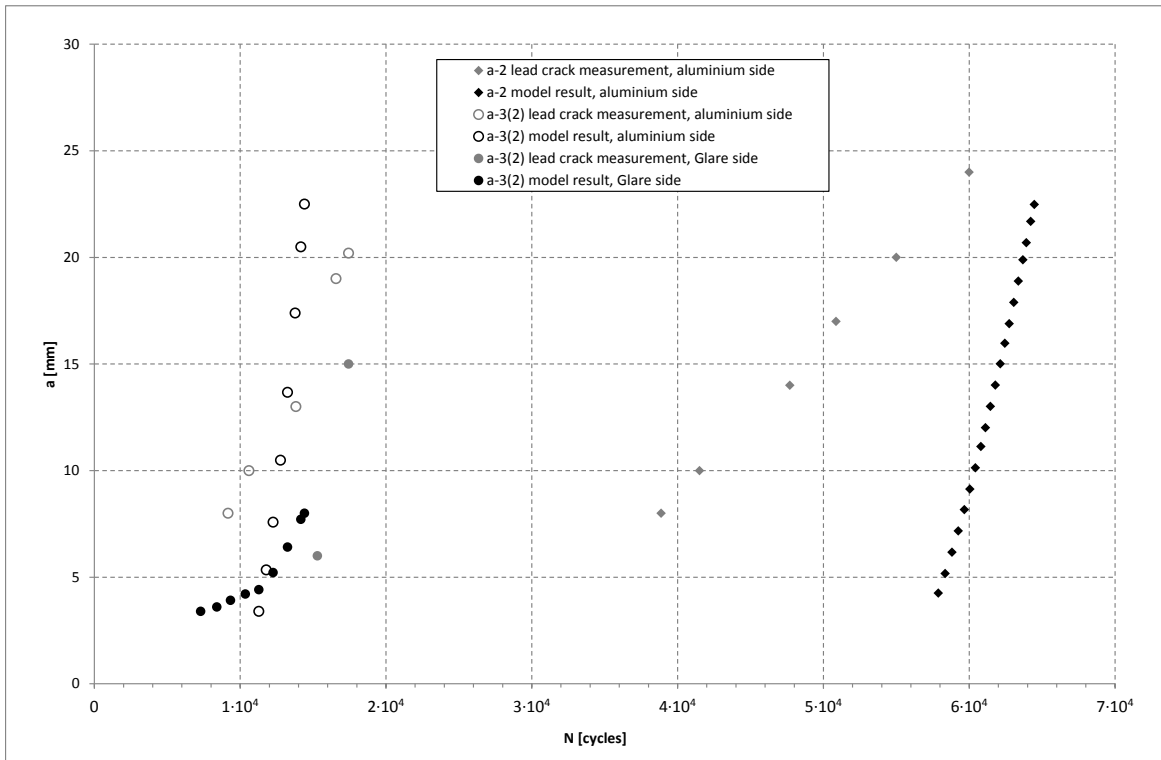


Figure 7-24. Comparing model output of combined FCI and FCP to results by Klein (2011)

7-5 The influence of run parameters

There are three numerical parameters that influence the way the FCP modules are run: b_0 , w_{\max} , and the number of updates per element. The effect of all three for both FCP codes is explained in this section.

b_0 is the initial delamination size in millimeters, it is inserted for $b(a_s)$ in equation 6-26 to calculate the initial delamination shape. For both the Alderliesten FCP code and the Wilson FCP code changing b_0 has little effect. Figure 7-25 shows that the only influence of changing b_0 on the produced result with the Alderliesten model is an initial vertical line. The absence of influence of the initial delamination shape on the final result was already found by Alderliesten (2005). Still he recommends a value of b_0 between 0.5 [mm] and 1.5 [mm], advising 0.6 [mm] for small crack lengths and 1.2 [mm] for large crack lengths, to prevent a large initial peak in either crack- or delamination growth rate. The same rule is applied to the Wilson model.

Lowering the value of w_{\max} results in a smoother curve for both the FCP modules, because the number of elements on a certain crack length is increased if their overall width is reduced. The crack propagation characteristics calculated using the Alderliesten code are highly dependent on the value of w_{\max} , see figure 7-17, while this is not the case for the Wilson code, see figure 7-21. The Alderliesten code needs a value of around 0.01 [mm] to produce correct results. The Wilson module produces smooth results for a w_{\max} below 0.05 [mm] for the simpler laminates, but using an output smoothing function can make results with $w_{\max} = 0.5$ [mm] already sufficiently accurate. The run-time increases exponentially with the decrease of w_{\max} ,

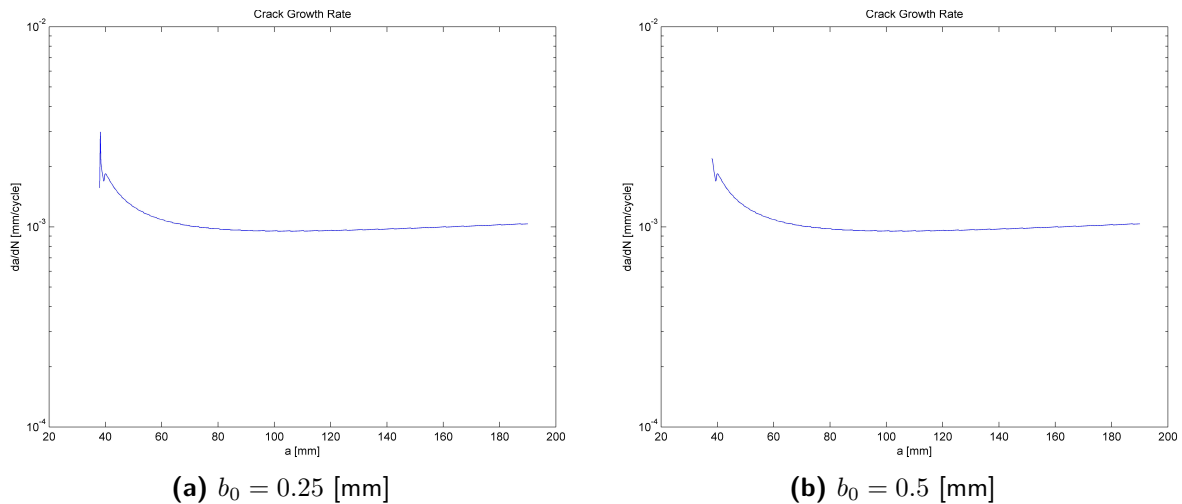


Figure 7-25. Running the Alderliesten FCP module for Glare 3-4/3-0.4 with different values of b_0

so care should be taken not to take its value too small.

Changing the number of updates per element has no effect on the accuracy of the Wilson code, it only makes the noise denser because a similar level of noise just appears more often. Increasing the number of updates per element produces smoother result without altering the answer for the Alderliesten code, compare figures 7-26a and 7-26b, which is an important feature considering the dependency of the result from the Alderliesten code on the number of elements. Five updates per element were used for all runs of the Alderliesten code in this research.

7-6 Limits of validity

The validity of the static strength module is probably very limited, because of the coarse assumptions made for the implementation of this module.

The FCI module should be valid for any laminate under any type of in-plane loading. The validity was proven for standard Glare laminates under CA tension and tension/bending loading, and for a Glare reinforced monolithic plate under CA tension, see table 7-8. No comments can be made on the validity of the initiation module for VA spectrum loading, since no test data was available with which to compare the model output.

The Alderliesten FCP module can rely on the validation analysis carried out by Alderliesten (2005), because the version adapted for the tool still produces very similar results. The limits of validity that were given in his thesis are given in table 7-9. No comment can be made about the validity of the model for Glare 2, because no Glare 2 test data was available with which this model could be validated.

The Wilson FCP module was also validated with the test data from Alderliesten (2005), and with a variety of different metals, lay-ups, adhesive additions and layer thickness values (Wilson, 2013), see table 7-10. The same limits of validity count for the adapted implementation

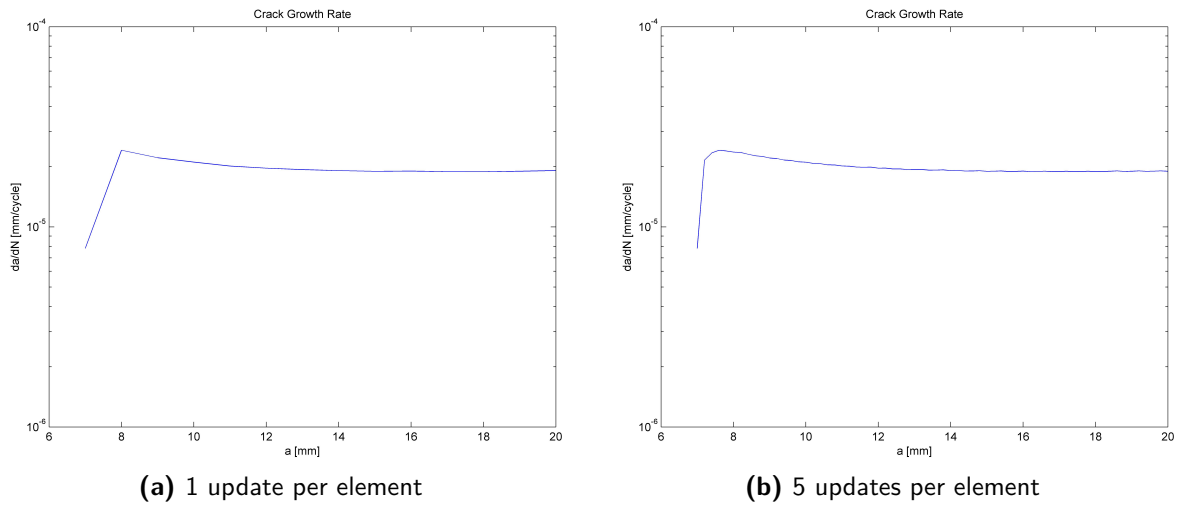


Figure 7-26. Running the Alderliesten FCP module for Glare 2A-4/3-0.4 with different numbers of updates per element

Table 7-8. Limits of validity of the FCI model

	Minimum	Maximum
FML types	Glare 2A, Glare 3, and Glare attached to a monolithic plate	
Lay-up	3/2	16/15
Aluminium thickness	0.3 [mm]	5.2 [mm]
Max. applied load	39 [MPa]	131.3 [MPa]
Stress ratio	0.05	0.1
Loading	Both tension and combined tension/bending	
Type	Both notched and unnotched	
Specimen widths	16 [mm]	100 [mm]

Table 7-9. Limits of validity of the Alderliesten FCP model (Alderliesten, 2005)

	Minimum	Maximum
Glare types	Glare 3 and Glare 4B (L-T and T-L)	
Lay-up	3/2	8/7
Aluminium thickness	0.3 [mm]	0.5 [mm]
Max. applied load	80 [MPa]	120 [MPa]
Stress ratio	0.05	0.5
Starter notch length	3 [mm]	75 [mm]
Crack lengths	1 [mm]	220 [mm]
Specimen widths	100 [mm]	500 [mm]

of the Wilson FCP model, because the results of the code used for the research reported here almost perfectly match the results of the original code.

Table 7-10. Limits of validity of the Wilson FCP model (Wilson, 2013)

	Minimum	Maximum
FML types	Glare 2A (L-T), Glare 3 and Glare 4B (L-T and T-L), including asymmetric lay-ups, extra adhesive layers, and the inclusion Al7055-T6, Al-Li and Al2524-T3 layers	
Number of layers	5	23
Metal layer thickness	0.4 [mm]	1.6 [mm]
Adhesive thickness	0.03 [mm]	0.36 [mm]
Max. applied load	80 [MPa]	140 [MPa]
Stress ratio	-0.3	0.5
Loading	Both tension and combined tension/bending	
Starter notch length	5 [mm]	20.7 [mm]
Crack lengths	1 [mm]	220 [mm]
Specimen widths	100 [mm]	500 [mm]

Validation of the VA addition was only done on the basis of tests of the effects of load variation on Glare 3-4/3-0.3 specimens (Khan et al., 2010), see table 7-11.

Table 7-11. Limits of validity of the VA addition

FML types	Glare 3-4/3-0.3
Max. overload	175 [MPa]
Standard max. load	120 [MPa]
Standard stress ratio	0.1
Loading	Tension
Starter notch length	5 [mm]
Crack lengths	4-22 [mm]
Specimen width	140 [mm]

There is no guarantee of correct results for combined FCI and FCP in a Glare reinforced strap loaded by a VA spectrum, even though the programme is currently capable of producing results for this type of situation. The author recommends validation of the programme using test results for VA FCI, and both CA and VA crack propagation in a Glare-reinforced monolithic plate.

7-7 Summary

The correct working of all the modules in the tool was verified and all modules have been validated using test results obtained from literature and the agreement between this data and the tool described here was relatively good in all cases. It is recommended to produce additional test results to which the model can be compared, to further validate the following situations:

- FCI due to VA loading
- FCP Glare 2A
- FCP due to VA loading in a variety of laminates, including a Glare-reinforced monolithic plate

Using the model for renewed reinforcement design

- 8-1 Introduction**
- 8-2 Evaluation of current design**
- 8-3 Reinforced frame design improvement**
 - 8-3-1 Constraints
 - 8-3-2 Variables
 - 8-3-3 Room for improvement
- 8-4 Summary**

8-1 Introduction

The accuracy of the method for justifying the A400M Glare reinforced frame flange by Airbus is evaluated in this chapter. This is done on the basis of a comparison with results generated using the programme that contains the calculation modules described in chapter 6. The limits of a possible future optimisation are discussed, and some fatigue life prediction results are shown for alternative reinforcement designs to allow for comments to be made on the availability of room for the improvement of the current Glare reinforced frame design from a fatigue perspective, which also shows the usefulness of the programmed tool. A general outline of how to include the tool in an optimiser is given.

8-2 Evaluation of current design

Only the fatigue crack propagation (FCP) results that were calculated by Airbus to justify the current design of the Glare strap reinforcement for frame 43 of the A400M are known

to the author (Th. Beumler, personal communication, April 4th, 2013). No fatigue crack initiation (FCI) data is available to the author. The current design of the Glare reinforced frame flange is therefore only evaluated on the basis of crack growth calculations starting from a crack that is 1 [mm] longer than the notch radius.

The loading data provided by Airbus is a set of combinations of minimum and maximum stress, sorted first from low to high minimum stress and sorted second, per level of minimum stress, from low to high maximum stress. The yield zone model will not produce results that match reality if this data is used, because in reality the experienced load history is far from ordered. The linear damage accumulation (LDA) model is therefore applied, which results in conservative outputs, because any crack growth retardation is neglected and calculated growth rates are thus higher than reality.

The input data that were used to run the code are summarised in table 8-1, the dimensions are based on a technical drawing of frame 43 of the A400M (Th. Beumler, personal communication, April 4th, 2013). The material data that was used to run the model can be found in tables 4-2, 4-3, and 7-3.

Table 8-1. Input data for the Glare reinforced frame flange

Specimen width W [mm]	90
Hole diameter D [mm]	4.8
Initial crack length a_0 [mm]	3.4
Laminate cure temperature [°C]	120
Test environment temperature [°C]	20

To verify whether the results produced by the model are close to the results that were used to justify the current design of the Glare reinforced frame flange, the applied loads are divided between the strap and the frame flange in the same way as was done by Airbus to justify the current design as was described in section 3-2. The reduced load is applied to only a strap made of a Glare 2A-12/11-0.4 laminate, even though this is outside the limits of validity of the Alderliesten model, which were given in table 7-9. The output of the variable amplitude (VA) Alderliesten module is shown in figure 8-1.

What is perhaps most striking in the figure, is the wavy pattern of the curve. This waviness is caused by the fact that the input spectrum is sorted on the basis of load severity as was explained earlier, making the crack grow significantly faster when the severest part of the spectrum is run through the simulation as compared to the rest of the simulation. The pattern shows that the complete load sequence is applied six times, after which the simulation reaches the final crack length before the application of a complete sequence could be finished.

It can be seen in the figure that after one complete spectrum, i.e. 10000 flights, the crack has grown to a length of 4.20 [mm], which is an increase of 0.8 [mm] from the initial crack length. This is a relatively large difference from the 0.28 [mm] growth that was calculated with the FML F&DT Toolbox for the justification by Airbus. This difference may be due to inapplicability of the empirical model in the Toolbox, or due to the absence of a notch during the justification, because the document that was provided by Airbus shows no information about whether or not the presence of a notch is taken into account (Th. Beumler, personal communication, April 4th, 2013).

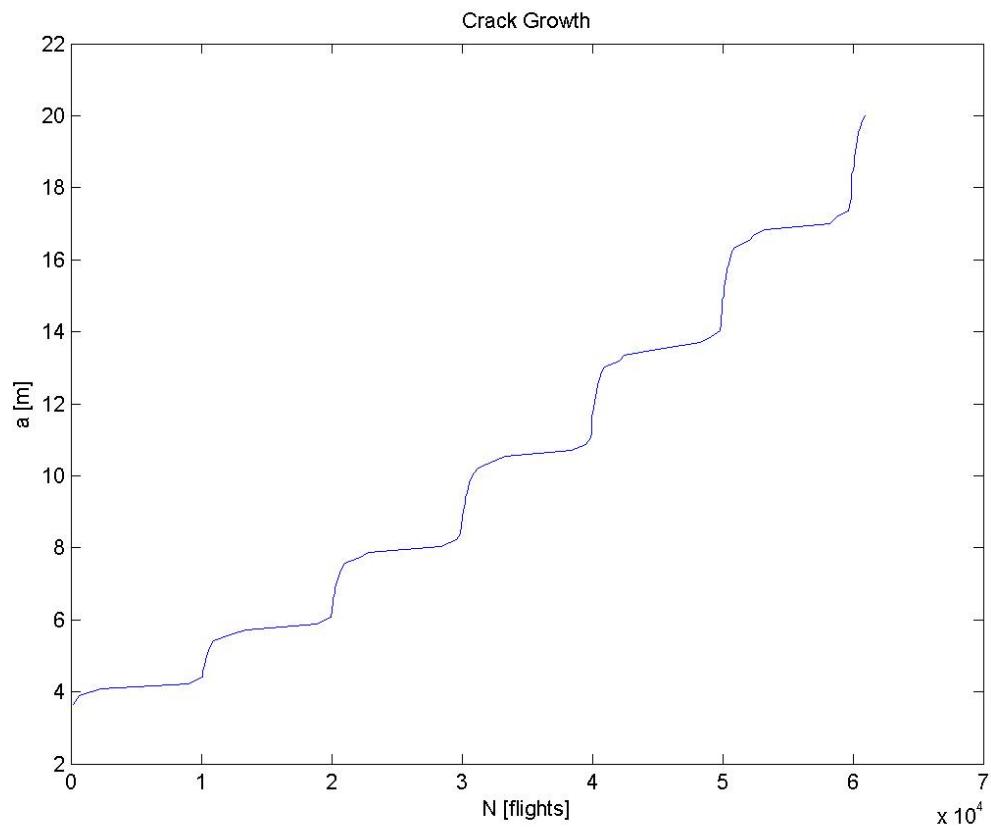


Figure 8-1. Fatigue crack growth of notched Glare 2A-12/11-0.4 under spectrum loading

The critical crack length, which was calculated by Airbus to be 11 [mm] (Th. Beumler, personal communication, April 4th, 2013), occurs at around 40000 flight cycles, which is about one third higher than the 29810 cycles that was estimated by Airbus. This difference could be the result of simulating crack growth in Glare 2A rather than Glare 3. Glare 2A has all the fibres in the prepreg layers aligned with the loading direction rather than half of them, resulting in a higher strength in loading direction. It is again uncertain whether the 11 [mm] stated by Airbus includes the notch radius.

The paragraphs above contain the reason to conclude that the analysis tool developed in this research reproduces the calculations by Airbus with an acceptable accuracy, despite the uncertainty around what exactly has been simulated by Airbus to justify their Glare reinforced frame flange design. The empirical model from the FML F&DT Toolbox used by Airbus thus seems reasonably accurate for describing crack propagation in Glare 2A-12/11-0.4, although a more thorough comparison is necessary to justify this conclusion.

Running the Glare strap and frame flange together using the VA Wilson code produces the result of figure 8-2. A through crack that was 1 [mm] longer than the hole radius was again given as an input. It was assumed that two prepreg layers with fibres in longitudinal direction and one adhesive layer were added to prevent excessive delamination of the strap from the flange, resulting in a layup that can be described as [Glare 2A-12-11-0.4/0.266 [mm] 0° S2+FM94/0.12 [mm] FM94/3.8 [mm] Al7085-T7068]. The load factor was adapted from the previous case to match the total load that is applied to the flange and strap together, rather than the strap alone.

Several curves are shown in figure 8-2, they are all resulting from a single FCP analysis. Each curve represents one metal layer, and a lighter shade of grey indicates that the curve belongs to a lower layer, i.e. a layer with a higher number according to the convention shown in figure 2-2. The flange is added to the bottom of the laminate and thus contains the lightest shade of grey in figure 8-2. It can be seen that the flange behaves significantly different than the metal layers in the strap. The crack length of the flange, visualised by the highest curve in figure 8-2, grows faster than the crack lengths in the strap, which all grow close together at a smaller crack growth rate than the flange.

The graph still shows a wavy pattern even though the analysis finishes when about half of the spectrum has been applied. The waves are far less pronounced this time, and are probably caused by the second tier of sorting in the input spectrum, i.e. the sorting on the basis of maximum stress level per level of minimum stress, as was explained above. This causes a variation in crack growth rate similar to the one seen in figure 8-1 to occur, albeit on a much smaller scale.

The crack in the monolithic flange reached the edge of the flange and caused the analysis to finish before the complete spectrum had been applied. The steep growth at the beginning of the curve in figure 8-1 reveals that the severest part of the spectrum is the beginning of the file, which matches the sorting scheme explained above because the most severe cycles have a combination of the lowest minimum stress and the highest maximum stress. Figure 8-2 should thus show conservative results, because in reality the severe cycles do not all fall in the beginning of the life of an aircraft, and because the LDA method is generally a conservative approximation of crack growth. Note, that this conclusion is in contrast with tests, where collecting all severe cycles in the beginning of the test leads to unconservative results because

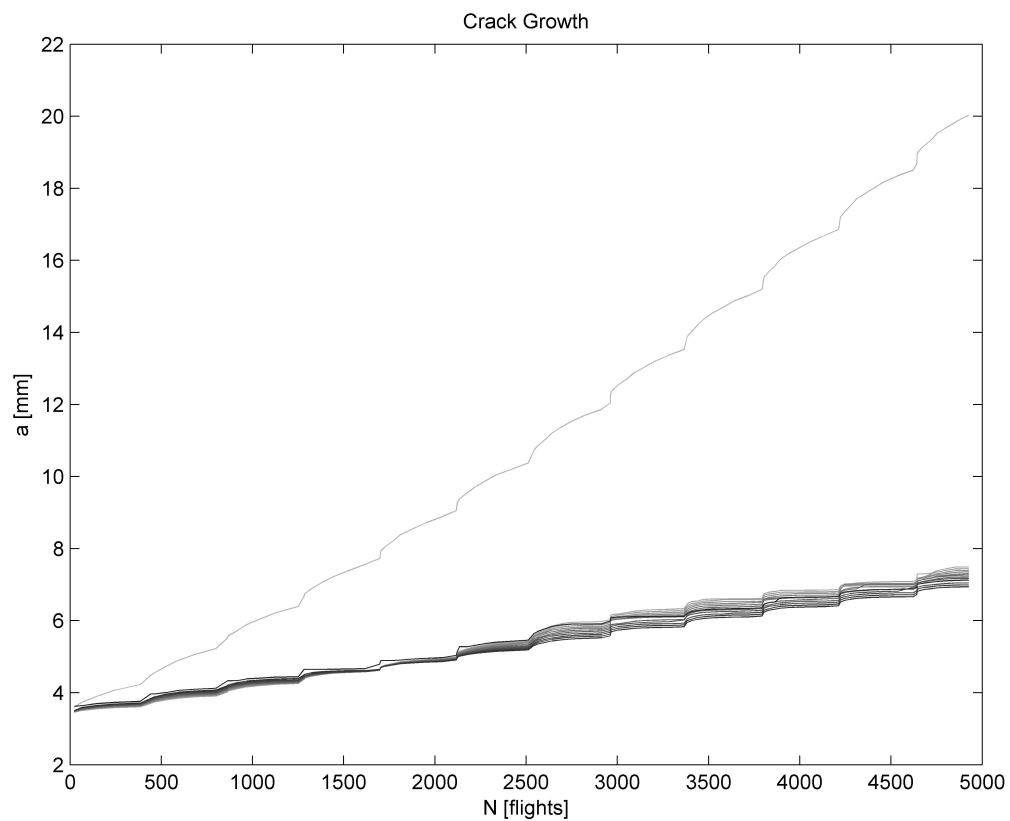


Figure 8-2. FCP of notched Glare 2A-12/11-0.4 attached to a 3.8 [mm] aluminium plate under spectrum loading, the crack propagation of each metal layer is visualised with a different line. The shade of grey of a line indicates the depth of the corresponding layer in the laminate, lighter shades corresponding to layers with a higher number, see also figure 2-2

of more crack growth delay is occurring than when the cycles are not sorted with decreasing severity (Schijve, 2009).

The cracks in the metal layers of the strap are all of almost equal length, as seen by the darker shaded curves in figure 8-2 which all lie close together, indicating that not much bending is occurring in the laminate. This matches the relatively small difference between Glare 2A and Al7085 in terms of in-plane stiffness.

At the end of the analysis, when the crack length in the flange has reached a length of 20 [mm], the maximum crack in the strap is close to 7 [mm], so the difference with the initial crack is 3.6 [mm]. This difference is significantly higher than the difference of 0.8 [mm] which was found after analysing the effect of applying a complete spectrum on the strap alone. The presence of the flange in the analysis thus seems to increase the crack growth rate of the reinforcing laminate, probably as a result of the Glare strap taking over the load that is initially carried by the flange. This suggests that the analysis as performed by Airbus to justify the design of the reinforcement might be unconservative.

8-3 Reinforced frame design improvement

There are two reasons why finding out whether the current design can be improved is useful. One, as mentioned before, the design of the Glare reinforcement was based largely upon static strength requirements which indicates the design might be suboptimal from a fatigue perspective. Two, as demonstrated in the previous section, the analysis shows that the crack growth rate might be higher in reality than anticipated on the basis of the justification method used by Airbus, and lowering this rate might thus even be a necessity.

It should be noted that an optimisation solely on the basis of the fatigue crack growth rate in a specific section of a frame of an aircraft will probably produce useless results, because there is much more to take into account when optimising an airframe. This is the reason that only possible room for improvement is shown in this report rather than an alleged ‘optimal solution,’ because the tool produced in this research cannot consider anything outside its scope when producing its results and will thus not deliver a globally optimal answer. How to set up an optimisation for the current problem, though, is discussed to provide a framework to assess the alternative designs that are made.

The objective of a study for improvement of the design of the Glare reinforced frame flange could be to reduce the crack growth rate while retaining a similar axial stiffness EA . Adding layers would be the obvious solution, ignoring the second part of the objective, and although the crack growth rate might be lowered by this simple alteration, the resulting design will probably become rather heavy and might even attract more load which will invalidate the analysis.

The performance of an alternative solution could thus be measured in terms of the amount of reduction in crack growth rate, or increase in cycles to a critical crack length, and weight in comparison to benchmark results.

8-3-1 Constraints

The discussion in the paragraphs above already suggest there are constraints for the allowed Glare reinforced frame flange design. The constraints listed below should be considered when carrying out an optimisation for the current case.

- Allowed metal layer thickness values
- Allowed material types
- Allowed prepreg direction
- Minimum flange thickness
- Required EA range of assembly
- The structure should always be capable of carrying limit load until the end of its life

The allowed material types and prepreg direction are fixed in the current case, because the reinforcement is limited to Glare and the flange to Al7085. Metal layer thickness values can be between 0.2 and 0.4 [mm] for Airbus. No minimum flange thickness is given, although the current design requires a flange to attach the strap to.

8-3-2 Variables

Variables that can be altered to change the design are summarised below.

- Metal layer thickness
- Flange thickness
- Number of prepreg plies between two consecutive metal layers
- Applying extra adhesive layers
- Total number of aluminium layers

8-3-3 Room for improvement

A constant amplitude loading spectrum was chosen to try to determine whether there is room for improvement of Airbus' Glare reinforced frame design, because of the much lower run times required to get to a result compared to variable amplitude simulations. The initiation module was also included, since changing the layout of the laminate can drastically affect the cycles to initiation of certain layers, and because of this addition, the choice was made to use Al2024-T3 for the flange because of the fact that, for this material, it is most likely that accurate SN-data is available for the stress cycles occurring in the layers, considering the largest variety of conditions for which there is data, see table 7-4. The performance is measured in terms of total number of cycles to reach a crack length of 20 [mm].

Since the situation has now chanced with respect to the beginning of this chapter, a new benchmark performance is necessary. The layup used for the benchmark is same layup as given earlier above for the Glare reinforced flange, which was described as: [Glare 2A-12-11-0.4/0.266 [mm] 0° S2+FM94/0.12 [mm] FM94/3.8 [mm] Al7085-T7068]. A laminate of this layup was tested under a load that applied the equivalent of a maximum average far-field stress value of 120 [MPa] to the laminate, which means a maximum line load of $1.09 \cdot 10^3$ [N/mm] was applied. This maximum load and a load ratio of $R = 0.1$, was used for this and the following cases, so the amount of load carried by the laminate did not change from case to case.

The result of the benchmark test can be seen in figure 8-3. It can be seen in the figure, that the line with the lightest shade of grey reaches a crack length of 20 [mm] first. This line corresponds to the lowest layer in the laminate, which is the frame flange. The growth rate in the flange is thus high enough to surpass the crack lengths of the other layers, of which the crack lengths all lie close together which is concluded from the darker shaded lines in figure 8-3. The model also shows the influence of the crack in the flange on the crack growth rate in the strap: as soon as the flange enters the crack growth phase, the other layers start experiencing a higher crack growth rate. This is concluded from the fact that the slope of the darker shaded lines in figure 8-3 increases significantly after the lightest shaded has surpassed them.

The benchmark problem has the performance in terms of fatigue properties given below.

- First initiation: 234880 cycles.
- First crack at 20 [mm]: 435588 cycles , so the FCP phase lasted 200708 cycles.

The three alternatives described below are tested to investigate whether the benchmark results can be improved.

1. Applying part of the Glare strap on the other side of the flange, thus requiring the strap to be cut for the inside application, but improving the bridging of the flange.
2. Making the assembly completely out of Glare, thus improving the crack bridging to a maximum extent.
3. Using thinner aluminium sheets, so the percentage of fibre layers to metal layers increases, reducing the mass due to the high specific strength of fibre layers.

Alternatives 1 and 3 contain two prepreg layers and 0.12 [mm] adhesive between the reinforcement and the flange.

The crack growth results of the three alternatives can be found in figures 8-4, 8-5, and 8-6. The performance of each alternative is given below in the format: cycles to first initiation + cycles from first crack at 1[mm] to first crack at 20 [mm] = total fatigue life.

1. 277242 + 114211 = 391463
2. 300477 + 742708 = 1043185

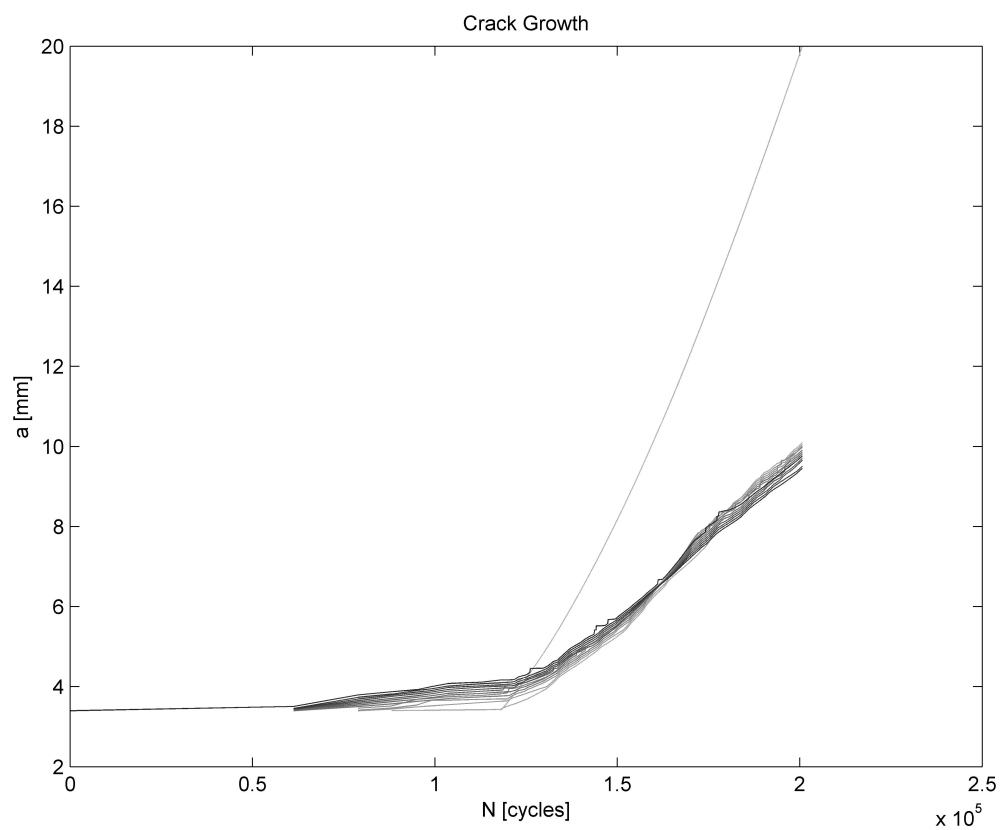


Figure 8-3. Benchmark solution: FCP of Glare 2A-12/11-0.4 adhered with two prepreg layers and 0.12 [mm] adhesive to a 3.8 [mm] Al2024-T3 flange. The crack propagation of each metal layer is visualised with a different line. The shade of grey of a line indicates the depth of the corresponding layer in the laminate, lighter shades corresponding to layers with a higher number, see also figure 2-2

$$3. 137789 + 339250 = 477039$$

A basic design space visualisation with the performance of the benchmark and the three alternatives is given in figure 8-7.

The reduction of internal moment is likely to be the cause of the increased number of cycles to initiation for alternative 1. The strong increase in crack growth rate is probably caused by the fact that a through crack is formed relatively soon, rather than leaving a larger part of the strap intact to bridge cracks. This is confirmed when looking at figure 8-4: the flange, indicated with the line with the lightest shade of grey, is cracked at a very early stage. The growth rates of the metal layers in the strap, indicated with the darker lines, are accelerated for almost the entire FCP phase.

Alternative 2 seems to be the best candidate, because there is no flange with a fast-growing crack that can accelerate the crack growth in the metal layers of the strap. Figure 8-5 shows only a single crack growth curve, because the Alderliesten model has run to analyse crack propagation in the now entirely Glare 2A laminate. Removing the flange completely is most probably not possible because the flange is needed to attach the strap to, but this analysis does show that much can be gained by increasing the ratio of Glare to monolithic aluminium in the cross-section of the Glare reinforced frame flange.

The increase in internal moment due to a larger stiffness difference between flange and strap causes alternative 3 to initiate sooner than the benchmark, but this is compensated by the larger number of cycles needed to reach the final crack length due to the increased amount of crack bridging and the delay in initiation in the flange, compare figure 8-6 with figure 8-3.

From the small set of runs carried out in the research described in this report, it can thus already be deduced that there is indeed room for improvement of the benchmark solution, which seems to lie in increasing the amount of crack bridging in the assembly which is achieved by increasing the fraction of prepreg to metal area in the cross-section. Looking at the design space in figure 8-7, there is most opportunity for an increase of performance of the benchmark solution towards the longer crack growth phase of alternative 2, although the performance of alternative 2 will never be reached, because it requires the entire flange to be replaced by Glare 2A, which is most probably not possible. The distance to the performance of alternative 2 will be dictated by the minimum required flange thickness.

8-4 Summary

There is reason to believe that the current justification method used for the Glare reinforced flange is unconservative, because the newly developed analysis tool discussed in this report shows a significantly larger crack growth rate when the FCP of the full assembly is analysed, rather than the FCP of just the strap with an equivalent stress cycle, as is done by Airbus to justify the current Glare reinforced frame design. The results of a small set of alternative solutions suggest that there is room for improvement of the current Glare reinforced frame flange design by increasing the ratio of Glare to monolithic aluminium in the cross-section.

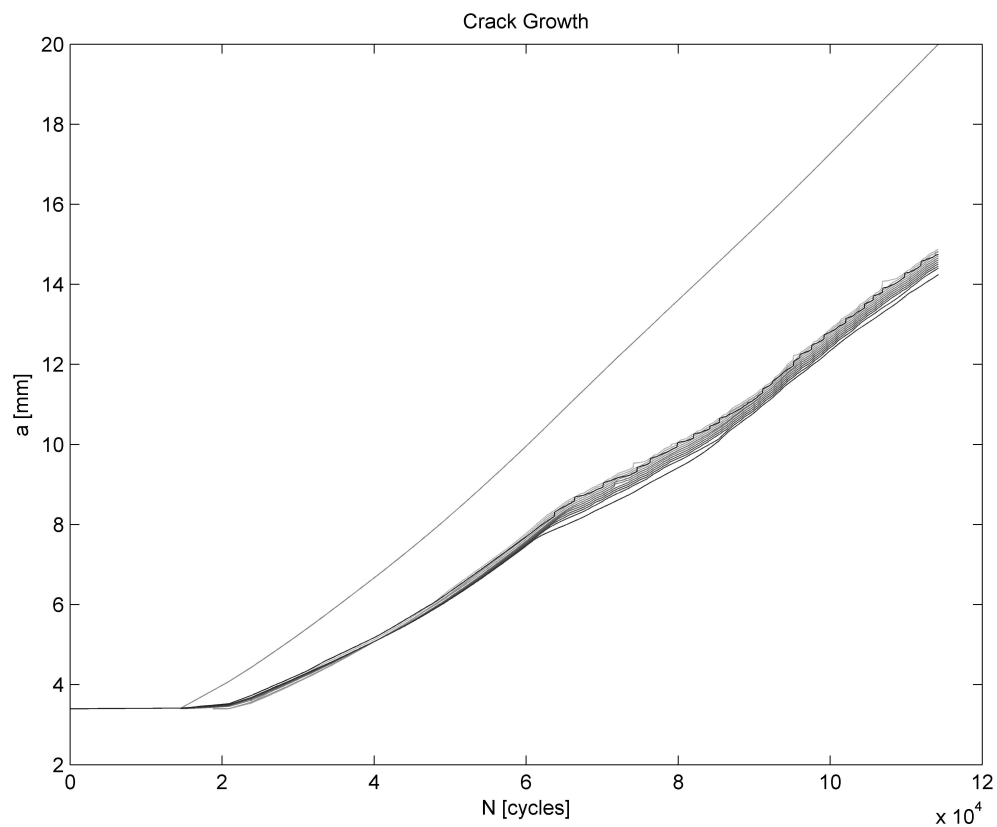


Figure 8-4. Alternative 1: FCP in Glare 2A-8/7-0.4 on one side and Glare-2A-4/3-0.4 on the other of a 3.8 [mm] Al2024-T3 flange. The crack propagation of each metal layer is visualised with a different line. The shade of grey of a line indicates the depth of the corresponding layer in the laminate, lighter shades corresponding to layers with a higher number, see also figure 2-2

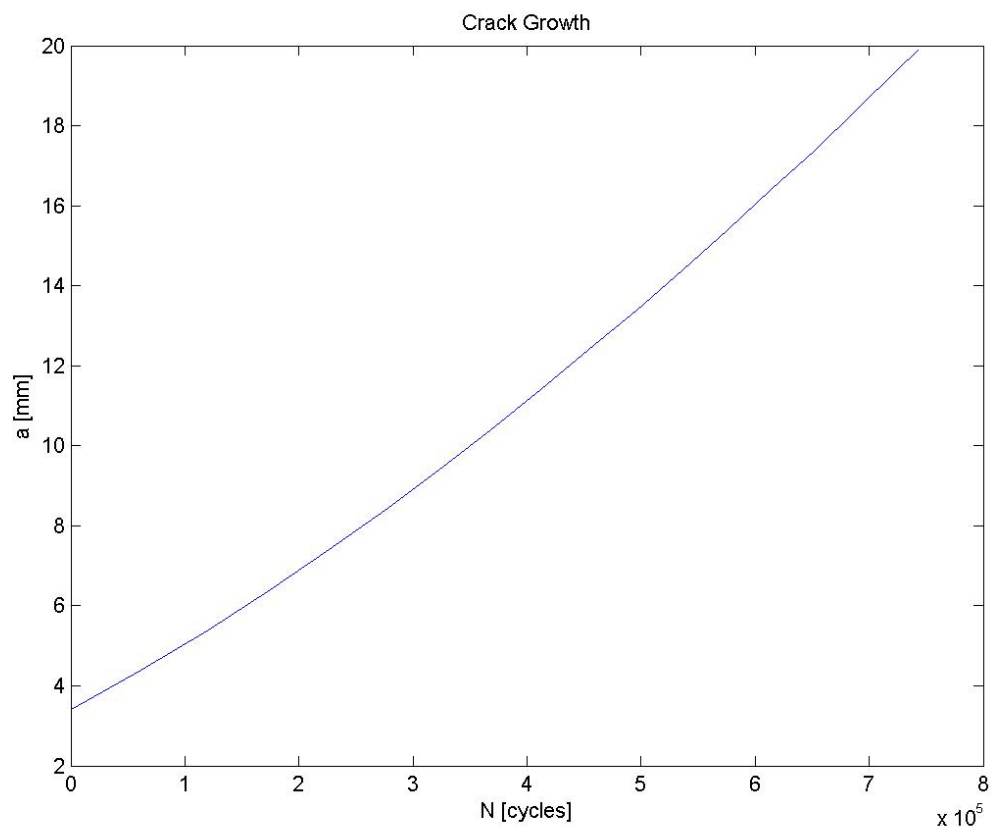


Figure 8-5. Alternative 2: FCP in Glare 2A-19/18-0.4. Only one curve is given to represent the crack growth in each layer because this graph is produced using the Alderliesten model.

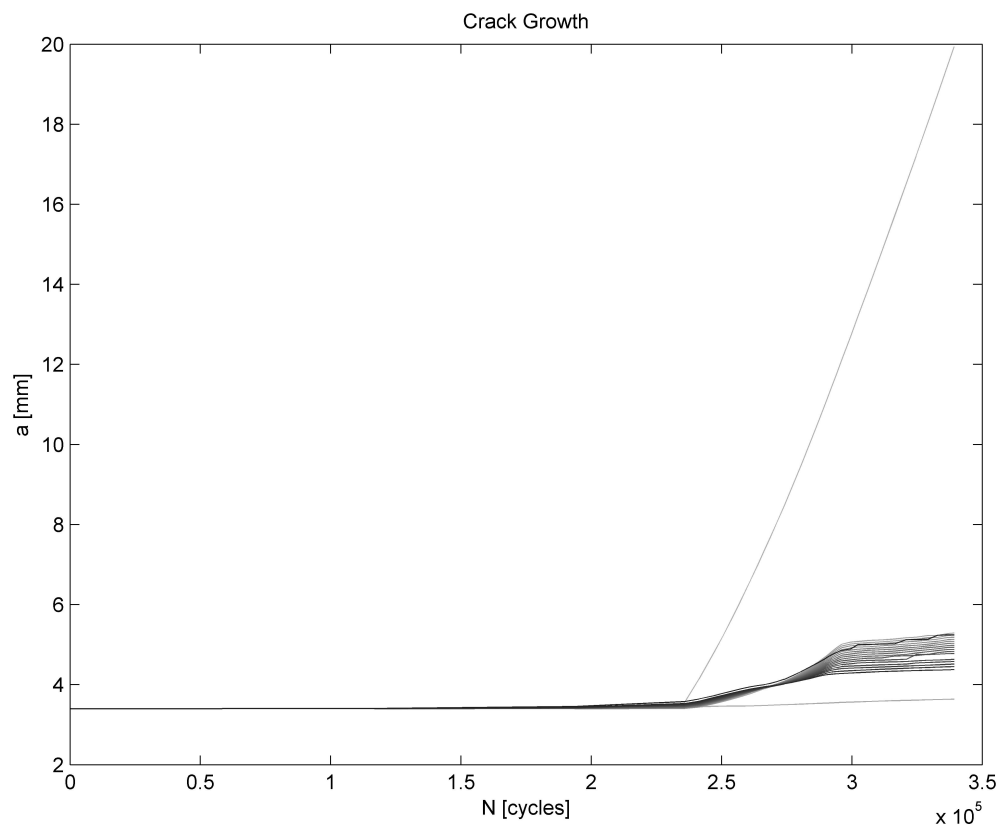


Figure 8-6. Alternative 3: FCP in Glare 2A-18/17-0.2 adhered with two prepreg layers and 0.12 [mm] adhesive to a 3.8 Al2024-T3 flange. The crack propagation of each metal layer is visualised with a different line. The shade of grey of a line indicates the depth of the corresponding layer in the laminate, lighter shades corresponding to layers with a higher number, see also figure 2-2

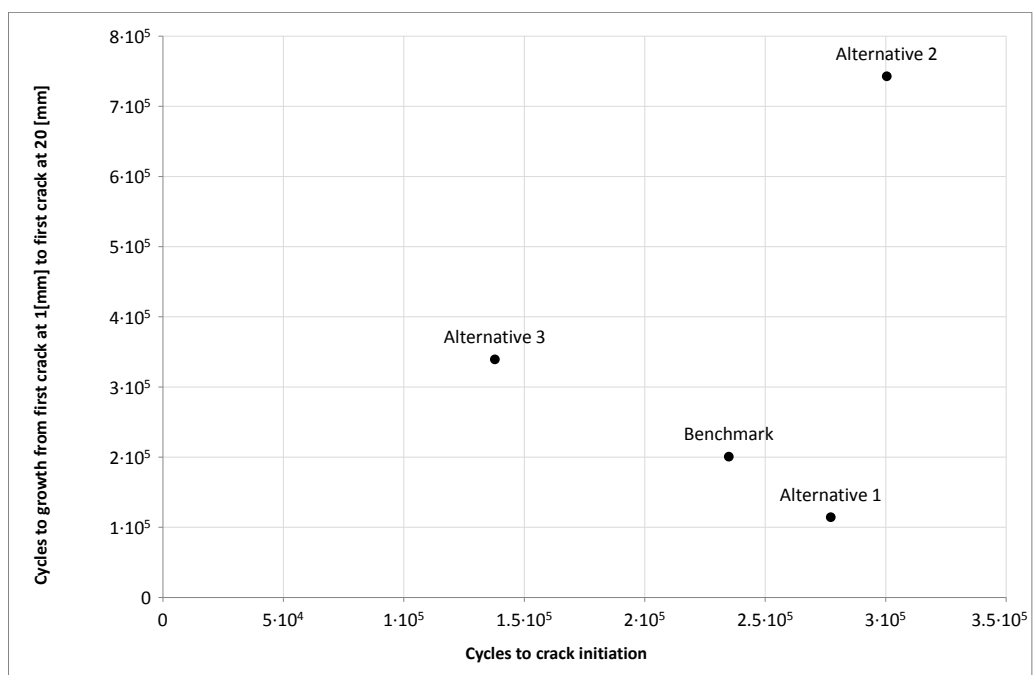


Figure 8-7. Basic design space of the Glare reinforced frame design. The benchmark and the three alternatives are shown. Performance is measured on the basis of distance to the origin.

Chapter 9

Evaluation

9-1 Complying to the requirements

The FML fatigue analysis tool that was developed for the research described here provides a solution to the need which exists within Airbus to have a model that can justify the Glare reinforced frame flange design in a more accurate way than previously possible. The basic requirement set in chapter 5 was fulfilled. In chapter 6 it is explained how a tool was developed that can be used to calculate fatigue crack initiation and subsequent propagation due to constant or variable amplitude loads in a Glare 2A laminate which is adhesively bonded to a plate that is of a different metal than the Al2024-T3 used in Glare. Chapter 7 contains the verification and validation results. It was shown that the program behaved correctly and that the output it generated matched well with test data.

The choice to use a model with an analytical basis, discussed in section 5-3, resulted in a versatile code that could handle many more cases than just the Glare reinforced flange, as shown by the diversity of validation cases in section 7-3, and thus the FML fatigue analysis tool meets the requirement of generality that allows one program to calculate all closely related cases. This would probably not have been the case the choice was made to use a phenomenological or finite element method, because the curve fit that validates the answer of the former is most probably only valid for a small region around the test data used to fit the curve to, and the type of elements and mesh layout used for the latter would limit its use to only a subset of the cases the analytical model presented here is currently capable of analysing.

The basic static strength estimation capability of the tool proved to provide a reasonable approximation of the static strength of the input laminate as shown in subsection 7-3-1. This thus allows the user to get an idea of the order of magnitude of the residual strength of the laminate and meets the requirement that the program should provide the user with some insight into whether the laminate can survive limit load or not.

9-2 Recommendations

The biggest shortcoming of the analysis tool in its current form is that there is no functionality to justify that the application of a limit load can be survived when a certain amount of fatigue loading has caused damage to appear inside the laminate. The static strength estimator is simply too coarse to provide this justification. The author highly recommends that the tool is completed with the addition of a residual strength calculation module, which can model the mechanism of a quasi-static failure on the laminate including cracks and delaminations to find the maximum load that can be sustained and thus providing the last step to justify a design.

There exist many more possible functionalities that could be added to the analysis tool to make it very generally applicable to FML related problems. These additions include, but are not limited to, the ability to analyse damage due to compression, off-axis loading, and biaxial loading, the ability to analyse configurations of multiple holes, filled holes, pin-loaded holes, lap joints and stringer runouts, and the ability to calculate the fatigue properties after a certain amount of external impact damage has been applied to the laminate.

The amount of validation performed in section 7-3 is dwarfed by the very large amount of possible cases that the tool could be used to provide an answer for. It is recommended that more validation is performed to ensure that the model produces results that match reality. Specifically for the case of the Glare reinforced flange, the following areas need further validation:

- Fatigue crack initiation due to variable amplitude loading
- Fatigue crack propagation in Glare 2A
- Fatigue crack propagation due to variable amplitude loading in a variety of laminates, including a Glare-reinforced monolithic plate

A long list of assumptions had to be made to get to a working model. Some of these are questionable and require further research, as is mentioned below.

- The applicability of the classical laminate theory to the assembly as a whole or the flange in particular is questionable, because the laminate is thicker than the normally used rule of thumb of ten per cent of the smallest in-plane dimension. The author recommends that research is done into the effect of the thick layer on the conservatism of the predictions. This research might lead to the conclusion that the internal stress and the connected deformation cannot be considered constant through the thickness of each layer.
- The assumption that cracking in one metal layer does not affect the initiation of the others is questionable, as shown by the initiation test results in section 7-3-2. It is recommended that the influence of a crack on the stress field in the intact layers of a fibre metal laminate is investigated further.
- The assumption that the influence of directionality and angularity is experienced equally by each layer in the laminate, does not cause the predicted cycles to initiation of the

flange to be unacceptably inaccurate for the test results considered. The almost consistent overestimation of the cycles to initiation at high loads of the test results by Klein (2011) suggests that the assumption does lead to prediction inaccuracy. Further research is recommended into the dependency of the influence of the anisotropy of one layer on the cycles to initiation of another to conclude whether the assumption made is valid.

- The origin of the exponent value of 2 for the Wheeler model is unclear, although it produces results that match well with test data. The author advises that more research is done into why this value is accurate and what the limits of applicability of this value are.

There are also implementation related recommendations. Further research into the cause of the poor convergence of the Alderliesten model is advised, because in the current form the answer is dependent on element density. The leapfrog mitigation scheme which is included in the Wilson code is probably the cause of delaminations growing together rather than alone, and it does not work in a case where variable amplitude loading is applied. The author recommends that effort is put into devising a better solution to tackle the leapfrogging issue.

Chapter 10

Conclusion

A tool was developed that can be used to analyse fatigue crack initiation and propagation due to constant or variable amplitude tensional or moment loading of general fibre metal laminates. The tool is based on data lookup for the initiation part and analytical models of the physics behind crack growth for the crack propagation part, although the analytical models require numerical methods to be solved. All the parts of the model were verified to work correctly using basic input variation or comparisons between the produced output and that of the original code it was based upon. All parts of the code, and some combinations thereof, were validated using of test data and the program showed a good agreement with all the test data that was used to validate it. The choice for analytical models thus resulted in a versatile program that can produce accurate predictions for a wide variety of cases.

The accuracy of the method as used for the design for the A400M Glare strap frame reinforcement was assessed, and it was shown that the method used to justify the current design might not be conservative. A small design exploration showed that the current design of the Glare reinforced frame can be improved, because the overall crack growth rate could be lowered by increasing the ratio of prepreg to metal in the cross-section of the frame.

Bibliography

- Airbus Military (2012). Airbus Military | A400 M. Available from: <http://www.airbusmilitary.com/Aircraft/A400M/A400MAbout.aspx>.
- Airbus S.A.S. (2007). *AM2377.7.5-A, Fatigue and Damage Tolerance Methods for GLARE*.
- Airbus S.A.S. (2012). Dimensions & key data | Airbus, a leading aircraft manufacturer. Available from: <http://www.airbus.com/aircraftfamilies/passengeraircraft/a380family/a380-800/specifications/>.
- Alderliesten, R. C. (1999). *Development of an empirical crack growth prediction model for the Fibre Metal Laminate Glare*. M.Sc. thesis, Delft University of Technology.
- Alderliesten, R. C. (2004). Energy release rate approach for delamination in a fatigue crack configuration in glare. In *Mechanics of 21st Century - ICTAM04 Proceedings*.
- Alderliesten, R. C. (2005). *Fatigue Crack Propagation and Delamination Growth in Glare*. Ph.D. dissertation, Delft University of Technology.
- Alderliesten, R. C. (2007a). Analytical prediction model for fatigue crack propagation and delamination growth in glare. *International Journal of Fatigue*, 29:628–646.
- Alderliesten, R. C. (2007b). On the available relevant approaches for fatigue crack propagation prediction in glare. *International Journal of Fatigue*, 29:289–304.
- Alderliesten, R. C. (2009). Fatigue and damage tolerance of hybrid materials & structures - some myths, facts & fairytales. In *ICAF 2009, Bridging the Gap between Theory and Operational Practice*, pages 1245–1260.
- Alderliesten, R. C. (2011). Lecture slides for the course AE4735: Fatigue of Structures and Materials.
- Alderliesten, R. C. and Vlot, A. (2001). Fatigue crack growth mechanism of glare. In *22nd International SAMPE Europe Conference*, pages 41–52, Paris, France.
- ASM International (1995). *Fatigue Data Book: Light Structural Alloys*.

- Guo, Y. J. and Wu, X. R. (1998). A theoretical model for predicting fatigue crack growth rates in fibre-reinforced metal laminates. *Fatigue & Fracture of Engineering Materials & Structures*, 21:1133–1145.
- Guo, Y. J. and Wu, X. R. (1999). Bridging stress distribution in center-cracked fiber reinforced metal laminates: modeling and experiment. *Engineering Fracture Mechanics*, 63:147–163.
- Gürdal, Z. and Kassapoglou, C. (2011). Lecture slides for the course AE4509 I: Advanced Design and Optimization of Composite Structures I.
- Homan, J. (2002). Crack growth properties of thin aluminium sheets. Report B2V-01-16 issue 2, Delft University of Technology, Faculty of Aerospace Engineering. (Restricted).
- Homan, J. J. (2006). Fatigue initiation in fibre metal laminates. *International Journal of Fatigue*, 28:366–374.
- Homan, J. J. and Schra, L. (2002). Application of aluminium alloy 2024-T3 fatigue life data to Glare laminates, GTP methods projects 2.4.3.2-b, 2.4.3.3-b and 2.3.3.4-b. NLR Report NLR-CR-2002-185, National Aerospace Laboratory of the Netherlands.
- IASB (1986). *Handbuch Struktur Berechnung (HSB) 63111-01: Fatigue strength of un-notched/notched specimen material: aluminum alloy 2024-T3 unclad.*
- IASB (1987). *Handbuch Struktur Berechnung (HSB) 63113-05: Fatigue strength of un-notched/notched specimen material: aluminum alloy 7475-T761 clad.*
- IASB (1994). *Handbuch Struktur Berechnung (HSB) 63110-02: Interpolation of S-N curves containing the mean stress as parameter.*
- Kassapoglou, C. (2010). *Design and Analysis of Composite Structures: With Applications to Aerospace Structures*. John Wiley & Sons Inc.
- Khan, S. (2013). *Fatigue crack & delamination growth in fibre metal laminates under variable amplitude loading*. Ph.D. dissertation, Delft University of Technology.
- Khan, S. U., Alderliesten, R. C., Rans, C. D., and Benedictus, R. (2010). Application of a modified wheeler model to predict fatigue crack growth in fibre metal laminates under variable amplitude loading. *Engineering Fracture Mechanics*, 77:1400–1416.
- Klein, S. (2011). A400M - Fatigue coupon testing of bonded and riveted Glare-aluminium specimens). FS01416, Industrieanlagen-Betriebsgesellschaft mbH (iABG).
- Lekhnitskii, S. G. (1968). *Anisotropic Plates*. Routledge, reprint edition.
- Marissen, R. (1980). *Fatigue properties of aramid reinforced aluminium laminates (in Dutch)*. M.Sc. thesis, Delft University of Technology.
- Marissen, R. (1988). *Fatigue Crack Growth in ARALL, A Hybrid Aluminium-Aramid Composite Material*. Ph.D. dissertation, Delft University of Technology.
- Marissen, R. (2011). Lecture slides for the course AE4634: Fracture of Advanced Materials.
- Peterson, R. E. (1974). *Stress Concentration Factors*. John Wiley & Sons.

- Pilkey, W. D. and Pilkey, D. F. (2008). *Peterson's Stress Concentration Factors*. John Wiley & Sons, third edition.
- Plokker, H. M. (2005). *Crack closure in GLARE*. M.Sc. thesis, Delft University of Technology.
- Plokker, M., Daverschot, D., and Beumler, T. (2009a). Hybrid structure solution for the A400M wing attachment frames. Presented at ICAF.
- Plokker, M., Daverschot, D., and Beumler, T. (2009b). Hybrid structure solution for the A400M wing attachment frames. In *ICAF 2009, Bridging the Gap between Theory and Operational Practice*, pages 375–385.
- Randell, C. E. (2005). *Subsurface Fatigue Crack Growth in Glare Fibre Metal Laminates*. Ph.D. dissertation, Delft University of Technology.
- Rensma, E. (2007). *Investigation of innovative concepts for hybrid structures*. M.Sc. thesis, Delft University of Technology.
- Roebroeks, G. H. J. J. and Vogelesang, L. B. (1987). Laminate of metal sheets and continuous glass filaments-reinforced synthetic material. EP 0312151 A1.
- Schijve, J. (1981). Some formulas for the crack opening stress level. *Engineering Fracture Mechanics*, 14:461–465.
- Schijve, J. (2009). *Fatigue of Structures and Materials*. Springer.
- Schijve, J., van Lipzig, H., van Gestel, G., and Hoeymakers, A. (1979). Fatigue properties of adhesive bonded laminated sheet material of aluminium alloys. *Engineering Fracture Mechanics*, 12:561–579.
- Schijve, J., Vogelesang, L. B., and Marissen, R. (1985). Laminate of aluminium sheet and aramid fibres. EP0056289.
- Schütz, W. (1996). History of fatigue. *Engineering Fracture Mechanics*, 54(2):263–300.
- Tada, H., Paris, P. C., and Irwin, G. R. (2000). *The Stress Analysis of Cracks Handbook*. The American Society of Mechanical Engineers, third edition.
- Tsai, S. W. and Hahn, H. T. (1980). *Introduction to composite materials*. Technomic Publishing Company Inc.
- Vlot, A. (2001). *Glare, history of the development of a new aircraft material*. Kluwer Academic Publishers, Dordrecht, The Netherlands.
- Vlot, A. and Gunnink, J. W. (2001). *Fibre Metal Laminates, an introduction*. Kluwer Academic Publishers, Dordrecht, The Netherlands.
- Wheeler, O. (1970). Spectrum loading and crack growth. *ASME Journal of Basic Engineering*, D94(1):181–186.
- William J. Hughes Technical Center, United States. (2011). *Metallic materials properties development and standardization (MMPDS): MMPDS-06*. Federal Aviation Administration, Washington, D.C.

- Wilson, G., Alderliesten, R. C., Rodi, R., and Lemmen, H. J. K. (2009). Practical Applications of Improvements in FML Crack Bridging Theory. In *25th International Committee on Aeronautical Fatigue*, pages 539–558, Rotterdam, The Netherlands.
- Wilson, G. S. (2007). Improving the Convergence of the Alderliesten Crack Growth Model for Glare. Structural Integrity group, internal document.
- Wilson, G. S. (2013). *Fatigue Crack Growth Prediction for generalized fiber metal laminates and hybrid materials*. Ph.D. dissertation draft, Delft University of Technology.
- Witasse, R., de Boer, H., and de Koppert, J. J. M. (2007). Simulation of Bonding Strength for A400M Reinforced Mainframes. 07204/RWI, Advanced Lightweight Engineering B.V. (ALE).

Appendix A

Classical laminate theory

Classical laminate theory (CLT) is a method to calculate the stresses in each individual layer of a flat, layered material (see, e.g. Kassapoglou (2010)). It is summarised here for clarity. First, the assumptions are stated which are required for the derivation that follows. Second, the derivation is explained, which starts from the individual ply stress, rotates this to laminate coordinates and then sums and integrates these stresses to get to laminate equations, and includes the effect of thermal stresses.

A-1 Assumptions

The assumptions made in the derivation of the CLT are summarised here.

- All plies are considered thin relative to their width and length, which usually implies $t < 0.1W$. This assumption is made so the plies can be assumed to be in a state of plane stress, which means $\sigma_z = \tau_{yz} = \tau_{xz} = 0$ and thus free straining in the z -direction.
- Every ply is assumed to be orthotropic, which means it contains two planes of symmetry.
- The z -axes of all plies are aligned.
- All plies are perfectly bonded to each other, which enforces strain compatibility throughout the laminate.
- The Kirchhoff hypothesis is assumed to hold, which means that all deformations of the laminate are a function of the mid-plane in-plane deformation, a rotation and a translation in z -direction. This implies that the z -coordinate does not change under deformation and that deformations thus need to remain small, and that a cross-section that was flat before deformation is still flat after deformation.
- Out-of-plane loads on the laminate are considered negligible.

A-2 Solution method

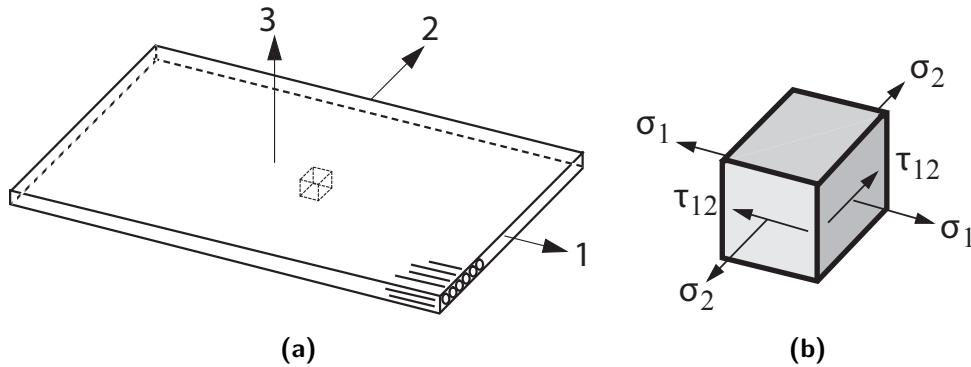


Figure A-1. (a) Ply coordinates. (b) Stresses existing in a plane stress state. (Courtesy Z. Gürdal)

The thickness dimension of a ply is small compared to the in-plane dimensions, hence each layer can be assumed to be in a state of plane stress, which makes the only stresses acting on a ply the in-plane normal stresses σ_1 and σ_2 , and the in-plane shear stress τ_{12} , see figures A-1a and A-1b, resulting in only in-plane normal strains ε_1 and ε_2 and in-plane shear strain γ_{12} . In plane stress, the generalised Hooke's Law becomes:

$$\bar{\sigma} = \mathbf{Q}\bar{\varepsilon} \quad (\text{A-1})$$

or:

$$\bar{\varepsilon} = \mathbf{C}\bar{\sigma} \quad (\text{A-2})$$

where, in the ply principle directions 1 & 2:

$$\bar{\sigma} = \begin{Bmatrix} \sigma_1 \\ \sigma_2 \\ \tau_{12} \end{Bmatrix} \quad (\text{A-3})$$

$$\bar{\varepsilon} = \begin{Bmatrix} \varepsilon_1 \\ \varepsilon_2 \\ \gamma_{12} \end{Bmatrix} \quad (\text{A-4})$$

and the plane stress compliance matrix \mathbf{C} and plane stress stiffness matrix \mathbf{Q} are:

$$\mathbf{C} = \begin{bmatrix} \frac{1}{E_1} & \frac{-\nu_{12}}{E_1} & 0 \\ \frac{-\nu_{12}}{E_1} & \frac{1}{E_2} & 0 \\ 0 & 0 & \frac{1}{G_{12}} \end{bmatrix} \quad (\text{A-5})$$

$$\mathbf{Q} = \begin{bmatrix} \frac{E_1}{1-\nu_{12}\nu_{21}} & \frac{\nu_{12}E_2}{1-\nu_{12}\nu_{21}} & 0 \\ \frac{\nu_{12}E_2}{1-\nu_{12}\nu_{21}} & \frac{E_2}{1-\nu_{12}\nu_{21}} & 0 \\ 0 & 0 & G_{12} \end{bmatrix} \quad (\text{A-6})$$

where ν is the Poisson's ratio. The response of a single off-axis layer that is rotated around the z -axis with an angle θ in terms of global coordinates x and y (see figure A-2), can be written

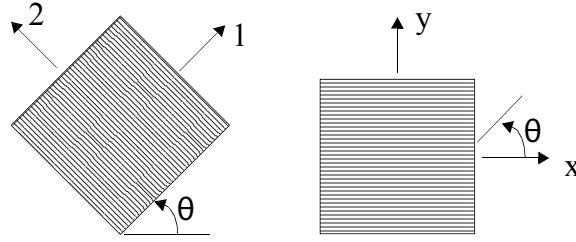


Figure A-2. Ply coordinate system and laminate (or global) coordinate system (Courtesy Z. Gürdal)

with the use of rotation matrices \mathbf{T}_1 and \mathbf{T}_2 which contain direction cosines $m = \cos(\theta)$ and $n = \sin(\theta)$:

$$\mathbf{T}_1 = \begin{bmatrix} m^2 & n^2 & 2mn \\ n^2 & m^2 & -2mn \\ -mn & mn & m^2 - n^2 \end{bmatrix} \quad (\text{A-7a})$$

$$\mathbf{T}_2 = \begin{bmatrix} m^2 & n^2 & mn \\ n^2 & m^2 & -mn \\ -2mn & 2mn & m^2 - n^2 \end{bmatrix} \quad (\text{A-7b})$$

$$(\text{A-7c})$$

The reason for two different rotation matrices instead of one is the use of the engineering stress and strain notations, rather than the tensor notation. Stress and strain in off-axis layers can be calculated using:

$$\begin{Bmatrix} \sigma_1 \\ \sigma_2 \\ \tau_{12} \end{Bmatrix} = \mathbf{T}_1 \begin{Bmatrix} \sigma_x \\ \sigma_y \\ \tau_{xy} \end{Bmatrix} \quad (\text{A-8})$$

and:

$$\begin{Bmatrix} \varepsilon_1 \\ \varepsilon_2 \\ \gamma_{12} \end{Bmatrix} = \mathbf{T}_2 \begin{Bmatrix} \varepsilon_x \\ \varepsilon_y \\ \gamma_{xy} \end{Bmatrix} \quad (\text{A-9})$$

Now the response in global coordinates (x, y) can be written in terms of ply properties that are defined in the ply coordinate system $(1, 2)$ by starting from the stress-strain relation in ply coordinates, equation A-1, and transforming the stress and strain vectors to global coordinates using equations A-8 and A-9:

$$\bar{\sigma} = \mathbf{Q}\bar{\varepsilon} \Rightarrow \mathbf{T}_1 \begin{Bmatrix} \sigma_x \\ \sigma_y \\ \tau_{xy} \end{Bmatrix} = \mathbf{Q}\mathbf{T}_2 \begin{Bmatrix} \varepsilon_x \\ \varepsilon_y \\ \gamma_{xy} \end{Bmatrix} \quad (\text{A-10})$$

or:

$$\begin{Bmatrix} \sigma_x \\ \sigma_y \\ \tau_{xy} \end{Bmatrix} = \mathbf{T}_1^{-1}\mathbf{Q}\mathbf{T}_2 \begin{Bmatrix} \varepsilon_x \\ \varepsilon_y \\ \gamma_{xy} \end{Bmatrix} = \bar{\mathbf{Q}} \begin{Bmatrix} \varepsilon_x \\ \varepsilon_y \\ \gamma_{xy} \end{Bmatrix} \quad (\text{A-11})$$

The following assumptions are needed for the part that follows:

- Layers are perfectly bonded together
- Each layer is in state of plane stress
- The Kirchhoff hypothesis holds for the laminate

The Kirchhoff hypothesis states that straight cross-sectional lines remain straight under deformation, and thus allows for every off-axis displacement to be written in terms of the mid-plane displacement, the distance to the midplane and the rotation of that part of the laminate. This leads to the following strain relations:

$$\begin{aligned}\varepsilon_x(x, y, z) &= \varepsilon_x^\circ(x, y) + z\kappa_x(x, y) \\ \varepsilon_y(x, y, z) &= \varepsilon_y^\circ(x, y) + z\kappa_y(x, y) \\ \gamma_{xy}(x, y, z) &= \gamma_{xy}^\circ(x, y) + z\kappa_{xy}(x, y)\end{aligned}\tag{A-12}$$

where the circle indicates the midplane value and the curvatures κ are defined as:

$$\begin{Bmatrix} \kappa_x \\ \kappa_y \\ \kappa_{xy} \end{Bmatrix} = - \begin{Bmatrix} \frac{\partial^2 w}{\partial x^2} \\ \frac{\partial^2 w}{\partial y^2} \\ 2 \frac{\partial^2 w}{\partial xy} \end{Bmatrix}\tag{A-13}$$

Now, the stress-strain relation for the k^{th} layer can be written as:

$$\begin{Bmatrix} \sigma_x \\ \sigma_y \\ \tau_{xy} \end{Bmatrix}_k = \bar{\mathbf{Q}}_k \begin{Bmatrix} \varepsilon_x^\circ(x, y) + z\kappa_x(x, y) \\ \varepsilon_y^\circ(x, y) + z\kappa_y(x, y) \\ \gamma_{xy}^\circ(x, y) + z\kappa_{xy}(x, y) \end{Bmatrix}\tag{A-14}$$

where $z_{k-1} < z < z_k$. With the definitions:

$$\int_{-\frac{h}{2}}^{\frac{h}{2}} \sigma_x dz = N_x \quad \int_{-\frac{h}{2}}^{\frac{h}{2}} \sigma_y dz = N_y \quad \int_{-\frac{h}{2}}^{\frac{h}{2}} \tau_{xy} dz = N_{xy}\tag{A-15}$$

$$\int_{-\frac{h}{2}}^{\frac{h}{2}} \sigma_x z dz = M_x \quad \int_{-\frac{h}{2}}^{\frac{h}{2}} \sigma_y z dz = M_y \quad \int_{-\frac{h}{2}}^{\frac{h}{2}} \tau_{xy} z dz = M_{xy}\tag{A-16}$$

the following relation holds after integration:

$$\begin{Bmatrix} N_x \\ N_y \\ N_{xy} \\ M_x \\ M_y \\ M_{xy} \end{Bmatrix} = \begin{bmatrix} A_{11} & A_{12} & A_{16} & B_{11} & B_{12} & B_{16} \\ A_{12} & A_{22} & A_{26} & B_{12} & B_{22} & B_{26} \\ A_{16} & A_{26} & A_{66} & B_{16} & B_{26} & B_{66} \\ B_{11} & B_{12} & B_{16} & D_{11} & D_{12} & D_{16} \\ B_{12} & B_{22} & B_{26} & D_{12} & D_{22} & D_{26} \\ B_{16} & B_{26} & B_{66} & D_{16} & D_{26} & D_{66} \end{bmatrix} \begin{Bmatrix} \varepsilon_x^\circ \\ \varepsilon_y^\circ \\ \gamma_{xy}^\circ \\ \kappa_x \\ \kappa_y \\ \kappa_{xy} \end{Bmatrix}\tag{A-17}$$

or in short:

$$\begin{Bmatrix} \bar{N} \\ \bar{M} \end{Bmatrix} = \begin{bmatrix} \mathbf{A} & \mathbf{B} \\ \mathbf{B} & \mathbf{D} \end{bmatrix} \begin{Bmatrix} \bar{\varepsilon}^\circ \\ \bar{\kappa} \end{Bmatrix}$$

where:

$$\begin{aligned}\mathbf{A} &= \sum_{k=1}^N \bar{\mathbf{Q}}_k (z_k - z_{k-1}) \\ \mathbf{B} &= \frac{1}{2} \sum_{k=1}^N \bar{\mathbf{Q}}_k (z_k^2 - z_{k-1}^2) \\ \mathbf{D} &= \frac{1}{3} \sum_{k=1}^N \bar{\mathbf{Q}}_k (z_k^3 - z_{k-1}^3)\end{aligned}$$

For convenience, the relation in equation A-17 can also be inverted when the strains are to be calculated from the loads, in which case the coefficients of the inverted matrix are written in lower case for clarity:

$$\begin{pmatrix} \varepsilon_x^\circ \\ \varepsilon_y^\circ \\ \gamma_{xy}^\circ \\ \kappa_x \\ \kappa_y \\ \kappa_{xy} \end{pmatrix} = \begin{bmatrix} a_{11} & a_{12} & a_{16} & b_{11} & b_{12} & b_{16} \\ a_{12} & a_{22} & a_{26} & b_{12} & b_{22} & b_{26} \\ a_{16} & a_{26} & a_{66} & b_{16} & b_{26} & b_{66} \\ b_{11} & b_{12} & b_{16} & d_{11} & d_{12} & d_{16} \\ b_{12} & b_{22} & b_{26} & d_{12} & d_{22} & d_{26} \\ b_{16} & b_{26} & b_{66} & d_{16} & d_{26} & d_{66} \end{bmatrix} \begin{pmatrix} N_x \\ N_y \\ N_{xy} \\ M_x \\ M_y \\ M_{xy} \end{pmatrix} \quad (\text{A-18})$$

A-3 Thermal stress

Variations in temperature cause thermal stresses in a laminate when plies of different coefficient of thermal expansion (CTE) are included in a single laminate. The thermal strain in the laminate is calculated by applying a fictitious thermal line load. The thermal line load and moment are calculated from the sum of the unconstrained thermal expansion or contraction in global coordinates of each ply as given below (Tsai and Hahn, 1980).

$$\bar{\mathbf{N}}^t = \sum_{k=1}^N \left[\bar{\mathbf{Q}}_k \begin{pmatrix} \varepsilon_x^t \\ \varepsilon_y^t \\ \gamma_{xy}^t \end{pmatrix} t_k \right] = \sum_{k=1}^N \left[[\mathbf{T}_1^{-1} \mathbf{E}]_k \begin{pmatrix} \alpha_1 \Delta T \\ \alpha_2 \Delta T \\ 0 \end{pmatrix} t_k \right] \quad (\text{A-19})$$

and similarly:

$$\bar{\mathbf{M}}^t = \sum_{k=1}^N \left[[\mathbf{T}_1^{-1} \mathbf{E}]_k \begin{pmatrix} \alpha_1 \Delta T \\ \alpha_2 \Delta T \\ 0 \end{pmatrix} \left(\frac{z(k) + z(k-1)}{2} \right) t_k \right] \quad (\text{A-20})$$

where the superscript t has been added to indicate that the quantities result from thermal expansion. The total strain in the laminate is calculated by using both the applied and the fictitious thermal line load:

$$\begin{pmatrix} \bar{\varepsilon}_{\text{total}}^\circ \\ \bar{\kappa}_{\text{total}} \end{pmatrix} = \begin{bmatrix} \mathbf{a} & \mathbf{b} \\ \mathbf{b} & \mathbf{d} \end{bmatrix} \begin{pmatrix} \bar{\mathbf{N}} + \bar{\mathbf{N}}^t \\ \bar{\mathbf{M}} + \bar{\mathbf{M}}^t \end{pmatrix} \quad (\text{A-21})$$

The stress occurring in layer k as a result of the combination of applied load and thermal expansion can now be calculated in ply coordinates using:

$$\begin{pmatrix} \sigma_{1, \text{total}} \\ \sigma_{2, \text{total}} \\ \tau_{12, \text{total}} \end{pmatrix}_k = [\mathbf{E} \mathbf{T}_2]_k \left(\bar{\varepsilon}_{\text{total}}^\circ + z \bar{\kappa}_{\text{total}} - \mathbf{T}_2^{-1} \begin{pmatrix} \alpha_1 \Delta T \\ \alpha_2 \Delta T \\ 0 \end{pmatrix} \right) \quad (\text{A-22})$$